Ore Geology Reviews 85 (2017) 64–106

Contents lists available at ScienceDirect

Ore Geology Reviews

journal homepage: www.elsevier.com/locate/oregeorev

Chimneys in Paleozoic massive sulfide mounds of the Urals VMS deposits: Mineral and trace element comparison with modern black, grey, white and clear smokers

V.V. Maslennikov [a,b,*], S.P. Maslennikova [a], R.R. Large [c], L.V. Danyushevsky [c], R.J. Herrington [d], N.R. Ayupova [a,b], V.V. Zaykov [a], A.Yu. Lein [e], A.S. Tseluyko [b,a], I.Yu. Melekestseva [a], S.G. Tessalina [f]

[a] Institute of Mineralogy, Ural Branch, Russian Academy of Sciences, Miass, Chelyabinsk District 456317, Russia
[b] Department of Geology, South Urals State University, 8 Oktyabrya str. 16, Miass 456301, Russia
[c] ARC Centre of Excellence in Ore Deposits, University of Tasmania, Hobart, Australia
[d] Department of Mineralogy, Natural History Museum, Cromwell Road, London SW7 5BD, United Kingdom
[e] Institute of Oceanology, Russian Academy of Sciences, Nakhimosvsky av., 36, Moscow 117997, Russia
[f] John de Laeter Centre, Department of Imaging and Applied Physics, Curtin University, GPO Box U 1987, Perth 6845, Western Australia, Australia

ARTICLE INFO

Article history:
Received 24 May 2016
Received in revised form 7 September 2016
Accepted 12 September 2016
Available online 14 September 2016

Keywords:
VMS deposits
The Urals
Chimneys
Black smokers
LA-ICP-MS
Mineral zonality and assemblages

ABSTRACT

In the Urals, a wide range of well-preserved chimneys are found in VMS deposits, which are associated with ultramafic (Atlantic type: Dergamysh), mafic (Cyprus type: Buribay), bimodal mafic (Uralian type: Yubileynoye, Sultanovskoye, Yaman-Kasy, Molodezhnoye, Uzelga-4, Valentorskoye) and bimodal felsic (Kuroko or Baymak type: Oktyabrskoye, Tash-Tau, Uselga-1, Talgan, Alexandrinskoye) sequences. Chimneys have also been found in the Safyanovskoye deposit (Altay type) that is hosted by intercalated felsic lavas and carbonaceous shales. A combination of geological, mineralogical and trace element data provide a general outline for comparison between chimneys from the Urals deposits and modern vent sites. The chimneys from the Dergamysh deposit show a broad affinity with those from the Rainbow and other vent sites associated with serpentinites of the Mid-Atlantic Ridge. The chimneys from the Buribay deposit are similar to the black smokers of the EPR vent sites including the scarcity of rare minerals. The chimneys from the Urals type of the VMS deposits show some similarities with grey smokers from the Brother Volcano and PACMANUS sites. The chimneys from the Baymak type of the VMS deposits resemble grey and white smokers of the PACMANUS and grey smokers of the Suiyo vent sites. The chimneys from the Safyanovskoye deposit are similar to the black and clear smokers from the Okinawa Trough. Mineral assemblages are controlled by the combination of host rock composition and physicochemical conditions of the ore-forming processes. Amount of colloform pyrite, isocubanite and pseudomorphic pyrite and marcasite after pyrrhotite decreases in the chimneys across the range from ultramafic and mafic to felsic-hosted deposits and is concomitant with increase in the contents of sphalerite, galena, bornite, fahlores, native gold and barite across this range. The chimneys from the Urals type contain abundant tellurides and sulfoarsenides, while these minerals are rare (except for hessite) in the Baymak type deposits. In the same range, the buffering capacity of host rocks decreases in contrast to the increase in fS_2 and fO_2. With the exception of the Safyanovskoye deposit, trace element assemblages in chalcopyrite vary to reflect the host rock: ultramafic (high Se, Sn, Co, Ni, Ag and Au) → mafic (high Co, Se, Mo and low Bi, Au and Pb) → bimodal mafic (high Te, Au, Ag, Bi, Pb, Co, moderate Se, and variable As and Sb) → bimodal felsic (high As, Sb, Mo, Pb, moderate Bi, and low Co, Te and Se). In sphalerite of the same range, the contents of Bi, Pb, Ag, Au and Sb increase versus Fe, Se and Co. The variations in trace elements in colloform pyrite coincide with these changes. The specific mineral changes in the local ranges from Cu- to Zn-rich chimneys in each VMS deposit are similar to the general changes in the range of host rock classes of the deposits. However, the local T, fS_2 and fO_2 changes can broadly be interpreted in terms of contribution of variable oxygenated cold seawater to the subseafloor and seafloor hydrothermal processes.

1. Introduction

The first fragments of the chalcopyrite–sphalerite and barite chimneys were found in the Hokuroko VMS deposits hosted by bimodal felsic

* Corresponding author at: Institute of Mineralogy, Ural Branch, Russian Academy of Sciences, Miass, Chelyabinsk District 456317, Russia.
E-mail address: mas@mineralogy.ru (V.V. Maslennikov).

http://dx.doi.org/10.1016/j.oregeorev.2016.09.012
0169-1368/

sequences (Scott, 1981; Shimazaki and Horikoshi, 1990; Shikasono and Kusakabe, 1999; Solomon et al., 2004). Chalcopyrite–isocubanite chimney fragments are widespread in the basalt-hosted Cyprus VMS deposits (Oudin and Constantinou, 1984). Chalcopyrite–pyrite chimneys in association with vent fauna occur at the Figaro deposit (the American Cordillera) (Little et al., 1999). Chalcopyrite–isocubanite–pyrite chimneys with glaucodot were described in the Bold Mountain VMS deposit hosted by bimodal-mafic rocks (Slack et al., 2003). Chalcopyrite–pyrite and chalcopyrite–sphalerite–pyrite chimneys also occur in VMS deposits of Pontides (Turkey), located in sequences transitional from bimodal mafic to bimodal felsic (Revan et al., 2014).

The Urals have yielded a mineral range of very well preserved sulfide vent chimneys within the Yaman-Kasy (Little et al., 1997; Herrington et al., 1998; Maslennikov et al., 2009) and Alexandrinskoye (Tessalina et al., 2008) VMS deposits. Many telluride-rich chalcopyrite–sphalerite–pyrite chimneys have been found at the Yubileynoye, Safyanovskoye, Valentorskoye, Molodezhnoye and Uzelga VMS deposits (Maslennikov et al., 2013). All these chimneys occur in VMS deposits hosted by bimodal mafic or bimodal felsic sequences only.

New samples have been found at the Dergamysh deposit hosted by ultramafic rocks, as well as the chimney fragments from the basalt-hosted Buribay, Yubileynoye and Sultanovskoye deposits and these are the closest in setting to chimneys described in modern black smoker systems. Chimneys have also been found at the Safyanovskoye deposit, a specific feature of which is an occurrence of the altered black shales among felsic lava flows. These findings together permit comparison between chimneys from the entire range of the igneous host rocks related to the VMS deposits and modern vent sites.

Numerous mineralogical data on modern black and white smokers are scattered through a number of publications (e.g., Halbach et al., 1993; Marumo et al., 2008; Hannington et al., 1995; Scott, 1997; Lein et al., 2003; Bogdanov et al., 2006a, 2006b, 2015; Rona, 2008; Fouquet et al., 2010; Berkenbosch et al., 2012). Little is published on the mineral peculiarities of chimneys from the ancient VMS deposits (Herrington et al., 1998; Maslennikova and Maslennikov, 2007; Maslennikov et al., 2009, 2013; Revan et al., 2014).

The bulk minor and trace element analyses indicate significant influence of host rocks on the metal inventory of the modern and ancient massive sulfide deposits. Ultramafic rocks from spreading ridges influence the higher concentration of Cu, Co, Ni and Sn (e.g., Fouquet et al., 2010; Bogdanov et al., 2006a, 2006b, 2015; Evrard et al., 2015), whereas felsic-hosted deposits are generally enriched in Zn, Pb, As, Sb, Ag and Au (e.g., Binns and Scott, 1993). In contrast, the results of the quantitative laser ablation inductively coupled plasma mass spectrometry (LA-ICP-MS) show that concentration of most trace metals in pyrite is a function of physico-chemical parameters of the fluid rather than a reflection of igneous host rock composition (Keith et al., 2016).

Local chemical analyses of chimney zones provided new insight into the processes and microenvironments involved in chimney growth (Kristall et al., 2011). Previous studies yield limited information on trace element distribution in individual crystals of sulfides within black smoker chimneys in each zone. The first semiquantitative data of Butler and Nesbitt (1999) illustrated the power of LA-ICP-MS analysis in documenting the non-random distribution of V, Ag, In, Te, Ba, Au and Pd within the chalcopyrite wall of an immature black smoker chimney from the Broken Spur hydrothermal field (29°10′N, MAR). LA-ICP-MS offers enormous potential in advancing trace element studies of sulfides through significantly improved detection limits for in situ analysis (e.g., Norman et al., 1998; Danyushevsky et al., 2011). A few studies reported on high variation in quantitative LA-ICP-MS trace elements on sulfide minerals from a variety of modern vent sites (Melekestseva et al., 2014; Wohlgemuth-Ueberwasser et al., 2015; Keith et al., 2016) and in zonal ancient chimneys from the VMS deposits of the Urals and Pontides (Maslennikova and Maslennikov, 2007; Maslennikov et al., 2009; Revan et al., 2014).

Trace and minor elements, which may be enriched in the same mineral phases under variable temperature, redox conditions or mixing, offer a method to identify physical and chemical microenvironments within zoned chimneys. In this paper, we use new LA-ICP-MS data on minor and trace elements in well preserved chimneys from abovementioned VMS deposits. Original LA-ICP-MS data on smokers from the Pacific and Atlantic oceans are used for comparison with the ancient chimney material.

2. Geological setting and types of VMS deposits

Several reviews describe the geological setting and geology of the VMS deposits of the Urals (Koroteev et al., 1997; Prokin and Buslaev, 1999; Maslennikov, 2006; Herrington et al., 2002, 2005a, 2005b; Zaykov, 2006; Puchkov, 2010; Seravkin, 2010; Kontar, 2013). The VMS deposits (hereafter, deposits) were formed in a range of tectonic settings (Fig. 1). The deposits formed in the Ordovician–Silurian Sakmara zone (e.g., Yaman-Kasy Zn–Cu deposit) are ascribed either to a marginal sea (Zaykov, 2006) or an island arc basin (Herrington et al., 2005b). The Valentorskoye deposit is situated in the northern part of the Ordovician to Early Silurian Tagil island arc basin (Krivtsov, 1999) formed on a narrow rifted continental crust in an active continental margin setting (Karetin, 2000). The Dergamysh Cu–Co deposit occurs in Main Uralian Fault (MUF), which is a 10–20-km wide suture zone with suprasubduction units (Zaykov, 2006; Melekestseva et al., 2013). The Early Devonian West Magnitogorsk island arc embraces three ore-bearing horizons, which occur within (Buribay Cu deposit) and on (Yubileynoye Cu–Zn deposit) the boninite–tholeiite basement and within the andesitic dacite upper unit (e.g., Oktyabskoye and Tash-Tau Zn–Cu deposits). The Uzelga-4 and Molodeznoye Zn–Cu deposits are confined to the lower level of the dacite–rhyolite unit close to basalt basement of the East Magnitogorsk island arc, whereas Uzelga-1, Talgan, Alexandrinskoye and many other Zn–Cu deposits occupy the upper ore-bearing levels of felsic units (Fig. 2). The Sultanovskoye Cu–Zn deposit is located in the Kunashak ore district within the Middle Devonian zone of the East Uralian uplift, which is interpreted as allochthonous fragments of evolved oceanic and epicontinental back-arc basins (Seravkin, 2010). There are, at least, three ore-bearing levels, including numerous fragments of ore bodies. The ore bodies with chimneys occur within or above the basalts in the bimodal sequence. The Safyanovskoye deposit is located in the central part of the East Uralian uplift, which is considered to be an ensialic island arc. The deposit occurs in the overturned sheet of the andesite–dacite–rhyolite volcanic edifice of the Early to Middle Devonian age (Koroteev et al., 1997). Most deposits are situated in the extensional graben or half-graben rift valleys not only in the back-arc basins, but also in the intra-arc rifted basement (Maslennikov, 1999) and are located in several stratigraphic levels (Fig. 2). The intra-arc rifts contained infrequently developed calderas (Seravkin, 2010).

The deposits are subdivided into five main types: Atlantic, Cyprus, Uralian, Baymak, and Altay. The ultramafic-hosted Co–Ni-bearing deposits with similar features to the Atlantic ultramafic-associated hydrothermal fields were recently distinguished in the Urals in addition to the basalt-hosted Cyprus type of the deposits (Zaykov et al., 2001; Zaykov, 2006; Melekestseva et al., 2013). The other types are also related to the geological and geodynamic formation conditions (Prokin and Buslaev, 1999; Herrington et al., 2002, 2005a; Zaykov, 2006; Seravkin, 2010). This classification can broadly be compared to the classification of Franklin et al. (2005) where Cyprus is Mafic, Besshi is Pelitic-mafic, Uralian is Bimodal-mafic and Baymak (Kuroko) and Altay are Bimodal-felsic types of deposits. The deposits of the Baymak type occur in the arc basins on the oceanic crust, whereas deposits of the Kuroko and Altay types of deposit are related to those on the continental crust (Prokin and Buslaev, 1999). The specific feature of the Altay type deposits is the presence of carbonaceous sediments instead of jaspers. Three subtypes (U1, U2, U3) were recognized in the Urals type of the deposits depending on the Cu/Zn ratio and host rock composition and

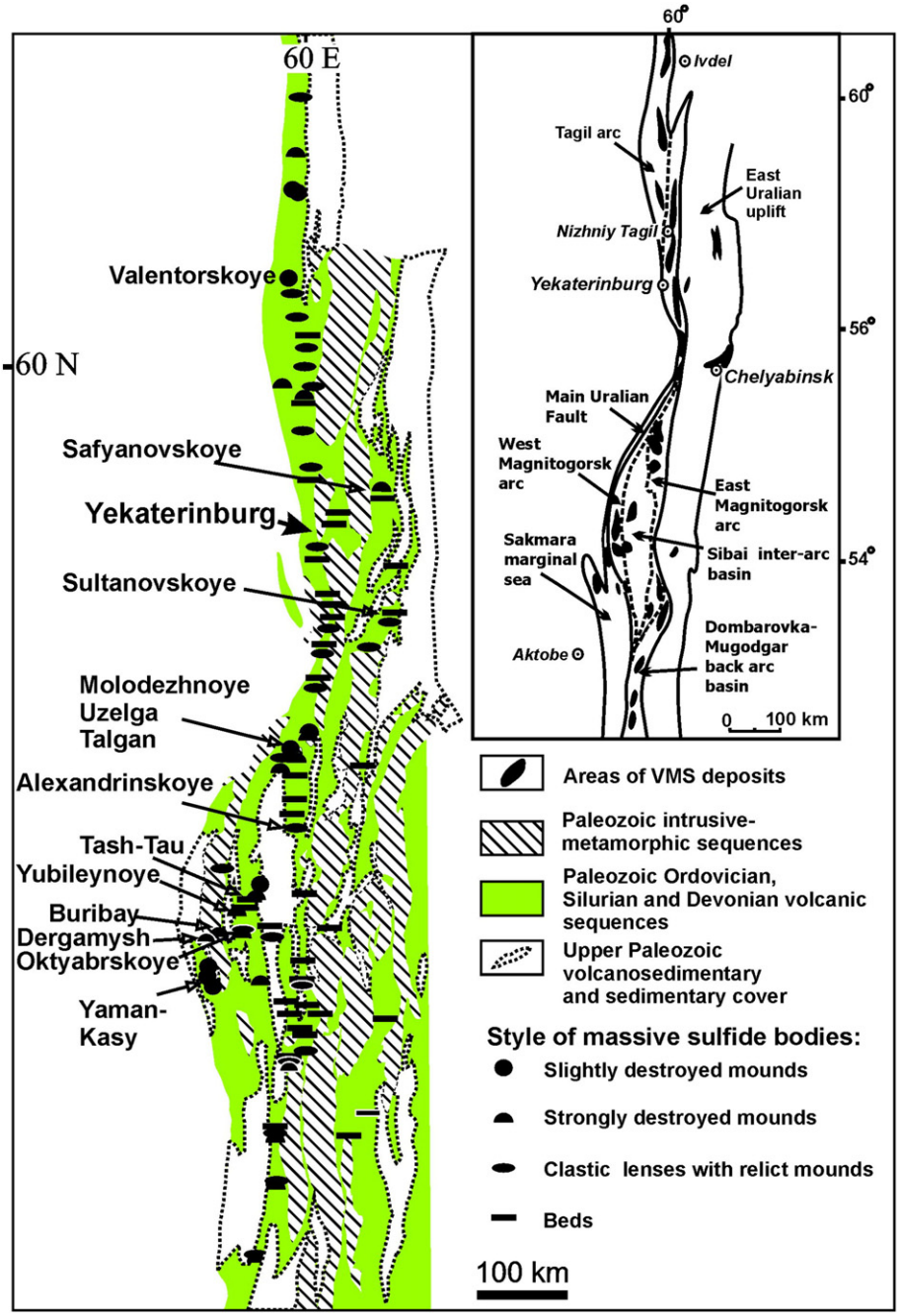

Fig. 1. Geological setting of the Urals VMS deposits with chimneys occurrences.

position in the bimodal mafic sequence (Seravkin, 2010; Prokin et al., 2011). The ore bodies located within or on basalt basement of the bimodal mafic units represent subtype U1. The ore bodies of subtype U2 and U3 are divided from the underlying basalt or andesitic basalt basement by a thin horizon of dacites or andesitic dacites, respectively. The Baymak type deposits could occur in the upper ore-bearing levels of the same sequences.

Generally, the Urals deposits can be ranged by host rock composition and associated ore types and subtypes: ultramafic (Atlantic type: Dergamysh) → mafic (Cyprus type: Buribay) → bimodal mafic (Uralian type, U1, U2, and U3 subtypes: Yubileynoye (U1) → Sultanovskoye (U1) → Yaman-Kasy (U2) → Molodezhnoye (U3) → Uzelga-4 (U3)) → bimodal felsic (Baymak type: Oktyabrskoye → Valentorskoye → Tash-Tau → Uzelga-1 → Talgan → Alexandrinskoye) sequences. In this range, footwall alteration is gradually changed from talc–chlorite–carbonate to chlorite, quartz–chlorite–sericite and quartz–sericite rocks. In the same direction, massive Cu–Co pyrite-rich ore facies, which are typical of the Atlantic and Cyprus types of the deposits, are followed by Au–Pb–As–Sb-rich chalcopyrite-, sphalerite-, bornite-, and barite-rich massive ore facies and sulfide stockworks. The amount of colloform pyrite, pyrrhotite or pseudomorphic pyrite and marcasite after pyrrhotite decreases in the same way. The Safyanovskoye Cu–Zn deposit may be a proxy of the Altay type (pelitic-felsic) hosted by intercalated felsic and black shale complex and displays specific mineral features, which are atypical of this range because of unpredictable predominance of colloform textures, pseudomorphic pyrite and marcasite after pyrrhotite and less abundant barite in comparison with Baymak or Kuroko types.

The Co-bearing sulfides are characteristic of the Dergamysh and other serpentinite-hosted deposits (Melekestseva et al., 2013). Accessory minerals are rare in the Buribay deposit (Prokin, 1977), as well as in

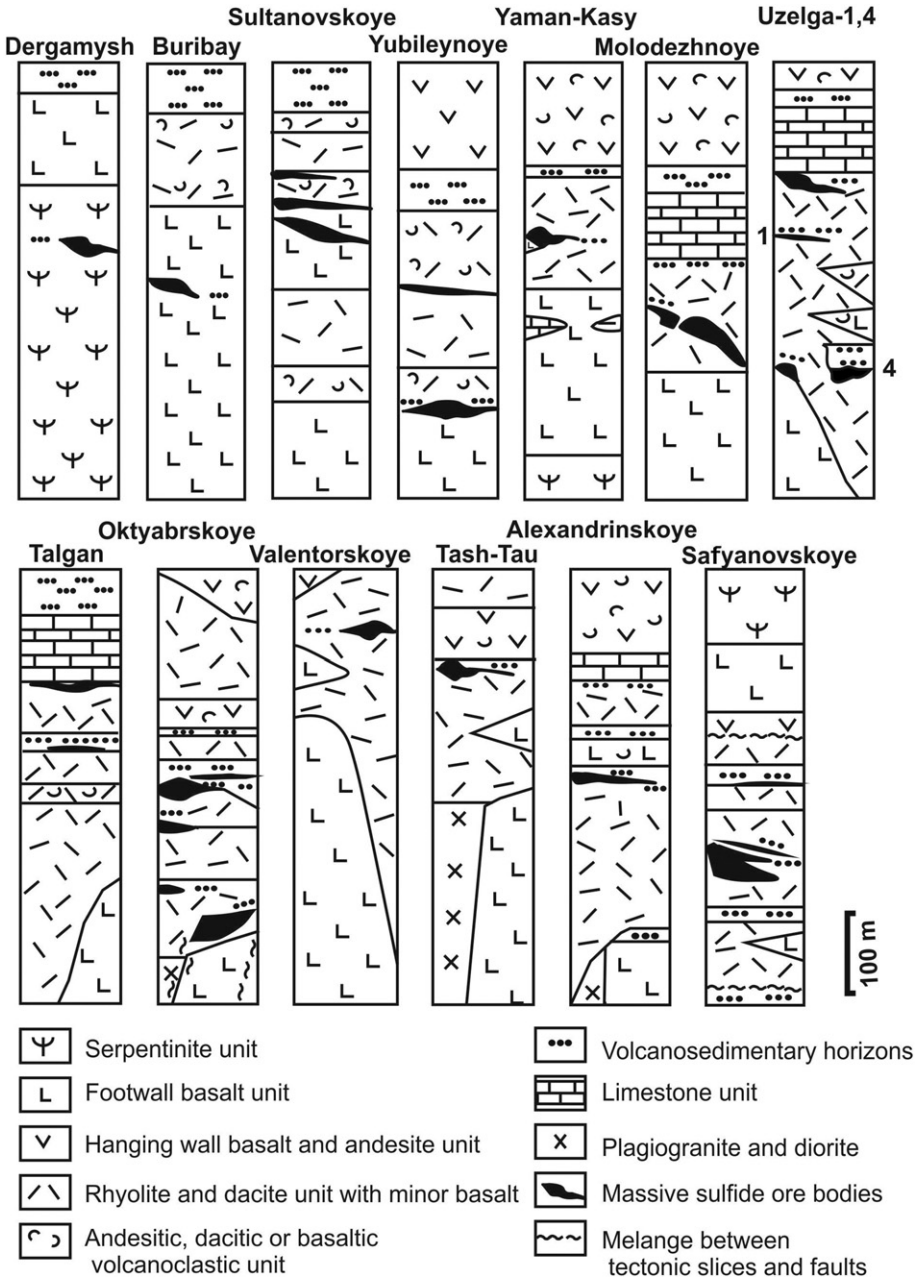

Fig. 2. Position of chimney-bearing Urals VMS deposits in stratigraphic columns.

other mafic-hosted Cyprus type of the deposits (Eremin et al., 2007). The deposits of the Urals type are characterized by abundant and diverse tellurides, sulfoarsenides and less pervasive gold–galena–fahlore assemblage, which are more typical of the Baymak or Kuroko types of the deposits (Moloshag et al., 2002; Vikentyev, 2006; Eremin et al., 2007; Maslennikov et al., 2013). Rare mineral assemblages of the Safyanovskoye deposit show signatures of both the Urals and Baymak types of the deposits (Table 1).

The Dergamysh deposit is very similar to Cyprus type by economic Cu contents in comparison to Zn and Pb and general low reserves (Table 2). The differences are in the higher Co contents and more diverse Au–Co–Ni mineral assemblages (Table 1) influenced by ultramafic host rocks. This deposit is similar to the ultramafic-hosted vent sites of the Atlantic Ocean (Melekestseva et al., 2013). By host basalts, high S and elevated Co contents and Cu/Zn ≫ 1, the Buribay deposit is similar to mafic class or Cyprus type of VMS deposits (Prokin and Buslaev, 1999), but is distinct in the higher Au contents. As well as many other Cyprus-type VMS deposits, the Buribay deposit has low ore reserves (Table 2). The Sultanovskoye and Yubileynoye deposits display the features typical of both Cyprus (Cu/Zn > 1) and Uralian (higher Te contents) types. The highest Te contents and low Cu/Zn (<1) ratio are characteristic related to subtype U2 (Yaman-Kasy) and subtype U3 (Molodezhnoye and Uzelga 4) of the Uralian type. In comparison with subtype U2, subtype U3 has the higher Pb contents (Table 2). In comparison with Uralian type, the Baymak type displays the lower S (<30 wt.%) and Te (<30 ppm) and higher total Cu + Zn and Pb contents (Table 2).

All the deposits with chimney fragments can be interpreted as variously eroded sulfide mounds (Zaykov and Maslennikov, 1987; Zaykov, 2006; Maslennikov, 2006; Herrington et al., 2005b) (Fig. 3). The cores of the mounds are composed of the pyrite-rich massive or porous ores related to the refining zone (e.g., Eldridge et al., 1983). Porous lenses of colloform pyrite and marcasite are located in the upper parts of the cores. The cores are surrounded by variable portions of breccias that are successively followed by sulfide turbidites, sulfide diagenites and

Table 1
Mineral composition of the Urals VMS deposits.

VMS deposit	Types	Distance from basalt basement (m)	**Main,** subordinate and *minor* minerals
Dergamysh	At	0*	**Pyrite, marcasite, chalcopyrite**, sphalerite, *mackinavite, pyrrhotite, isocubanite, cubanite and magnetite in assemblage with minor gersdorffite, cobaltite, nikeline, pylsenite, cassiterite and native gold, calcite*
Buribay	C	0	**Pyrite, chalcopyrite**, sphalerite, *native gold, pyrrhotite, tennantite, bornite, enargite, magnetite*
Sultanovskoye	U1	0	**Pyrite, chalcopyrite**, sphalerite, marcasite, *covellite, chalcocite, bornite, galena, enargite, pyrrhotite, hematite, native gold, tellurobismuthite, galena*
Yubileinoye	U1	0	**Pyrite, chalcopyrite, sphalerite**, *marcasite, pyrrhotite, arsenopyrite, magnetite, tennantite, tellurobosmuthite, coloradoite, cervelleite, clausthalite, hessite, native gold and electrum, talc, calcite*
Yaman-Kasy	U2	0–100	**Pyrite, marcasite, chalcopyrite, sphalerite**, *bornite, arsenopyrite, pyrrhotite, altaite, tellurobismuthite, coloradoite, empressite, galena, hessite, tennantite, barite, hematite, magnetite, galena, enargite, petzite, stützite, loellingite, volynskite, greenockite, digenite, cervelleite, benleonardite, covellite, goldfieldite, sylvanite, frohbergite, native tellurium, native gold*
Molodezhnoye	U3	30–120	**Pyrite, chalcopyrite, sphalerite**, bornite, marcasite, *arsenopyrite, pyrrhotite, altaite, tellurobismuthite, coloradoite, empressite, hessite, tennantite, barite, hematite, magnetite, galena, enargite, stromeyerite, arsenosulvanite, jalpaite, mackinstryite, stannoidite, mowsonite, native gold, cassiterite, naumannite, clausthalite, kurilite, bohdanowichite, roquesite*
Uzelga-4	U3	40–150	**Pyrite, chalcopyrite, sphalerite, pyrrhotite,** *altaite, tellurobismuthite, sylvanite, petzite, coloradoite, shützite, hessite, native tellurium, native gold, tennantite, tetrahedrite, magnetite, arsenopyrite, coloradoite, siderite*
Uzelga-1	U3/B1	250	**Pyrite, chalcopyrite,** sphalerite, tennantite, tetrahedrite, *galena, native gold, hessite, calcite*
Talgan	U3/B1	>350	**Pyrite, sphalerite, chalcopyrite**, bornite, barite, *hessite, galena, electrum, kustelite, stromeyerite, wittichenite, stannoidite, germanite*
Oktyabrskoye	U3/B1	200	**Pyrite, chalcopyrite, sphalerite**, bornite, digenite, quartz, barite, *hessite, altaite, tennantite, tetrahedrite, native gold*
Valentorskoye	B1	90 ≥ 300	**Pyrite, chalcopyrite, sphalerite,** bornite, *hessite, tellurobismuthite, stützite, tetradymite, empressite, kochkarite, tennantite, cervelleite, wittichenite, renierite, native gold*
Tash-Tau	B1	150–300	**Pyrite, sphalerite, chalcopyrite**, bornite, tennantite, galena, *hessite, cervellite, native gold, electrum, enargite, digenite, stromeyerite, jalpaite, germanite, calcite, barite*
Alexandrinskoye	B2	310	**Pyrite, chalcopyrite, sphalerite**, bornite, barite, galena, tennantite, *hessite, diagenite, stromeyerite, renierite, germanite, acanthite, pearseite, native gold, electrum*
Safyanovskoye	Alt	>300	**Pyrite, chalcopyrite, sphalerite,** galena, *pyrrhotite, tennantite, tetrahedrite, glauckodot, tellurobismuthite, hessite, Bi-telluride, enargite, stannoidite, mowsonite, native gold, Pb sulfosalts*

The table is composed after Prokin (1977), Zaykov (2006), Moloshag et al. (2002), Tessalina et al. (1998), Vikentyev et al. (2000), Vikentyev (2006), Seravkin (2010), Prokin et al. (2011), Maslennikov et al. (2009; 2013), and Ayupova et al. (2015). The types of the VMS deposits: At – Atlantic; C – Cyprus; U – Uralian with subtypes U1, U2, U3; B – Baymak (Kuroko) with subtypes B1 (Cu-rich) and B2 (Zn-rich); Alt – Altai; * – distance from serpentenite.

ferruginous sediments (Maslennikov et al., 2012; Ayupova et al., 2015) or alternatively black shales (Safyanovskoye deposit; Safina et al., 2016). Most chimneys were found as fragments in the sulfide breccias along with clasts of various ores. Chimneys actually preserved *in situ* within colloform pyrite crusts are rare.

The deposits studied are located in tectonically preserved fragments of low-metamorphosed terrain. In spite of being part of the Uralian orogen, the host rocks are locally undeformed and have only undergone metamorphism of zeolite or prehnite–pumpellyite facies (Grabezhev et al., 2001). The primary colloform textures, sulfidized fauna and chimneys in ores indicate the low degree of metamorphic overprint (Zaykov and Maslennikov, 1987; Shadlun, 1991; Herrington et al., 1998; Little et al., 1997; Maslennikov, 2006; Zaykov, 2006; Maslennikov et al., 2009) and account for the exceptional degree of preservation of some deposits (Herrington et al., 2005a).

3. Analytical techniques

Macroscopic mineralogical study of samples was followed by analysis of chemical composition on a REMMA-2M SEM equipped with an Oxford Link energy dispersive X-ray and JXA JEOL 733 microprobe (Institute of Mineralogy UB RAS) and CAMECA SX-50 and JEOL-JXL-8600 (Natural History Museum, London) and JEOL JXA 8900RL (University of Tasmania, Australia and Freiberg Mining Academy, Germany) microprobes at an accelerating voltage of 15–25 kV, a beam current of 20–35 nA, a counting time of 10–20 s for peaks and background, and a beam size of 1 μm (EDAX) and 2 μm (CAMECA SX-50). For all microprobe analyses, the standard deviation of results was <0.1%.

Quantitative LA-ICP-MS analysis of sulfides from chimneys for a wide range of major and trace elements (Fe, Cu, Zn, Co, Ni, Au, Ag, Bi, Pb, Tl, Cd, As, Te, Se, Mo, Sn, V, Ti and Mn) was carried out using a New Wave 213 nm solid-state laser microprobe coupled to an Agilent 4500 quadrupole ICP-MS housed at the CODES LA-ICP-MS analytical facility, University of Tasmania. The laser microprobe is equipped with an in-house small volume (~2.5 cm^3) ablation cell characterized by <1 s response time and <2 s wash-out time. Ablation was performed in an atmosphere of pure He (0.7 l/min). Helium gas carrying the ablated aerosol was mixed with Ar (1.23 l/min) right after the ablation cell and the mixture was passed through a pulse homogenising device prior to direct introduction into the torch. For this study, quantitative analyses were performed by ablating spots ranging in diameter from 40 to 60 μm and depth 80 μm. Laser repetition rate was typically 5 Hz and laser beam energy at the sample was maintained between 4 and 5 J/cm^2. The analysis time for each sample was 100 s, comprising a 30 s measurement of background with the laser off and a 70 s analysis with the laser on. Acquisition time for all masses was set to 0.02 s. Data reduction was undertaken according to standard methods (Danyushevsky et al., 2011). Iron was used as the internal standard for quantification of pyrite and chalcopyrite and Zn was used as an internal standard for quantification of sphalerite. Concentrations of the internal standard were calculated assuming stoichiometry. In cases when a significant degree of fine-grained mineral intergrowth occurred within the ablated volume, values for the internal standard concentration were adjusted such that the total of major elements (Fe, Cu, Za and S, the latter calculated assuming stoichiometry) was 100%. An in-house Li-borate fused glass of a pyrite/sphalerite mixture (Danyushevsky et al., 2011) was used as the primary calibration standard. The standard was analyzed twice every 90 min to account for the instrument drift, with a 100 μm spot size at 10 Hz. The LA-ICP-MS was also used for detection of rare mineral microinclusions in the sulfides studied and for analysis of trace elements in telluride phases. The entire LA-ICP-MS dataset is included in Appendix A.

4. Results

4.1. Mineral composition and zonation of chimneys

4.1.1. Chimneys from the Urals deposits

In previous papers, we recognized the presence of chimney types with various proportions between sphalerite and chalcopyrite

Table 2
Average composition and sizes of the Urals VMS deposits yielded the chimneys.

Deposit	Cu	Zn	Pb	S	Se	Te	Au	Ag	Co	Size
	wt.%				g/t					Mt
Dergamysh	1.3	0.3	<0.005	47	54	16	2.0	12	0.01–0.25	1.0
Buribay	3.5	0.5	<0.005	>43	>50	20	5.5	<10	0.03	3.2
Sultanovskoye	1.4	0.7	0.009	42.64	52	38	1.1	128	<0.01	9.3
Yubileynoye	1.4	1.0	<0.005	43.8	50	30	1.6	18	<0.01	108.8
Yaman-Kasy	2.6	5.6	0.03	42.4	22	325	3.3	34	<0.01	1.7
Uzelga	1.3	2.6	0.15	37.4	110	101	1.8	34	<0.01	77.4
Molodezhnoye	2.1	3.3	0.17	29.4	82	89	1.6	46	<0.01	15.9
Talgan	3.2	3.6	0.45	29.2	15	10	1.7	44	<0.01	2.8
Oktyabrskoye	4.16	2.0	0.10	25.9	30	22	2.4	24	<0.01	11.2
Valentorskoye	2.4–6.0	3.2	0.24	17.1	22	28	1.72	26	<0.01	1.6
Tash-Tau	6.8	2.1	0.25	29.5	<10	5	4.0	58	<0.01	0.7
Alexandrinskoye	2.7	4.6	0.52	27.4	8	39	1.1	37	<0.01	3.8
Safyanovskoye	2.2	0.7	0.13	25.44	60	9.2	0.5	20	<0.01	19.4

The dataset is from unpublished reports of the Ministry of Base Metals, USSR and Maslennikov (1999).

depending on the high-temperature fluid/seawater interaction (Herrington et al., 1998; Maslennikova and Maslennikov, 2007; Maslennikov et al., 2009, 2013). Our recent work broadly classifies the chimney types into three chemical and mineral ranges:

Type 1 Cu–Fe (chalcopyrite–pyrite) to Fe–Cu (quartz–pyrite–chalcopyrite);
Type 2 Cu–Fe–Zn (chalcopyrite–pyrite–sphalerite) to Zn–Fe–Cu (quartz–sphalerite–pyrite–chalcopyrite);
Type 3 Cu–Zn (chalcopyrite-sphalerite) to Zn-rich (sphalerite-rich with minor chalcopyrite and pyrite).

Each mineral range reflects the decrease in amount of chalcopyrite and the increase in amount of quartz + pyrite (range 1), sphalerite + quartz (range 2) and sphalerite + quartz + barite (range 3). The type 1 is typical of chimneys from Atlantic, Cyprus and some Uralian (U1) types of deposits. In the Uralian type of deposits, the chimneys related to range 2 are widespread. The chimneys of ranges 1 and 2 contain abundant colloform pyrite, isocubanite, pseudomorphic pyrite and marcasite after pyrrhotite in contrast to the chimneys from the Baymak (Kuroko) type of deposits. The Baymak chimneys correspond to the range type 3. The chimneys from the Safyanovskoye deposits exhibit features typical of all chimney ranges. In the other hand, all these ranges form a general range with increase in sphalerite from type 1 to type 3. In the general range, tellurides and sulfoarsenides substitute the galena-tennantite assemblages with native gold, as well as in the ranges 1 and 2 of the Uralian type of deposits. The range 2 displays most contrasting and diverse mineral and textural signatures in comparison with range 1 and 3.

Our previous papers described chimney fragments with clear evidence for the high-temperature fluid flow through the axial zone, passing to a temperature-zoned chimney wall (Herrington et al., 1998; Maslennikov et al., 2009, 2013). The authors recognized the presence of three types of the chimneys. The chimneys consist of three radial zones, which can be described from the outer wall formerly in contact with seawater to the inner axial hydrothermal flow conduit thus: A – external zone – typified by the presence of pyrite, marcasite and/or sphalerite; B – internal zone – typified by the presence of chalcopyrite, and C – lining of the axial zone – normally infilled with sphalerite, quartz or barite (Figs. 4, 5). Our recent work showed that each Uralian deposit yields its own specific features of chimneys and the entire classification is more complex. The general mineral composition of the chimneys studied is shown in Table 3.

At the *Dergamysh* deposit, the outer wall of some chalcopyrite–pyrite chimneys is locally composed of colloform pyrite (Figs. 4a, 5a). Pseudomorphic pyrite and marcasite after subhedral pyrrhotite crystals occur in the middle part of the outer wall (Fig. 5a). Euhedral pyrite crystals are common to the inner part of the outer walls. Chimneys with a sphalerite outer wall are rare (Figs. 4b, 5b). The inner wall (zone B) is infilled with crystals of chalcopyrite and isocubanite, often showing exsolution lamellae texture. The euhedral pyrite crystals are disseminated within the chalcopyrite of zone B. The Co-bearing pyrite (2–22 wt.% Co) occurs as veinlets in chalcopyrite. Inclusions of electrum 5–10 μm in size are enclosed in isocubanite. Microinclusions of an unresolved Sn–Fe–Cu sulfide (17.9 wt.% Sn) 1–2 μm in size and cassiterite are dispersed in chalcopyrite (Table 3). Colloform calcite–pyrite-rich chimneys (Figs. 4c, 5c) and diffuser-like structures are widespread in this deposit. Single subhedral crystals of chalcopyrite, isocubanite, and pyrite encrust the inner wall of the conduit. The axial part of the conduit was sealed by calcite.

Rare fragments of chalcopyrite–pyrite chimneys (Fig. 4d) were found in the dumps of the *Buribay* deposit in association with fragments of colloform pyrite, pseudomorphic pyrite after subhedral pyrrhotite and rare sphalerite clasts. The mineral zonation of the chimneys could be reconstructed due to combination of ore clasts (Fig. 5d). The chimneys contain no rare mineral assemblages (Table 3).

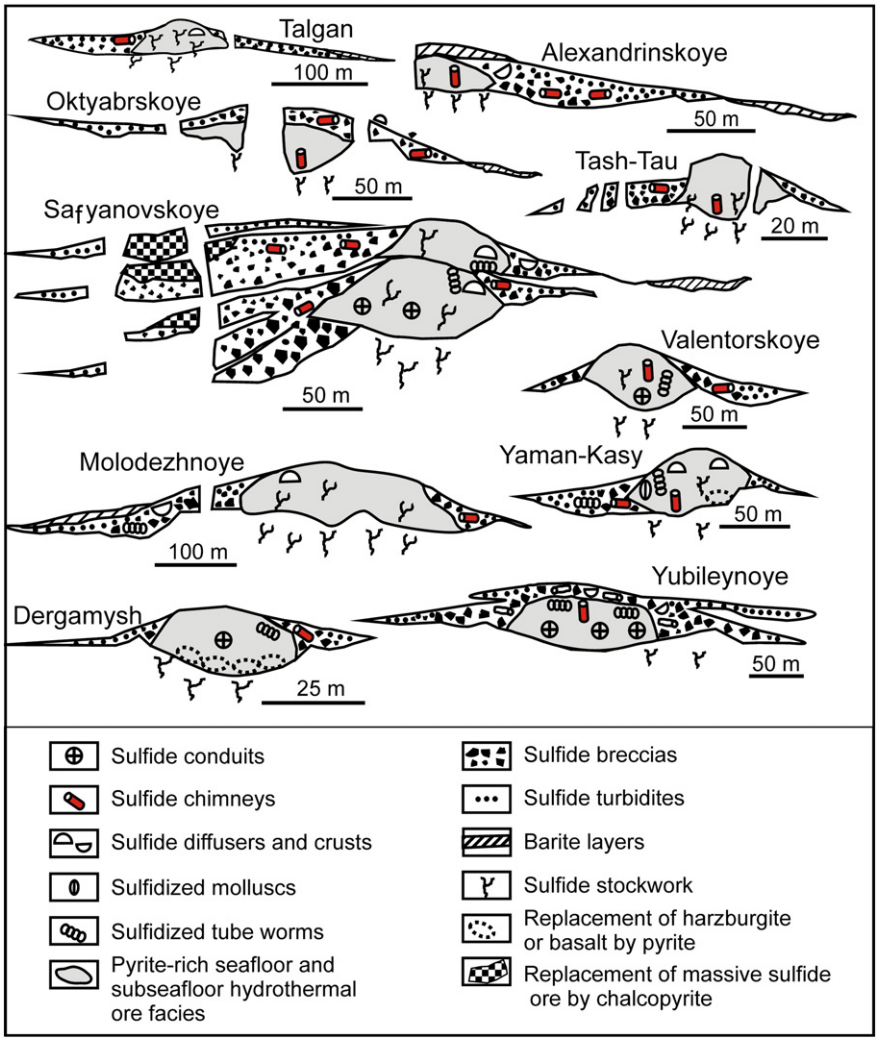

Fig. 3. Position of sulfide chimneys in the ore bodies of the Urals VMS deposits.

At the *Sultanovskoye* deposit, sulfide breccias host abundant small (1–2 cm in diameter) zoned chalcopyrite–pyrite chimneys with minor sphalerite (Figs. 4e, 5e). Fragments of colloform pyrite and sooty pyrite after subhedral pyrrhotite are also widespread. The outer part of zone A is occupied by colloform pyrite and pseudomorphs pyrite and marcasite after subhedral pyrrhotite, which was recrystallized in the inner part of this zone (Fig. 5e). The chalcopyrite of zone B contains rare microinclusions of pyrrhotite, galena, native gold tellurobismuthite (Fig. 6a) and other tellurides (Table 3). The axial parts of the conduits (zone C) are infilled with quartz, subhedral pyrite, marcasite and rarer sphalerite (Fig. 5e).

The *Yubileynoye* deposit yields a range of chalcopyrite–pyrite ± quartz (Figs. 4f, 5f), chalcopyrite–calcite ± talc–pyrite–sphalerite (Figs. 4g, 5g) and sphalerite–pyrite–chalcopyrite (Figs. 4h, 5h) chimneys. In the chimneys, the outermost zone is composed of laminated and botryoidal colloform pyrite and its direction indicates centrifugal growth of botryoids. Toward the inner part of the zone, colloform pyrite becomes more medium-grained. The thickness of zone B decreases from 15 cm to 1 mm in this range of chimneys accompanied by increasing amount of sphalerite and gradual exchange of the telluride minerals to galena–electrum–tennantite assemblage (Fig. 6d, c; Table 3).

At the *Yaman-Kasy* deposit, two ranges of the chimneys are recognized: 1) from chalcopyrite–pyrite (Figs. 4i, 5i) to pyrite–chalcopyrite (Figs. 4j, 5j) and quartz–pyrite–chalcopyrite (Figs. 4k, 5k) varieties; 2) from chalcopyrite–pyrite–sphalerite (Figs. 4l, 5l) to sphalerite–quartz–barite–pyrite–chalcopyrite (Figs. 4m, 5m) varieties (type 3, Fig. 6b). The outer walls of chimneys are composed of laminated, botryoidal or globular colloform pyrite. Pseudomorphic pyrite or marcasite after subhedral pyrrhotite crystals occurs in the central part of this zone. Euhedral pyrite is cemented by chalcopyrite or sphalerite. In this range of chimneys, the thickness of chalcopyrite zone B progressively decreases from 2–10 cm to 1 mm and, in zones A and C, the amount of sphalerite and/or pyrite and quartz and/or barite increases consequently. In the same direction, the altaite–tellurobismuthite, greenockite–coloradoite, sulfoarsenide and arsenide assemblages (Fig. 6d–g) pass to hessite–galena–tennantite assemblage with native gold (Table 3). However, any accessory minerals are out of chalcopyrite–pyrite chimneys as well as in most of modern black smokers (Maslennikov et al., 2009).

At the *Molodezhnoye* deposit, most chimneys belong to the chalcopyrite–pyrite–sphalerite–quartz ± barite (Figs. 4n, 5n) and sphalerite–pyrite–chalcopyrite (Figs. 4o, 5o) varieties which represent the gradual mineral range with consequent increasing amount of sphalerite. In the first variety of the chimney, the outermost part of zone A is composed of the laminated and botryoidal colloform pyrite with interstitial sphalerite, quartz and marcasite. In the second variety, sphalerite-rich outer walls contain no collofrom pyrite. In the middle part of zone A, granular aggregates of pyrite and marcasite enclose rare pseudomorphs

after subhedral pyrrhotite. Altaite and hessite intergrown with galena and tennantite are widespread in chalcopyrite zone B (Fig. 6h). Native gold and arsenopyrite occur in the same zone (Fig. 5n, Table 3). Tenantite and galena versus tellurides are more typical for sphalerite-rich chimneys. The axial part of conduits (zone C) is infilled with pyrite, marcasite, sphalerite and occasional quartz and barite (Fig. 5n, o).

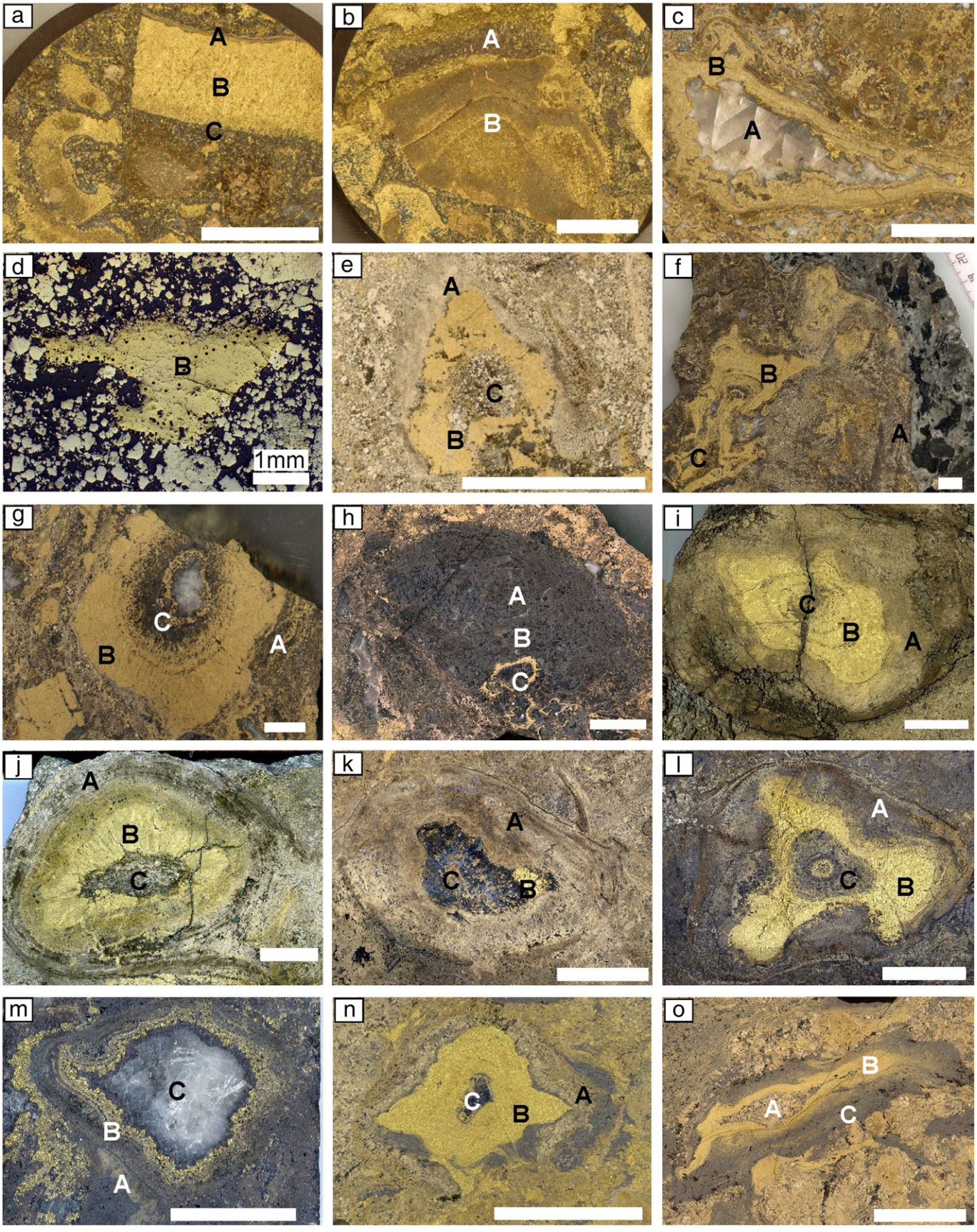

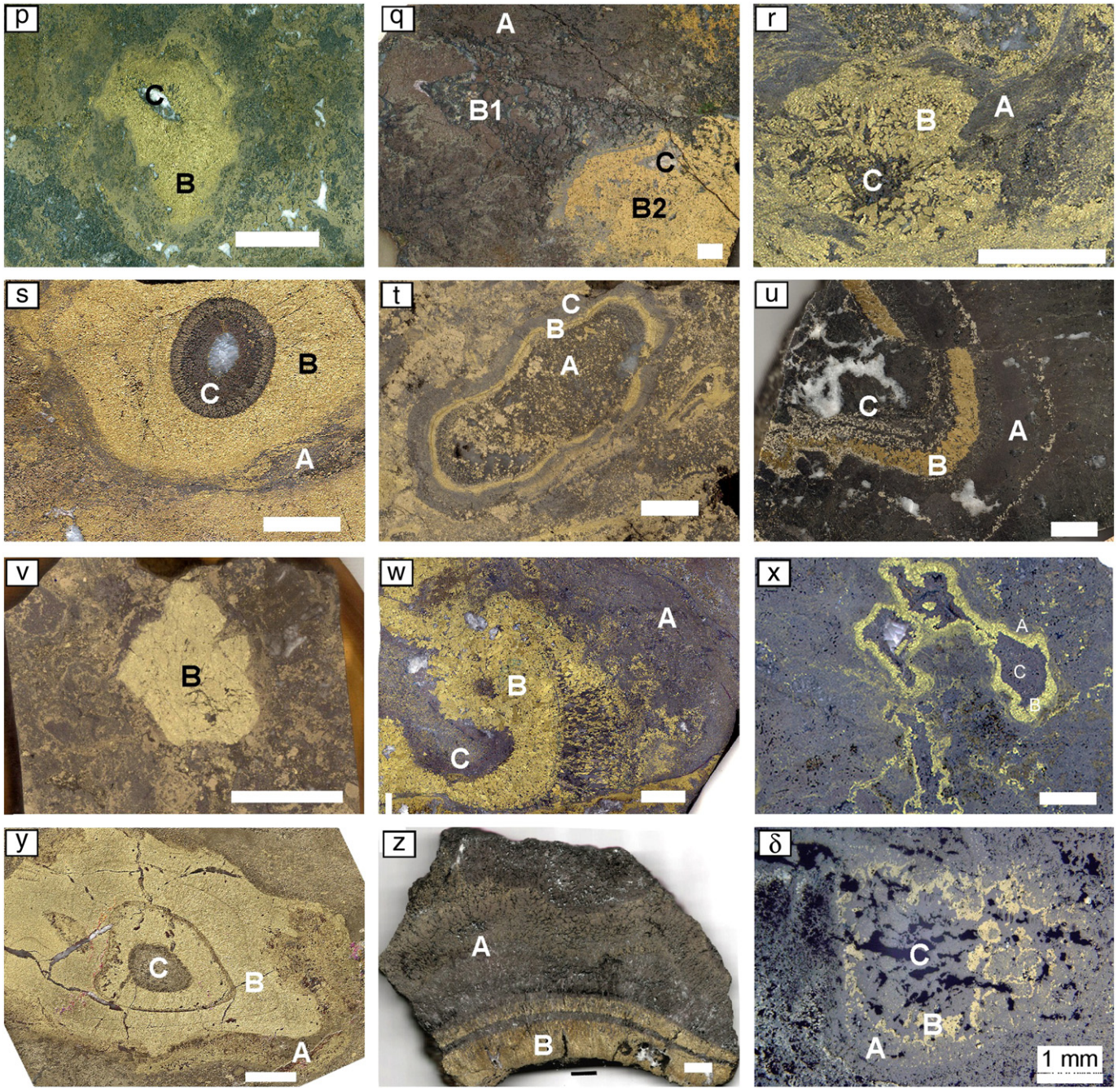

Fig. 4. Chimneys of the Urals VMS deposits: Dergamysh: a – chalcopyrite–pyrite (D13-6-7), b – isocubanite–chalcopyrite–sphalerite–pyrite (D13-6-18), c – calcite-pyrite-chalcopyrite (D-30-60); Buribay: d – chalcopyrite-pyrite chimney fragment of zone B (Bur-14-3); Sultanovskoye: e – chalcopyrite–pyrite–quartz with minor sphalerite (Sult-14-1-8); Yubileynoye: f – chalcopyrite–pyrite–quartz (Yb-12-19), g – chalcopyrite–sphalerite–quartz–pyrite-talc (Yb-12-78), h – sphalerite–pyrite–chalcopyrite (Yb-11-63);Yaman-Kasy: i – chalcopyrite–pyrite (7380-32), j – pyrite–chalcopyrite (YK-2001-189), k – pyrite–quartz–chalcopyrite (YK-SV-47), l – chalcopyrite–pyrite–sphalerite (YK-2001-346), m – sphalerite–quartz–barite–pyrite–chalcopyrite (YK-SV-91); Molodezhnoye: n – chalcopyrite–pyrite–sphalerite (Mol-08-24), o – sphalerite–chalcopyrite–pyrite(Mol-08-13b); Uzelga-4: p – chalcopyrite–pyrite–sphalerite–quartz (Uz-09-1); Uzelga-1: q – sphalerite–chalcopyrite (UZ-15-1); Oktyabrskoye: r – chalcopyrite–sphalerite–pyrite chimney with minor barite and quartz O-886-82); Valentorskoye: s – chalcopyrite–sphalerite–pyrite–quartz (Val-06-51); t – sphalerite–pyrite–chalcopyrite-barite (Val-06-48); Tash-Tau: u – sphalerite–chalcopyrite–calcite with minor pyrite (sample TT-201-1); Talgan: v – chalcopyrite–sphalerite with minor pyrite and barite (Tal-09-1); Alexandrinskoye: w – chalcopyrite–sphalerite with barite (Al-SV-I), x – sphalerite–chalcopyrite–barite (A-SV-19a); Safyanovskoye: h – chalcopyrite–pyrite (Saf-07-a), pyrite–sphalerite–chalcopyrite (Saf-11-101), sphalerite–chalcopyrite (Saf-0691b). Polished samples. A sample number is in brackets. Scale bar is 1 cm.

Chalcopyrite–pyrite–sphalerite–quartz ± barite chimneys are most dominant at the *Uzelga-4* deposit (Figs. 4p, 5p). Colloform pyrite is less abundant and no pseudomorphic pyrite after pyrrhotite occurs in the outer wall of these chimneys in comparison with those from the Molodezhnoye deposit. The galena–tetrahedrite–tennantite assemblage with coloradoite is common in the chalcopyrite of zone B (Fig. 6i).

In the *Uzelga-1* deposit, a sphalerite–chalcopyrite–barite chimney was found in the hanging wall of the sulfide–volcanoclastic breccias (Figs. 4q, 5q). The outer wall of the chimney is composed of sphalerite, barite and calcite with subordinate euhedral and subhedral pyrite. The largest conduits are infilled with chalcopyrite and the smaller ones consist of tetrahedrite. Native gold is associated with galena, hessite and rare petzite (Fig. 6j).

In chimneys from the *Oktyabrskoye* deposit, the outer walls (zone A) are enriched with sphalerite including colloform to subhedral pyrite (Figs. 4r, 5r). Chalcopyrite (zone B) contains no any accessory minerals

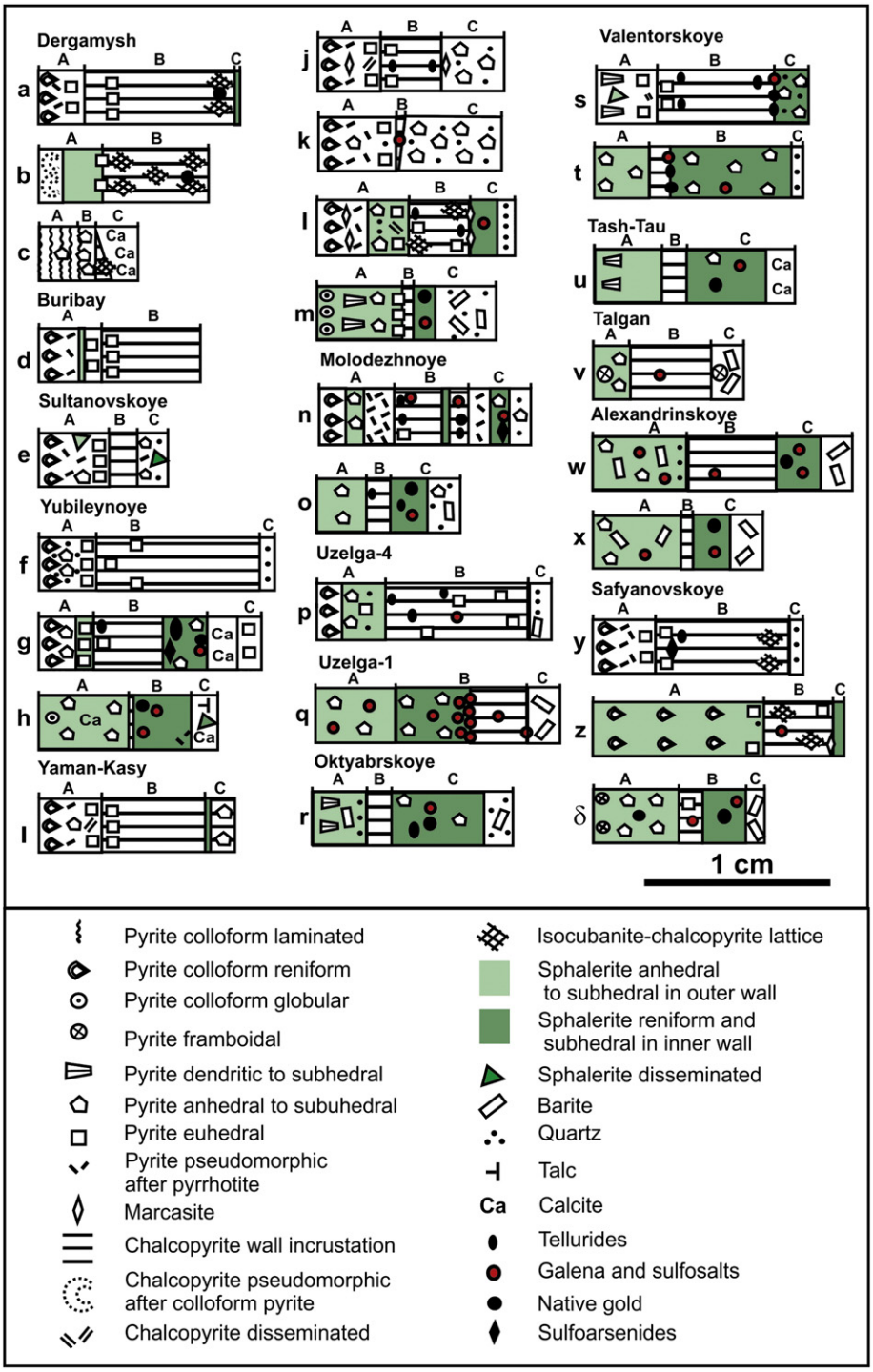

Fig. 5. Wall zonation of chimneys from the Urals VMS deposits. A – external zone – typified by the presence of pyrite, marcasite and/or sphalerite; B – internal zone – typified by the presence of chalcopyrite, C – lining of the axial zone – normally infilled with sphalerite, quartz or barite.

unlike chimneys relating to Uralian type of deposits (Yaman-Kasy, Molodezhnoye). In contrast to chalcopyrite, sphalerite (zone C) encloses altaite, galena and hessite intergrown with native gold and tennantite (Maslennikov et al., 2013).

The *Valentorskoye* deposit yields abundant chalcopyrite–pyrite–sphalerite (Figs. 4s, 5s) and sphalerite–pyrite–chalcopyrite (Figs. 4t, 5t) chimneys. In the outer wall (zone A) of the chalcopyrite–pyrite–sphalerite chimneys, the aggregates of crystalline dendritic pyrite cemented by chalcopyrite occur instead of colloform pyrite. No pseudomorphic marcasite and pyrite after pyrrhotite were found in contrast to chimneys from the Uralian type of deposits. In the first variety of the chimneys, chalcopyrite of zone B contains small inclusions of tellurides including the most abundant rucklidgeite-kochkarite intermediate solid solutions (Maslennikov et al., 2013). In the second variety of the chimneys, native gold in assemblage with tennantite, galena and hessite is abundant in the contacts of chalcopyrite with sphalerite (Table 3).

At the *Tash-Tau* deposit, the gold-rich core of the sulfide mound contains sphalerite–chalcopyrite conduits (Zaykov, 2006) (Figs. 4u, 5u). The chalcopyrite–sphalerite and sphalerite–chalcopyrite chimney fragments are abundant in sulfide breccias. The chimneys contain no

Table 3
The mineral composition of hydrothermal chimneys of the Urals VMS deposits.

Deposits	Chimney type		**Major**, subordinate and *minor* minerals
Dergamysh	Cu-Fe	bs	**Cp** > **Pyc,s,e,p,f,** marcasite, isocubanite, *calcite, pyrrhotite, electrum, arsenopyrite, Co-pyrite, Sn-Cu-Fe-sulfide unresolved, cassiterite*
	Cu-Zn	gs	**ISS** > **Cp** > **Sp**> > **Py-e,** *electrum, calcite, Co-pyrite, cassiterite*
	Fe-Ca-Cu	cs	**Py-c,f,s,p** > **Ca**> > **Cp**> > **Sp**
Buribay	Cu-Fe ± Zn		**Cp** > **Pyc,s,e,p**> > **Sp**
Yubileynoye	Cu-Fe	bs	**Cp** > **Pyc,s,e,p** quartz, *pyrrhotite, tellurobismuthite*
	Cu-Fe-Zn	gs	**Pyc,s,e = Cp = Sp, talc, calcite,** *arsenopyrite, tellurobismuthite, coloradoite, hessite, native gold, tennantite, electrum, galena*
	Zn-Fe-Cu	ws	**Sp** > **Pyc,s,e,p**> > **Cp,** calcite, talc, *electrum, tennantite, galena*
Sultanovskoye	Cu-Fe ± Zn	bs	**Cp ≥ Pyc,s,e,p**> > **Sp**, marcasite, isocubanite, quartz, *pyrrhotite, tellurobismuthite, tsumoite, coloradoite, hessite, galena, native gold*
Molodezhnoye	Cu-Fe-Zn	gs	**Pyc,s,e,p ≥ Cp ≥ Sp**, marcasite, quartz, barite**,** *altaite, hessite, tennantite, native gold, arsenopyrite, cobaltite(?), galena, barite, tennantite*
Uzelga-4	Cu-Fe-Zn	gs	**Cp** > **Pyc,s,e** > **Sp,** marcasite, barite, *coloradoite, hessite, tennantite-terahedrite, native gold*
Uzelga-1	Zn-Cu	ws	**Sp** > **Cp** > **Pye,s,** barite, calcite, *hessite, tennantite-terahedrite, native gold*
Yaman-Kasy	Cu-Fe	bs	**Cp = Py**> > **Sp**
	Fe-Cu		**Py** > **Cu**, marcasite, *frohbergite, cobaltite, hessite coloradoite, sylvanite*
	Fe ± Cu		**Pyc,s,e,p** > **Q**> > **Cp,** marcasite, *tetrahedrite, tennantite, bornite, digenite*
	Cu-Fe-Zn	gs	**Pyc,s,e,p = Cp** > **Sp,** isocubanite, marcasite, quartz, *altaite, galena, loellingite, sylvanite, cobaltite, hessite coloradoite, volynskite, tennantite, goldfieldite, native gold, pyrrhotite, barite*
	Zn-Fe-Cu	ws	**Sp** > **Pyc,s,e** > **barite** > **Cp**, quartz, *tennantite, galena, hessite, magnetite*
Talgan	Cu-Zn-Fe	ws	**Cp** > **Sp** > **Pyf,e,** *tennatite, magnetite*
Oktyabrskoye	Zn-Cu-Fe	gs	**Sp** > **Cp** > **Pys,e,c,** quartz, barite, hessite, altaite, tennantite, native gold
Valentorskoye	Cu-Zn-Fe	gs	**Cp** > **Sp** > **Pys,e,c**, quartz, *rucklidgeite-kochkarite, hessite, native gold, petzite, sylvanite, tennantite, galena*
Tash-Tau	Zn-Cu ± Fe	ws	**Cp ≥ Sp** > **Pye,s,a,** bornite, tennantite, *galena, quartz, native gold*
Alexandrinskoye	Zn-Cu	ws	**Cp** > **Pye,s,a** > **Sp** barite, galena, tennantite, bornite, *hessite, native gold*
Safyanovskoye	Cu-Fe ± Zn	bs	**Cp** > **Pye,s,a** > **Sp,** marcasite, *glaucodot, arsenopyrite, tetrahedrite, tennantite, Bi-tellurides, hessite*
	Cu-Fe-Zn	gs	**Cp ≥ Py** > **Sp, barite, quartz,** marcasite, barite, *native gold, stannoidite*, mawsonite, quartz, *enargite*
	Zn-Cu	ws	**Sp** > **Cp** > **Pye,s,a,** galena, *native gold, tennantite-tetrahedrite, barite*

The table presents original data with the addition of Herrington et al. (1998), Maslennikova and Maslennikov (2007), and Maslennikov et al. (2009; 2013). Cp – chalcopyrite, ISS – isocubanite; Sp – sphalerite, Py – pyrite: c – colloform, f – framboidal, p – pseudomorphic after pyrrhotite, e – euhedral, s – subhedral, a – anhedral. Supposed color of the smokers: bs – black, gs – grey, ws – white (greyish), cs – clear.

colloform pyrite and pseudomorphic pyrite after pyrrhotite. Chalcopyrite and sphalerite of chimneys host inclusions of euhedral pyrite, native gold, galena and galena (Table 3).

At the *Talgan* deposit, fragments of the chalcopyrite–pyrite–shalerite chimneys were found in sulfide breccias (Figs. 4v, 5v). The outer wall of chimneys consists of framboidal and euhedral pyrite cemented by sphalerite. Galena–tennantite assemblage with magnetite and sphalerite inclusions occurs in chalcopyrite zone B (Table 3). Axial conduits are infilled with framboidal pyrite and barite (Fig. 5v).

At the *Alexandrinskoye* deposit, the chalcopyrite–sphalerite–barite (Fig. 4w, 5w) and sphalerite-barite-chalcopyrite (Figs. 4x, 5x) chimneys are dominant varieties. Their outer wall consists of major sphalerite with disseminated euhedral and subhedral pyrite. Rare colloform, dendritic crystalline or framboidal pyrite is typically replaced by chalcopyrite. Barite, quartz, galena and tennantite inclusions are common in all zones. Dendritic intergrowths of sphalerite and chalcopyrite occur in zone C. In some chimneys, sphalerite in the chimneys hosts bornite with latticed chalcopyrite. Native gold was found in sphalerite of the chimney conduit in assemblage with galena and tennantite (Fig. 6k). Hessite is a very rare mineral in sphalerite of axial conduits (Maslennikov et al., 2013).

At the *Safyanovskoye* deposit, the chimneys include three varieties: 1) chalcopyrite–pyrite (Figs. 4y, 5y); 2) pyrite–sphalerite–chalcopyrite (Figs. 4z, 5z) and 3) sphalerite-rich with subordinate chalcopyrite (Figs. 4δ, 5δ). The outer zones of pyrite-rich chimneys are made up of botryoidal colloform, framboidal and dendritic pyrite. Rare primary tabular–hexagonal pyrrhotite crystals are replaced by non-stoichiometric cryptocrystalline or fine-grained pyrite in the central parts of the outer walls of chalcopyrite–pyrite and pyrite–sphalerite–chalcopyrite chimneys. In the innermost parts of the outer wall, the fine-grained pyrite was recrystallized to euhedral crystals cemented by chalcopyrite or sphalerite. The outer wall of sphalerite-rich chimneys contains no colloform pyrite. Sphalerite encloses inclusions of euhedral pyrite, barite and galena. The relative amount of chalcopyrite (zone B) decreases in this chimney range. In the same direction, sphalerite and barite substitute quartz and pyrite in the axial part of conduits. Chalcopyrite in chalcopyrite–pyrite chimneys hosts no accessory minerals except for glaucodot and hessite, partly replaced by tennantite (Fig. 6l). In some pyrite–sphalerite–chalcopyrite chimneys, galena, enargite, stannoidite and mawsonite occur in chalcopyrite zone B (Fig. 6m). Galena, tennantite and native gold are typical minerals in sphalerite of sphalerite-rich chimneys (Table 3).

4.1.2. Chimneys of the modern vent sites

The studied modern vent sites with chimneys occur in a various geological setting of the Pacific and Atlantic oceans. In Atlantic Ocean, the black and clear smokers were collected from the serpentinite-hosted *Rainbow* vent site (Bogdanov et al., 2015). The outer walls (zone A) of some active chalcopyrite-rich black smokers from this site are made up of anhydrite with disseminated chalcocite, digenite, bornite and rare pyrrhotite (Fig. 7a). Digenite and chalcocite in assemblage with magnetite are followed by bornite toward the inner part of the outer wall. The inner wall of the conduit is incrusted by chalcopyrite. The outer part is partly replaced by bornite, while the inner part of zone B contains Y-phase $Cu_2Fe_3S_5$ (Borodaev et al., 2004; Mozgova et al., 2008). Diverse Co-Ni-As-Te-Au rare mineral assemblages (Table 4) occur in assemblage with bornite veinlets in chalcopyrite (Mozgova et al., 1996, 2008; Vikentyev et al., 2000; Lein et al., 2003; Bortnikov et al., 2004; Bortnikov and Vikentyev, 2005; Marques et al., 2007; Fouquet et al., 2010; Bogdanov et al., 2015). Sphalerite and pyrrhotite crystals are abundant in the outer and inner walls of clear smokers (Fig. 7b). The outer walls of some clear smokers are covered by colloform pyrite or Ca–Fe–Mn carbonate and laminated iron hydroxide crusts (Borodaev et al., 2004).

In the *Logachev* vent sites, chalcopyrite-rich black smokers are widespread. The outer wall of a studied chimney fragment displays relic texture of colloform pyrite and pyrrhotite replaced by chalcopyrite. Bornite inclusions occur in chalcopyrite zone B (Fig. 7c).

In *EPR 9°50′N*, the black smokers were collected during initial stage of hydrothermal activity on the fresh lava flows (Bogdanov et al., 2006a). The chimneys display a typical mineral zonation (Graham et al., 1988). The presence of an outer hematite and anhydrite wall with minor bornite and chalcopyrite in the inner wall is the characteristic feature of immature black smoker vents (Fig. 7d). In mature black smokers, anhydrite is eventually dissolved in ambient cold seawater (Haymon, 1983). The outer walls of most mature black smokers are overgrown by crusts of colloform pyrite (Fig. 7e). Pyrrhotite is also abundant in some black smokers, but, in older chimneys, it tends to be replaced by marcasite and pyrite. Rare mineral assemblages are not common for the black smokers (Table 4).

Active black smokers were collected in the *Broken Spur* vent site (Mid-Atlantic Ridge) (Bogdanov et al., 2008). The black smoker

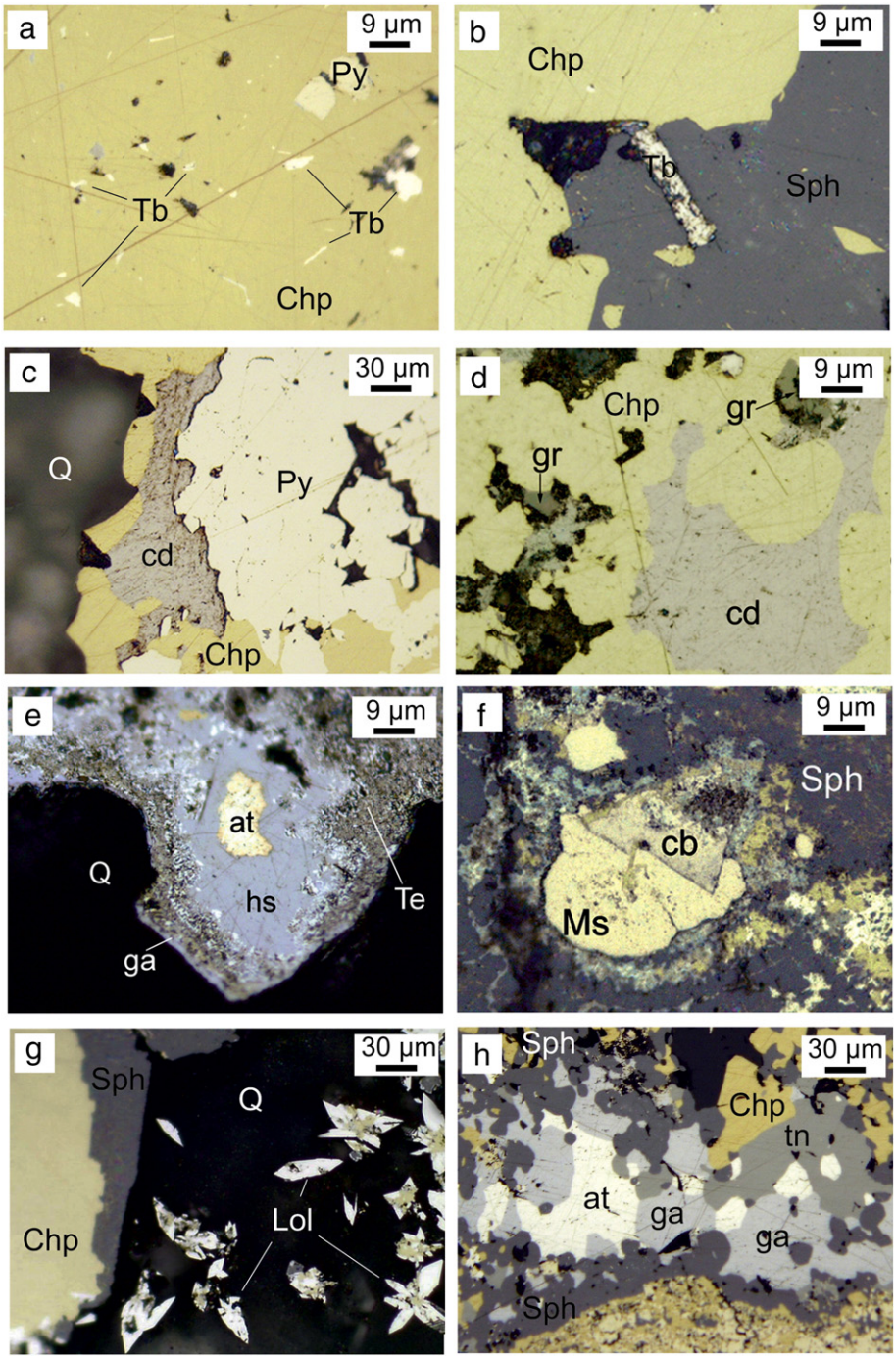

Fig. 6. Accessory minerals in chimneys from the Urals VMS deposits. a – inclusions of tellurobismuthite (Tb) in chalcopyrite (Chp) of zone B (Sultanovskoye); b – tellurobismuthite crystal at the boundary of subhedral chalcopyrite (zone B) and sphalerite (Sph) of zone C (Yubileynoye); c – coloradoite (cd) at the chalcopyrite and pyrite (Py) boundary of zone B (Yubileynoye); d – greenockite (gr) and coloradoite of zone B (Yaman-Kasy); e – successive intergrowths of altaite (at), hessite (hs), native tellurium (Te), galena (ga) at the boundary of zones B and C (Yaman-Kasy); f – cobaltite (cb) overgrowing by marcasite (Ms) in sphalerite at the boundary of zones B and C (Yaman-Kasy); g – euhedral loellingite (Lol) in quartz (Q) in assemblage with sphalerite and chalcopyrite at the boundary of zones B and C (Yaman-Kasy); h – intergrowths of altaite, galena, tennantite (tn), chalcopyrite and sphalerite of zone C (Molodeznnoye); i – intergrowths of coloradoite, galena, tennantite, sphalerite and quartz of zone C (Uzelga-4); j – intergrowths of native gold (Au), hessite and galena in tennantite of zone B (Uzelga-1); k – intergrowths of native gold, tennantite and galena in sphalerite at the boundary of zones B and C (Alexandrinskoye); l – replacement of glaucodot (gld) by tennantite in chalcopyrite of zone B (Safyanovskoye); m – intergrowths of stannoidite (sta) and mawsonite (maw) in chalcopyrite of zone B (Safyanovskoye); n – tellurobismuthite and hessite at the boundary of chalcopyrite and tennantite of zone B (PACMANUS). Reflected light.

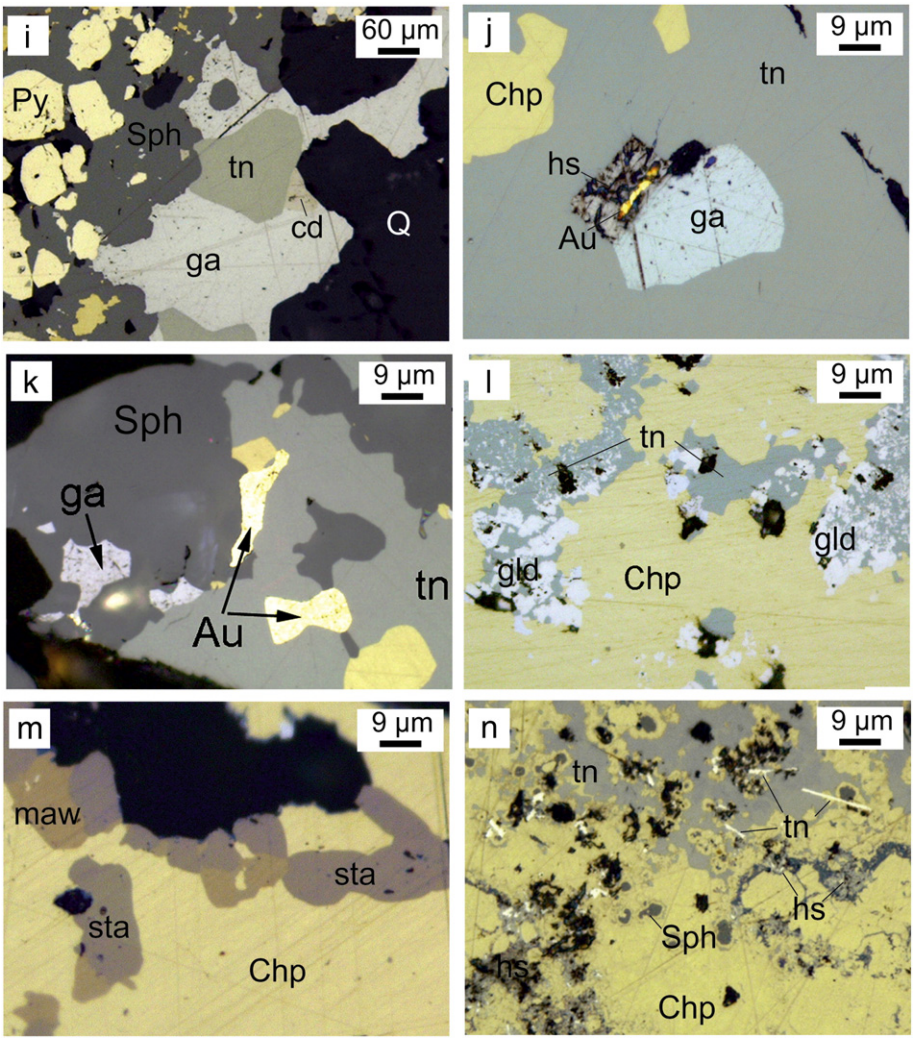

Fig. 6 (*continued*).

chimneys are similar to chimneys from EPR 9°50′N vent site except for abundant bornite and digenite at the boundaries of the chalcopyrite wall (Fig. 7f). The presence of bismuth tellurides in euhedral pyrite of the outer wall of some chimneys is detected by LA-ICP-MS (Table 4).

In outer wall of chalcopyrite-rich black smokers collected in the *Snake Pit* vent site (Mid-Atlantic Ridge) (Bogdanov et al., 2006b), outer walls are characterized by abundant colloform and dendritic pyrite, subhedral pyrrhotite, partly replaced by marcasite and euhedral pyrite in sphalerite and chalcopyrite intergrowths (Fig. 7g). Chalcopyrite and γ-phase $Cu_2Fe_3S_5$ form zone B. Dendritic pyrite is overgrown by marcasite and subhedral pyrite is typical of the outer walls of the sphalerite-rich clear smokers (Bogdanov et al., 2006b) (Fig. 7h). In both smoker types, the accessory minerals are rare similar to the smokers from EPR 9°50′N. The exceptions are rare small inclusions of native gold, cobaltite, and realgar detected by EPMA (Table 4).

The chimneys from instinct vent site of the *Galapagos Center* are similar to black smokers of EPR 9°50′N except for occurrence of pyrrhotite (Fig. 7i). In other vent sites of the Pacific (Galapagos Center, Axial Seamount) and Atlantic (Lucky Strike, Menez Gwen) MOR influenced by hot spots, the chimneys are distinct from typical black smokers of other parts of the MORs. First, they contain barite in the outer walls or inner channel (Fig. 7j–l). In these chimneys, pyrrhotite is largely absent except for its minor amount in the sphalerite-rich active grey smokers of *Axial Seamount* collected by I. Jonasson (Fig. 7j, Table 4). In sphalerite–pyrite–chalcopyrite–barite chimneys of Axial Seamount, Pb–Sb–As sulfosalts were found (Bogdanov et al., 2006b). Active chalcopyrite–pyrite-rich black smokers of the *Lucky Strike* vent site (Bogdanov et al., 2006b) lack rare minerals like to black smokers from EPR 9°50′N. Inclusions of native gold and tennantite were revealed by SEM in the barite–chalcopyrite-rich chimney fragments collected from sulfide–barite breccias of the *Menez Gwen* vent site (Lein et al., 2010; Fig. 7l). The grey smoke of inactive chimneys could be supposed due to specific mineral composition which is similar to grey smokers at the West Pacific island intra-arc basins.

At the flank of inactive *MIR vent site* (TAG field, Atlantic Ocean), Yu.A. Bogdanov collected the Au-rich chimney fragments, which are distinct from smokers related to different vent sites of MORs. The outer chimney wall, as usual, shows successive change from colloform to granular pyrite toward the inner part (Fig. 7m). At the boundary with zone B, sphalerite, barite and bornite are widespread (Table 4) with interstitial inclusions of native gold. This is probably chalcopyrite-rich analog of grey or white smokers located at the main TAG mound (Bogdanov et al., 2006a).

Samples from the West Pacific back-arc basins include two varieties of sphalerite-rich clear smokers. These chimneys emanate shimmering fluids at the seazed stage typical of diffusers (Bogdanov et al., 2006a). At the *Vienna Wood* and *Northern Lau* vent sites, the first variety contains barite (Fig. 7n, o; Table 4). Invisible native gold is detected in opal of the Vienna Wood chimney by LA-ICP-MS analyses. At the *Central Lau*, the second variety comprises subhedral pyrrhotite and isocubanite instead of chalcopyrite (Fig. 7p; Table 4) and is probably similar to clear smokers described in MOR-related vent sites (Bogdanov et al., 2006b).

Dacite-hosted chimneys from the Suiyo volcano at the Izu-Ogasawara arc, PACMANUS vent site of the Pual Ridge, Eastern Manus, Suzette vent site from the SuSu Knoll and Hakurei vent site from the Okinawa Trough show distinct mineral characteristics.

At *Suiyo* volcano, the chalcopyrite-rich chimneys of black and grey smokers are widespread (Watanabe and Kajimura, 1994; Ishibashi and Urabe, 1995; Marumo et al., 2008). The studied sample of black to grey chalcopyrite–pyrite smokers was presented by T. Urabe. In general, the chimney is similar to chalcopyrite–pyrite black smokers of MORs except for abundant galena and tennantite, the occurrence of realgar and orpiment and absence of pyrrhotite (Fig. 7q, Table 4). It is suggested, that this chimney belongs to dark grey smokers rather than to MOR-type black smokers.

The *PACMANUS* is a vent site with abundant active grey and white smokers (Reeves et al., 2011; Monecke et al., 2016). Galena, tennantite, enargite, native gold and sulfur are common in chimneys from this site (Moss and Scott, 2001; Petersen et al., 2003). The samples of chalcopyrite-rich (Fig. 7r) and sphalerite–barite-rich (Fig. 7s) chimneys from the PACMANUS (Solwara-4) site presented by M. Gibbson (Nautilus Company) are supposed to be grey and greyish white smokers, respectively. The chalcopyrite-rich chimneys host fine inclusions of tellurobismuthite, hessite, native tellurium and gold in assemblage with tennantite and bornite. Galena, tennatite and Pb–As–Sb sulfosalts are abundant in sphalerite–barite-rich chimney (Table 4). At the *Suzette* vent site, the inactive sphalerite–barite–chalcopyrite chimney is similar by mineral zonation to typical greyish white smoker (Fig. 7t).

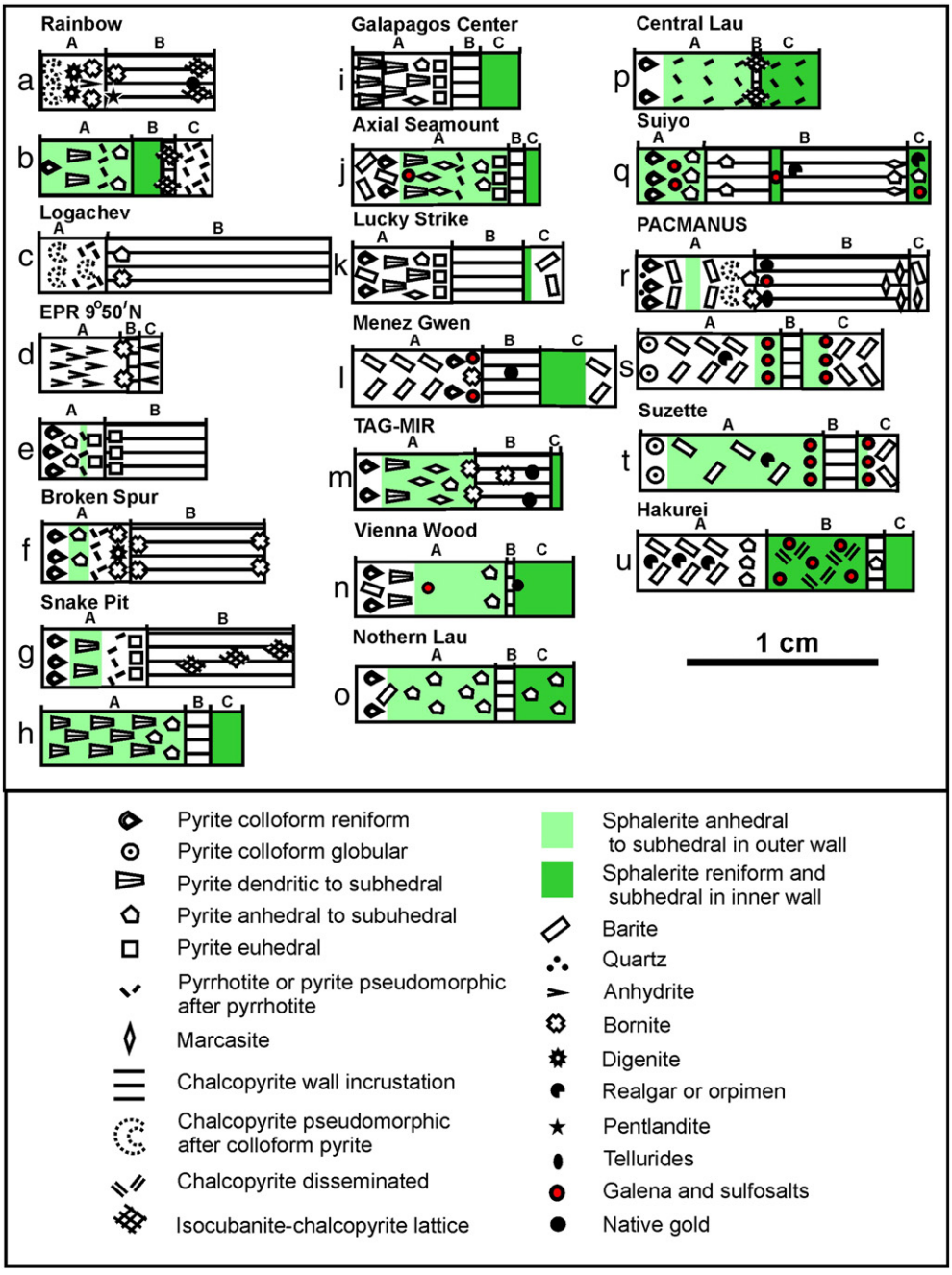

Fig. 7. Wall zonation of chimneys of modern smokers. A – external zone – typified by the presence of pyrite, marcasite and/or sphalerite; B – internal zone – typified by the presence of chalcopyrite, C – lining of the axial zone – normally infilled with sphalerite, quartz or barite.

Black, grey, white and clear smokers are widespread in several vent sites of the Okinawa Trough (Kimura, 1990; Sakai et al., 1990; Halbach et al., 1993; Marumo and Hattori, 1997; Glasby and Notsu, 2003; Gena et al., 2005). The fragment of the active sphalerite-rich diffuser or clear smoker from the *Hakurei* vent site was presented for study by T. Urabe. The outer wall of the chimney consists of barite and abundant realgar and orpimen (Fig. 7u; Table 4). Numerous small conduits of the chimney are infilled with detritic overgrowths of sphalerite, tetrahedrite and chalcopyrite with galena.

In general, galena, tennantite, Pb–As–Sb sulfosalts, native gold, orpiment and realgar were found in most chimneys hosted by dacites (Monecke et al., 2016). Meanwhile, these minerals can also be found in the vent sites of the Mid-Atlantic Ridge (Table 4).

4.2. Trace elements in major sulfides of chimneys

4.2.1. Chalcopyrite

4.2.1.1. Se–Te. Chalcopyrite from the chalcopyrite–pyrite chimneys of the *Dergamysh* deposit is characterized by high contents both of Se (429–517 ppm) and Te (67–114 ppm), which are comparable to those of the modern black smokers associated with serpentinites (Tables 5, 6). Contents of these elements are lower in chalcopyrite from the calcite–pyrite-chalcopyrite chimneys and diffusers: Se (76–268 ppm) and Te (0.03–0.9 ppm). The positive correlation between Se and Te is not as clear as in chalcopyrite of the modern black smokers (Fig. 8a).

The high Se contents in chalcopyrite from the chalcopyrite–pyrite chimneys of the *Buribay* (2685 ppm), *Yubileynoye* (up to 780 ppm) and *Sultanovskoye* (up to 688 ppm) deposits are slightly below than those from typical MOR modern black smokers associated with basalts (Fig. 8b, c). The Se/Te ratio (0.6–29) of most chalcopyrite samples from the Sultanovskoye deposit and some samples from the Yubileynoe deposit is lower than that of chalcopyrite from the modern black smokers (14–78,837) and is related to microinclusions of rare tellurides. The Se (20–206 ppm) and Te (1–186 ppm) contents in chalcopyrite from the calcite–talc–sphalerite–pyrite–chalcopyrite chimneys of the Yubileynoe deposit most likely correspond to those in chalcopyrite of the barite–chalcopyrite chimneys of the felsic-associated modern grey smokers from the West Pacific. Chalcopyrite from the sphalerite–pyrite chimneys of the Yubileynoe deposit is characterized by the lowest Se (1–10 ppm) and Te (0.01–0.1 ppm) contents, which are typical of modern white smokers or clear diffusers. In general, chalcopyrite from the chimneys of the Buribay, Yubileynoe and Sultanovskoye deposits retains the Se–Te correlation, which is characteristic of chalcopyrite from the MOR black smokers (Fig. 8b, c).

The Se contents (106–2153 ppm) in chalcopyrite from chimneys of the *Molodezhnoye* and *Uzelga-4* deposits are similar to those of chalcopyrite from the modern black smokers (Tables 5, 6; Fig. 8d). In terms of Se and Te contents, chalcopyrite from the pyrite–chalcopyrite and sphalerite–pyrite chimneys of the *Yaman-Kasy, Oktyabrskoye* and *Valentorskoye* deposits lie between black and grey smokers (Fig. 8e, f). Chalcopyrite of the sphalerite- , pyrite-, quartz- and barite-rich chimneys is characterized by the lower Se content (5–17 ppm) and higher Te content (34–1613 ppm) due to the presence of microinclusions of hessite or Ag-bearing tennantite. This variety of chimneys is comparable with modern white smokers, probably (Maslennikov et al., 2009).

At the *Tash-Tau* deposit, the low contents of Se in chalcopyrite are slightly declined in the range from chalcopyrite-rich to sphalerite-rich chimneys independently on Te contents (Fig. 8f) The Te content in chalcopyrite from the sphalerite–chalcopyrite chimneys of the *Tash-Tau* deposit is lower than that of chalcopyrite of the Yaman-Kasy, Oktyabrskoye and Valentorskoye chimneys (Table 5; Fig. 8e, f). The

Table 4
Mineral composition of hydrothermal chimneys of the vent sites studied.

Vent site		Chimney type	**Major**, subordinate and *minor* minerals
Rainbow	bs	Cu ± Ca	**Cp** > **Bo** > **Di** > **An,** isocubanite, magnetite, pyrrhotite, wurtzite–sphalerite, goethite, *opal, quartz, barite, native gold, electrum, Co-pentlandite, stannite, safflorite–löllingite, $Cu_2Fe_3S_5$ phase, millerite, acantite, atacamite, molibdenite, melonite, chalcocite-covellite group*
	cs	Zn-Cu-Fe	**ISS** > **Cp** > **Wu** > **Po** > **Py$_{c,a,e}$, marcasite,** *electrum, cassiterite, calcite, galena, tennantite,* goethite
Logatchev	bs	Cu	**Cp**> > **Py$_{e}$,** bornite, pyrrhotite**,** *sphalerite*
EPR 9°11′ N	bs	Cu-Fe ± Zn	**Cp** > **Py$_{c,s,e,p}$**> > **Sp,** wurtzite, pyrrhotite, *galena*
Axial Seamount	gs	Zn-Ba-Fe-Cu	**Sp**> > **Ba** > **Py$_{c,a,e}$** > **Cp**, pyrrhotite, iordanite, galena
Galapagos Ridge	gs	Fe-Cu-Zn	**Py** > **Ms.** > **Cp** > **Sph,** *chalcocite-covellite group, tellurobismuthite***
Broken Spur	bs	Cu-Zn-Fe	**Cp** > **Sp** > **Bo** > **Py$_{c,p,a,s,e}$, anhydrite,** isocubanite, marcasite, opal, quartz, aragonite, $Cu_5Fe_3S_5$ phase, digenite, pyrrhotite, minerals of the chalcocite–covellite series, *magnetite, hematite, goethite, galena, realgar*, jordanite-geocronite, tellurobismuthite***
Snake Pit	bs	Cu-Fe-Zn	**Cp** > **Py** > **Sp**, marcasite, pyrrhotite, isocubanite, cobaltite*, realgar*, minerals of the chalcocite–covellite series, native gold, bornite, atacamite, talc, calcite, hematite, anhydrite, quartz,
	cs	Zn-Cu-Fe	**Sp** > **Py** > **Ms.** > **Cp,** *jordanite-geocronite, tennantite, galena*
TAG-MIR	ws	Fe-Cu-Zn	**Py** > **Cp** > **Sp,** opal, goethite, barite, native gold, digenite, bornite, tennantite
Lucky Strike	bs	Cu-Fe ± Zn	**Sp** > **Py**> > **Sp**, marcasite, barite
Menez Gwen	gs	Ba-Cu-Zn-Fe	**Ba** > **Cp** > **Sp** > **Py$_{a,c,e}$,** native gold, tennantite
Northern Lau	cs	Zn-Fe-Cu	Sp > Py$_{c,s}$> > Cp, marcasite, bornite, barite
Central Lau	cs	Zn-Fe-Cu	**Cp** > **Po** > **Pya,s,c** > **ISS**
Vienna Wood	cs	Zn-Fe-Cu	**Spp** > **Op** > **Py$_{c,s}$** > **Cp,** marcasite, *proustite–pyrargirite, stephanite, native gold*
Suiyo volcano	bgs	Cu-Fe ± Zn	**Cp** > **Py$_{c,a,e}$** > **Sp,** opal, barite, *orpimen, realgar, native gold, mimetite, tennantite, galena*
PACMANUS	gs	Cu ± Fe ± Zn	**Cp** > **Py$_{c,s,e,f}$** > **Sp** > **Ba,** marcasite, bornite, digenite, *galena, native gold, tellurobismuthite*, native tellurium*, hessite**
	ws	Ba-Zn-Fe-Cu	**Ba** > **Sp** > **Py$_{c,e,s,f}$**> > **Cp,** marcasite, galena, native gold, tennantite, jordanite–geocronite
Suzette	ws	Ba-Zn-Fe-Cu	**Ba** > **Sp** > **Py**> > **Cp,** marcasite, galena, native gold
Hakurei	cs	Zn-Ba-Fe-Cu	**Sp** > **Ba** > **Cp** > **Py,** marcasite, realgar, orpimen, tetrahedrite, *native gold*

Table presents original data and data from Detrick et al. (1986), Hannington and Scott (1988), Hannington et al. (1991), Shadlun et al. (1993), Duckworth et al. (1995), Mozgova et al. (1996), Scott (1997), Petersen et al. (2003), Vikentyev (2004), Borodaev et al. (2004), Lein et al. (2010), Binns (2014), Bogdanov et al. (2015), Fouquet et al. (2010), and Monecke et al. (2016). The reference include data on color of the smokers: bs – black; gs – grey; ws – white (greyish white); cs – clear; bgs – black or grey. Cp – chalcopyrite, ISS – isocubanite; Sp – sphalerite, Po – pyrrhotite; Bo – bornite; Ba – barite; Py – pyrite: c – colloform, f – framboidal, p – pseudomorphic after pyrrhotite, e – euhedral, s – subhedral, a – anhedral.* and ** – the first finding by SEM and LA-ICP-MS, respectively (Institute of Mineralogy, UB RAS).

Table 5
Average contents of trace elements in chalcopyrite of chimneys from the Urals VMS deposits (LA-ICP-MS, ppm).

Dep	CH	SM	n/sd	Co	Ni	Zn	As	Se	Mo	Ag	Sn	Sb	Te	W	Au	Pb	Bi
Der	Cu-Fe	bs	39	3970	173	4849	80	541	1.7	33	43	38	83	0.01	4.0	165	11
			sd	4463	194	4591	108	185	3.0	22	23	46	38	0.02	7.3	145	13
Der	Cu-Zn	gs	30	5237	568	63,343	29	464	8.4	47	46	55	122	0.01	8.2	416	435
			sd	3861	600	58,522	21	86	9.0	43	39	41	86	0.02	31.1	269	413
Der	Fe-Ca-Cu	cs	23	19	18	531	0.6	184	0.2	6.0	126	12	0.02	0.07	0.02	7.9	0.03
			sd	39	64	772	1.1	51	0.4	12	55	27	0.03	0.13	0.01	8.2	0.13
Bur	Cu-Fe ± Zn	bs	25	1.2	2.6	1316	3.5	1536	651	89	4.0	10	75.3	0.02	1.3	168	2.7
			sd	0.8	3.8	3396	2.8	556	819	91	0.3	7.6	75	0.02	0.9	110	3.1
Sult	Cu-Fe ± Zn	bs	56	61	1.6	8170	73	510	112	197	44	29	502	0.04	6.9	3552	124
			sd	202	4.9	15,351	166	375	205	368	70	30	647	0.08	18	6380	101
Yub	Cu-Fe	bs	41	0.01	0.1	264	2.7	114	3.8	60	24	3.2	21	0.3	0.4	66	1.0
			sd	0.01	0.2	177	2.6	63	16	69	7.3	3.1	46	0.6	0.4	293	2.0
Yub	Cu-Fe-Zn	gs	40	2.0	0.4	238	4.0	416	11	8.6	10	6.6	12	4.4	0.3	16	5.8
			sd	7.4	1.2	303	10	245	32	8.6	4.0	7.6	25	17	0.3	12	10
Yub	Zn-Fe-Cu	ws	28	0.04	0.1	438	3.0	20	0.8	14	22	2.0	0.6	0.01	0.2	21	0.05
			sd	0.04	0.3	489	10	7.7	2.4	11	6.5	2.1	0.5	0.02	0.1	21	0.12
Mol	Cu-Fe-Zn	gs	48	311	1.4	5255	813	499	6.3	138	225	48	3381	5.6	7	12,327	79
			sd	412	2.6	15,435	1054	470	13	209	850	49	7140	30	9	23,490	152
Uz-4	Cu-Fe-Zn	gs	20	1.8	3.2	531	21	731	5.2	158	23	6	207	0.06	1.5	4138	3.7
			sd	7.9	14	1475	54	449	21	354	5.1	21	519	0.14	4.8	5187	4.0
Uz-1	Zn-Cu	ws	64	0.8	0.1	3186	26	120	4.7	7.6	55	25	6.4	0.02	0.05	57	0.02
			sd	1.7	0.3	24,507	91	59	11	17	248	104	45	0.08	0.14	284	0.08
Tal	Cu-Zn-Fe	ws	6	0.09	0.1	118	20	21	105	14	11	13	1.3	0.06	0.07	175	31
			sd	0.12	0.2	23	15	10	255	9.0	1.6	22	0.9	0.05	0.10	263	66
YK	Cu-Fe	bs	17	0.10	0.2	1765	12	103	0.06	7.0	107	38	27	0.04	0.16	42	0.13
			sd	0.09	0.1	1407	12	53	0.11	3.8	87	34	14	0.05	0.15	21	0.25
YK	Cu-Fe-Zn	gs	96	118	1.3	8893	1418	64	23	718	23	465	7006	2.2	148	3393	857
			sd	570	3.1	23,785	3355	32	43	1272	32	873	14,161	5.0	381	5655	3428
YK	Zn-Fe ± Cu	ws	23	0.5	0.2	26,388	393	8.4	4	371	164	145	373	0.08	0.14	504	0.4
			sd	0.8	0.5	49,269	609	4.0	11	592	273	153	541	0.17	0.18	738	0.5
Okt	Zn-Cu-Fe	gs	22	0.4	0.5	912	5.0	134	11	5.6	3.8	1.7	8	0.02	0.19	25	8.1
			sd	1.4	1.4	2153	4.1	50	22	14	0.4	1.7	18	0.06	0.49	35	10
Val	Cu-Zn-Fe	gs	52	0.20	1.8	9333	27	139	25	70	37	5.6	138	0.7	1.2	1393	100
			sd	0.45	4.9	17,486	37	79	53	108	16.4	5.9	464	1.9	2.2	2610	333
TT	Zn-Cu ± Fe	ws	57	0.08	0.4	409	9.0	84	32	22	3.4	1.3	1.0	0.04	0.1	28	1.3
			sd	0.32	1.5	2773	48	36	137	33	2.4	2.9	2.3	0.11	0.6	75	3.2
Alex	Zn-Cu	ws	52	0.03	0.4	332	243	23	22	7.5	6.1	90	6.8	0.56	0.3	208	2.7
			sd	0.1	2.3	1307	1427	40	40	6.2	6.3	542	23	1.6	1.0	739	5.8
Saf	Cu-Fe ± Zn	bs	26	66	0.2	6114	170	1316	69	84	133	48	28	0.12	0.5	6345	52
			sd	148	0.3	16,294	330	612	266	58	163	115	41	0.23	1.7	7056	64
Saf	Cu-Fe-Zn	gs	8	0.05	0.2	937	13	238	0.05	377	2009	9.0	20	0.02	0.06	732	7.4
			sd	0.03	0.2	571	6.6	303	0.06	543	1248	16	26	0.04	0.05	1904	7.5
Saf	Zn-Cu	ws	6	0.02	0.1	17	2.9	36	0.05	17	4.9	12	1.2	0.04	0.22	3294	0.01
			sd	0.01	0.1	6.7	1.5	24	0.06	8.0	1.1	6.2	1.0	0.04	0.28	6795	0.00

Dep – massive sulfide deposits: Der – Dergamysh, Bur – Buribay, Sult – Sultanovskoye, Yb – Yubileynoye, Mol – Molodezhnoye, Uz – Uzelga, Tal – Talgan, YK – Yaman-Kasy, Okt – Oktyabrskoye, Val – Valentorskoye, TT – Tash-Tau, Alex – Alexandrinskoye, Saf – Safyanovskoye.
CH – chemical chimney types; SM – supposed chimney smoke: bs – black, gs – grey, ws – white (greyish); cs – clear; n – number of analyses; sd – standard deviation.

Table 6
Average contents of trace elements in chalcopyrite of chimneys from the modern vent sites (LA-ICP-MS, ppm).

VS	CH	CS	n/sd	Co	Ni	As	Se	Mo	Ag	Sn	Sb	Te	Au	Tl	Pb	Bi
Rb	Cu ± Ca	bs	82	2045	928	15	934	8.5	20	19	1.5	68	4.3	0.1	16	5.7
			sd	1408	572	20	390	17	16	12	2.0	31	5.3	0.2	42	5.6
Rb	Zn-Cu-Fe	cs	34	2811	0.4	42	3.2	2.7	289	1601	35	0.1	0.8	0.1	20	5.2
			sd	2011	0.4	159	3.0	7.2	144	1669	61	0.1	2.0	0.1	35	19
Log	Cu	bs	20	4.5	0.7	2.5	1035	1.1	14	45	2.0	38	3.5	30	49	6.8
			sd	7.2	0.8	1.1	584	1.0	6.1	28	1.5	15	1.8	20	23	4.7
EPR	Cu-Fe ± Zn	bs	48	57	6.6	42	1184	122	63	31	15	26	0.0	0.23	30	7.4
			sd	62	11	106	652	332	57	34	55	24	0.1	0.77	52	15
BS	Cu-Zn-Fe	bs	87	113	4.4	21	1983	28	12	4.2	1.2	92	0.1	0.18	9.0	8.1
			sd	41	5.1	87	1088	158	12	4.0	3.5	65	0.4	0.50	18	24
TM	Fe-Cu-Zn	ws	15	0.02	0.6	3.5	3.2	51	54	7.3	19	0.1	24	0.15	13	0.05
			sd	0.02	1.0	3.4	2.6	116	37	7.5	16	0.2	56	0.22	13	0.06
SP	Cu-Fe-Zn	bs	26	1817	0.4	11	516	0.1	214	29	4	23	0.1	0.01	4.9	6.2
			sd	1556	0.4	27	257	0.1	67	26	12	9.1	0.1	0.02	16	10
SP	Zn-Fe-Cu	cs	9	0.02	0.1	0.9	8.9	0.1	442	498	0.03	0.04	0.2	0.01	1.1	0.005
			sd	0.02	0.2	1.0	2.2	0.1	106	358	0.03	0.05	0.1	0.01	1.5	0.005
LS	Cu-Fe ± Zn	bs	15	28	0.2	35	928	8	16	4	1.1	0.4	0.04	0.8	13	0.013
			sd	48	0.2	77	379	18	9.3	2.2	2.2	0.3	0.04	1.7	18	0.035
GR	Fe-Cu-Zn	gs	46	18	0.13	1.0	857	0.85	63	65	0.5	0.14	0.01	0.02	4.7	0.141
			sd	11	0.18	1.8	946	2.73	55	69	0.9	0.17	0.02	0.09	10	0.247
MG	Ba-Cu-Zn-Fe	gs	30	8	0.2	10	1517	69	83	4.5	9.1	0.5	0.2	0.8	34	0.040
			sd	16	0.6	30	1160	185	110	5.0	24	1.5	0.5	2.3	92	0.15
AS	Zn-Ba-Fe-Cu	gs	13	26	0.5	28	1248	20	120	8.6	3.7	1.3	0.1	0.2	23	0.01
			sd	20	0.5	63	881	37	107	6.6	7.3	1.6	0.1	0.4	49	0.02
VW	Zn-Fe-Cu	cs	12	2.49	0.1	0.9	27	0.4	130	66	0.1	0.2	0.1	0.02	6	0.003
			sd	0.80	0.1	1.2	2.6	0.8	11	15	0.2	0.2	0.04	0.02	11	0.002
NL	Zn-Fe-Cu	cs	16	0.02	0.1	0.3	6.3	0.1	19	15	0.03	0.2	0.01	0.03	0.1	0.009
			sd	0.04	0.1	0.3	1.8	0.1	2	9	0.03	0.2	0.01	0.1	0.2	0.012
CL	Zn-Fe-Cu	cs	5	7.9	2.2	1.0	17.2	0.06	254	33	0.06	0.17	0.21	0.01	0.29	0.002
			sd	1.4	4.1	1.7	3.0	0.04	14	12	0.05	0.11	0.06	0.02	0.55	0.001
SV	Cu-Fe ± Zn	gs	20	1.05	0.05	8.1	147	0.6	98	63	5.8	0.1	0.2	0.1	4.1	2.38
			sd	0.70	0.08	19	49	2.2	95	25	25	0.1	0.3	0.4	14	8.10
Pac	Cu ± Fe ± Zn	gs	56	0.03	0.3	6694	21	183	45	65	930	123	7.1	10	223	271
			sd	0.04	1.1	12,534	20	440	70	78	1118	552	7.8	36	309	632
Pac	Ba-Zn-Fe-Cu	ws	28	6	0.2	3599	79	211	95	0.5	2456	0.28	8.4	12	521	0.005
			sd	11	0.5	4742	35	189	84	0.3	2953	0.25	12	52	668	0.006
Suz	Ba-Zn-Fe-Cu	ws	30	1.3	0.5	1628	47	130	139	0.6	1007	0.17	8.6	26	441	0.004
			sd	3.2	1.7	2923	29	213	250	0.4	2440	0.17	19	104	1248	0.004
Hak	Zn-Ba-Fe-Cu	cs	18	0.03	0.04	32	2.9	0.7	188	0.5	63	0.03	0.0	0.01	9	0.004
			sd	0.07	0.03	45	0.6	1.1	73	0.3	104	0.02	0.0	0.02	20	0.005

VS – vent sites: Rb – Rainbow, EPR – East Pacific Rise 9°11′N, AS – Axial Seamount, BS – Broken Spur, TM – TAG-MIR, SP – Snake Pit, LS – Lucky Strike, GR – Galapagos Ridge; MG – Menez Gwen, VW – Vienna Wood, NL – Northern Lau, CL – Central Lau, SV – Suiyo Volcano, Pac – PACMANUS (Solwara-4), Suz – Suzette (Solwara-1); Hak – Hakurei. CH – chemical type of a chimney; SM – supposed color of chimney smoke: bs – black; gs – grey; ws – white (greyish white); cs – clear; n – number of analyses; sd – standard deviation.

Tash-Tau chimneys are similar to grey smokers of Suiyo volcano by moderate to low Se and Te contents in chalcopyrite (Table 6).

The contents of Te and Se are lower in chalcopyrite from the barite–chalcopyrite–sphalerite chimneys of the *Alexandrinskoye* deposit (Table 5, Fig. 8g). The barite- and sphalerite-rich chimneys from this deposit are most likely resemble modern white smokers of the PACMANUS vent site (Table 6).

Chalcopyrite from the chalcopyrite-rich chimneys of the *Safyanovkoye* deposit, as well as chalcopyrite from typical black smokers associated with basalts and ultramafic rocks, is characterized by significantly variable Se (157–3139 ppm) and Te (1–220 ppm) contents (Tables 5, 6). The increase in amount of sphalerite in chimneys is accompanied by the decrease in Se and Te contents in chalcopyrite. Their contents in chalcopyrite from sphalerite- and barite-rich chimneys are the lowest: 12–70 ppm Se and 0.1–6 ppm Te. These chimneys belong to grey and white/or clear smokers (Fig. 8g).

Generally, the Se contents in chalcopyrite from the smokers decrease as a role of felsic volcanic rocks increases in the sequences. In the both mineralogical ranges of modern and ancient smokers, the Se and Te contents in chalcopyrite (with rare exceptions, e.g., Yaman-Kasy deposit)

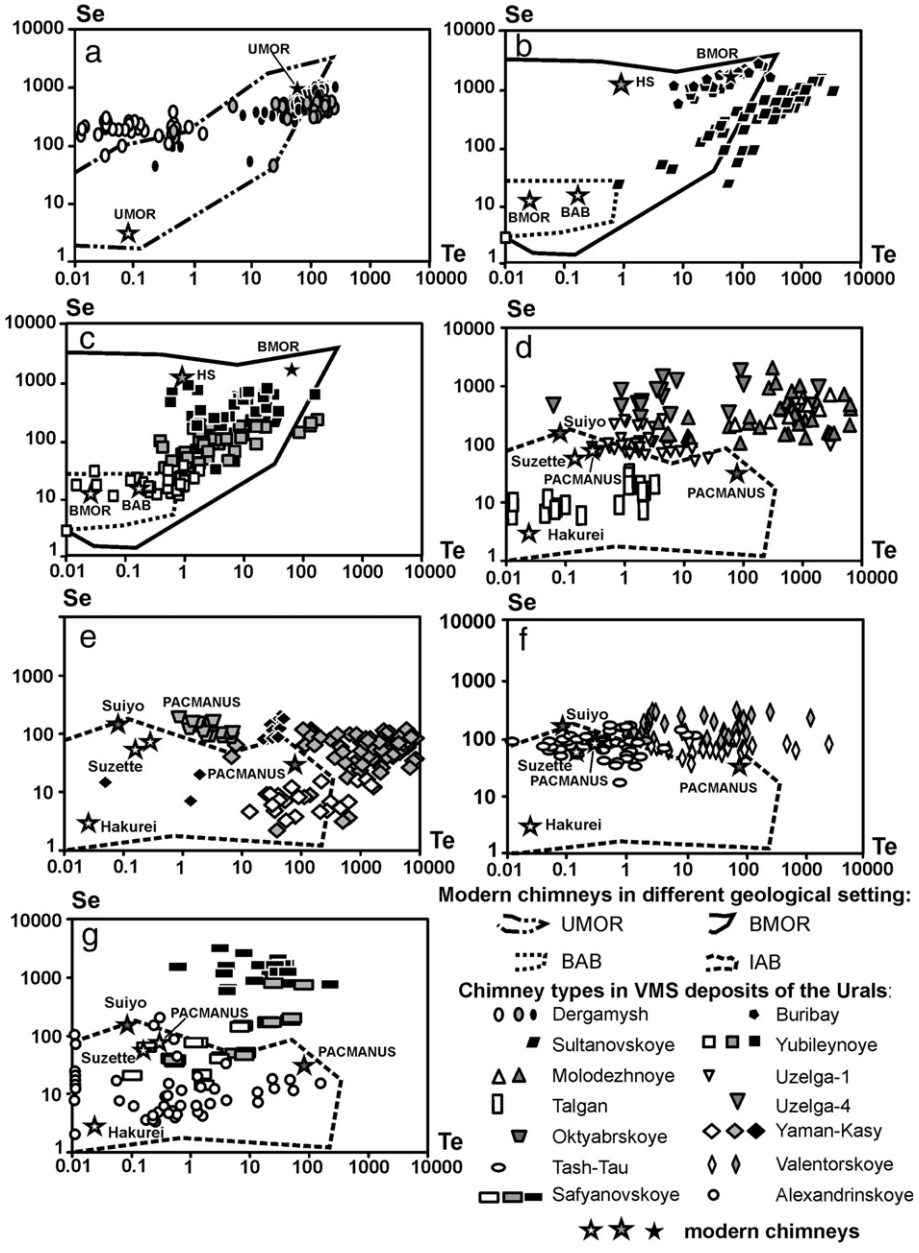

Fig. 8. Log–log plots of Se vs. Te in chalcopyrite from chimneys of the Urals VMS deposits and modern vent sites. The contents of Se and/or Te increase in the ranges from clear and white to grey and black smokers. The Se–Te positive correlation in black smokers declines with increasing amount of felsic volcanic host rocks in order from ultramafic (a) → mafic (b) → bimodal mafic (c, d) → bimodal felsic and felsic (e, f). In the same direction, as is suggested, the substitution of Se^{2-} and Te^{2-} for S^{2-} leads to formation diverse telluride and then Te-rich tennantite, Te-rich pyrite and native gold–galena–hessite assemblages. This pattern is also consistent with mineral change in the range from black to grey and white or clear smokers. The exception is chalcopyrite of chimneys from the felsic- and black shale-hosted Safyanovskoye deposit, where positive Se and Te correlation is due to influence of organic-rich sediments located in the foot wall. The color of black, grey and white symbols corresponds to black, grey and white (or clear) smokers, respectively. The line counters are field of data points of chalcopyrite composition for chimneys from different host rocks and of geological setting: UMOR – ultramafic-rich mid-ocean ridge; BMOR – basalt-rich mid-ocean ridge; HS – hot spots of the mid-ocean ridge; BAB – basalt basement of back-arc basins; IAB – bimodal mafic- and felsic-hosted vent sites in intra-arc or proximal arc basins. Here and hereafter in Figs. 11–19, LA-ICP-MS data, ppm.

decrease with decreasing amount of chalcopyrite and increasing amount of sphalerite and pyrite. In most cases, the average Te contents in chalcopyrite from chimneys of the Urals deposits are much higher than those in chalcopyrite of the modern black smokers (Tables 5, 6). The presence of tellurides and tellurium-bearing tennantite negates the positive correlation between Se and Te in the modern and ancient black smokers.

4.2.1.2. Co–Sn and Ni. The Sn contents in chalcopyrite of the modern smokers increases in the range from bimodal to basaltic and ultramafic ore-hosting rocks, reaching economic concentrations (0.8–1 wt.%) in the latter. The Co and Ni contents display opposite distribution (Tables 5, 6; Fig. 9).

The *Dergamysh* chalcopyrite is characterized by the highest Co contents (up to 3295 ppm) at moderate Sn contents (10–91 ppm) and falls to the boundary between overlapping fields of modern black smokers associated with basalts and ultramafic rocks (Fig. 9a). In opposite to modern clear smokers, the chalcopyrite of the Dergamish pyrite-rich chimneys display lower contents of Co in comparison to chalcopyrite-rich varieties. While Sn contents in chalcopyrite are much higher in modern clear diffusers and pyrite-rich chimneys of the Dergamish deposit.

The Co contents (0.01–2, up to 41 ppm) of the *Buribay, Yubileynoye* and *Sultanovskoye* chalcopyrite are lower than that of chalcopyrite of the modern black smokers (Fig. 9b, c). Most Sn and Co data points are located within the field of the modern grey smokers associated with island-arc basalts. The high Co content in chalcopyrite from the pyrite–chalcopyrite chimneys of the Sultanovskoye deposit attains values, which are characteristic of the modern black smokers. Chalcopyrite of chimneys with abundant sphalerite is depleted in Co and Sn similarly to most modern clear smokers and diffusers.

The Co (0.01–1432 ppm) and Sn (5–5737 ppm) contents of chalcopyrite from the *Molodezhnoye* chimneys strongly vary and are similar, on average, to those of chalcopyrite from the modern black smokers (Fig. 9d). The Sn and Co contents in chalcopyrite from the *Uzelga-1* chimneys with abundant sphalerite, calcite, tetrahedrite–tennantite and barite are similar to those in chalcopyrite of grey and clear smokers (Fig. 9d).

The highly variable Co contents (28–981 ppm, rarely, up to 0.5 wt.%) and moderate Sn contents (4–48 ppm, rarely, up to 166 ppm) are typical of chalcopyrite from the pyrite–sphalerite–chalcopyrite chimneys of the *Yaman-Kasy* deposit. The enrichment in Co is related to the microinclusions of cobaltite (Fig. 9e), Co-bearing loellingite (Fig. 9e) and Co-bearing frohbergite (Maslennikov et al., 2013). The Co contents are much lower (0.01–2.6 ppm) in chalcopyrite from the sphalerite-rich chimneys with abundant pyrite, quartz and barite; Sn contents in this case are 21–981 ppm. These chimneys represent a transitional type between grey to white or clear smokers (Fig. 9e).

Much lower Co (0.01–10 ppm) and Sn (0.2–7 ppm) contents are typical of chalcopyrite from the chimneys of the Baymak and/or Kuroko type *Valentorskoye*, *Oktyabrskoye*, *Tash-Tau* and *Alexandrinskoye* deposits (Table 5). They occupy the field data points related to chimneys of the West Pacific grey and clear smokers (Fig. 9e–g).

Chalcopyrite from the *Safyanovskoye* pyrite–chalcopyrite chimneys is enriched in Co (0.01–704 ppm) and Sn (75–886 ppm) (Table 5, Fig. 9g). Part of Sn and Co is isomorphic in chalcopyrite, whereas some part of Co is related to microinclusions of glaucodot (Fig. 6l). Chalcopyrite from these chimneys shows high Co contents similar to those of the modern black smokers (Tables 5 and 6). The Sn contents in chalcopyrite from the pyrite–sphalerite–chalcopyrite chimneys attain 389 ppm at the lowest Co contents (0.02–0.1 wt.%). In these chimneys, Sn is fixed in microinclusions of stannoidite and mawsonite (Fig. 6m). Further increase in the amount of sphalerite, quartz and barite in chimneys results in decreasing Sn and Co contents in chalcopyrite. The lowest Co (0.01–00.4 ppm) and Sn (4–6 ppm) contents are identified in the chalcopyrite zone, which incrusts the channel walls of barite–sphalerite chimneys (Fig. 9g).

Chalcopyrite of the Dergamysh chimneys display the highest Ni and Co contents in comparison with chalcopyrite from others deposits (Table 5). The Ni enrichment is typical of modern chimneys associated with ultramafic rocks. In most chimneys of the Atlantic, Cyprus and Uralian types, the Co/Ni ratio is much higher than 1. The Baymak type of the deposits yields the chimneys with low Ni contents and Co/Ni ration of < 1.

4.2.1.3. Pb–Bi. At the *Dergamysh* deposit, chalcopyrite of the chalcopyrite-rich chimneys are depleted in Pb (4–63 ppm) and Bi (4–16 ppm) (Table 5, Fig. 10a). The lowest Bi contents (<0.001–0.29 ppm) are typical of chalcopyrite from pyrite-rich chimneys and diffusers. Isocubanite and chalcopyrite with isocubanite ingrowths are enriched in these elements: 16–726 ppm Pb and 1–1133 ppm Bi.

Chalcopyrite from the *Buribay* chalcopyrite–pyrite chimneys, as well as chalcopyrite of the modern black smokers, is characterized by low Pb (51–450 ppm) and Bi (0.1–4, up to 13 ppm) contents (Fig. 10b; Tables 5 and 6). The Pb (400–4975 ppm) and Bi (78–563 ppm) contents are much higher in chalcopyrite from the *Sultanovskoye* chalcopyrite-rich chimneys (Fig. 10b). Numerous microinclusions of galena, tsumoite and tellurobismuthite frequently occur in chalcopyrite from these chimneys. At the *Yubileynoye* deposit, Pb contents in chalcopyrite from all chimneys are 5–60 ppm and, locally, reach 1453 ppm due to rare microinclusions of galena (Fig. 10c). In this deposit, chalcopyrite from the chalcopyrite-pyrite chimneys is characterized by the high Bi contents (up to 57 ppm) because of rare fine inclusions of tellurobismuthite. None of these inclusions were identified in chalcopyrite from the calcite–talc–pyrite–sphalerite–chalcopyrite chimneys comparable with the modern grey smokers, where this mineral is common (f.e.PACMANUS vet site). The Bi contents in chalcopyrite from these chimneys vary from 0.01 to 4 ppm and Bi contents of chalcopyrite from the sphalerite-rich chimneys are <1 ppm.

At the *Molodezhnoye* deposit, the enrichment in Pb (up to 1–2 wt.%) and Bi (1–643 ppm) in chalcopyrite of chimneys (Fig. 10d) is mostly related to microinclusions of Bi-bearing altaite and galena, as well as unresolved Pb–Bi–Te solid solutions. At the *Uzelga*-4, the Bi contents of chalcopyrite (<15 ppm) are related to microinclusions of galena. The Bi (<0.07 ppm) and Pb (1–20, rarely, up to 60–2230 ppm) contents are much lower in chalcopyrite from calcite–barite–tetrahedrite–tennantite–chalcopyrite and chalcopyrite–tetrahedrite–sphalerite chimneys of the Uzelga-1 deposit (Fig. 10d).

The high contents of Pb (up to 7682 ppm) and Bi (6067 ppm) in chalcopyrite of the *Yaman-Kasy* chalcopyrite-rich chimneys are related to microinclusions of altaite, galena and tellurobismuthite (Fig. 6e; Maslennikov et al., 2009). The Bi contents in chalcopyrite of the sphalerite-rich chimneys are much lower (10–0.01 ppm) (Fig. 10e). At the *Valentorskoye* deposit, chalcopyrite, along with galena, from chimneys hosts inclusions of the Pb–Bi–Te intermediate solutions of tellurobismutite → kochkarite → rucklidgeite series (Maslennikov et al., 2013) ensuring the highest Pb (6–11,518 ppm) and Bi (2–2306 ppm) contents. The highest contents of Pb are detected in chalcopyrite of sphalerite-rich chimneys (Table 5, Fig. 10f).

Altaite, galena and tellurobismuthite are found only in sphalerite from the *Oktyabrskoye* sphalerite–chalcopyrite–barite–pyrite chimneys. Accessory minerals lack in the chalcopyrite, which yielding the low contents of Bi (1–42 ppm) and Pb (2–132 ppm) (Fig. 10e). The lower Pb (1–40 ppm, rarely, up to 200–4000 ppm) and Bi (0.01–11 ppm) contents are characteristic of chalcopyrite from sphalerite–chalcopyrite chimneys of the *Tash-Tau* and *Alexandrinskoye* deposits (Table 5, Fig. 10f, g). Strong positive correlation between Pb and Bi is due to microinclusions of galena, according to following equation of a well-known scheme of heterovalent isomorphism: $Bi^{3+} + Ag^{+} \leftrightarrow 2Pb^{2+}$. The positive correlation coefficients, which are slightly higher than critical level (minimum $r = 0.3$), seem to support this idea: Pb–Bi

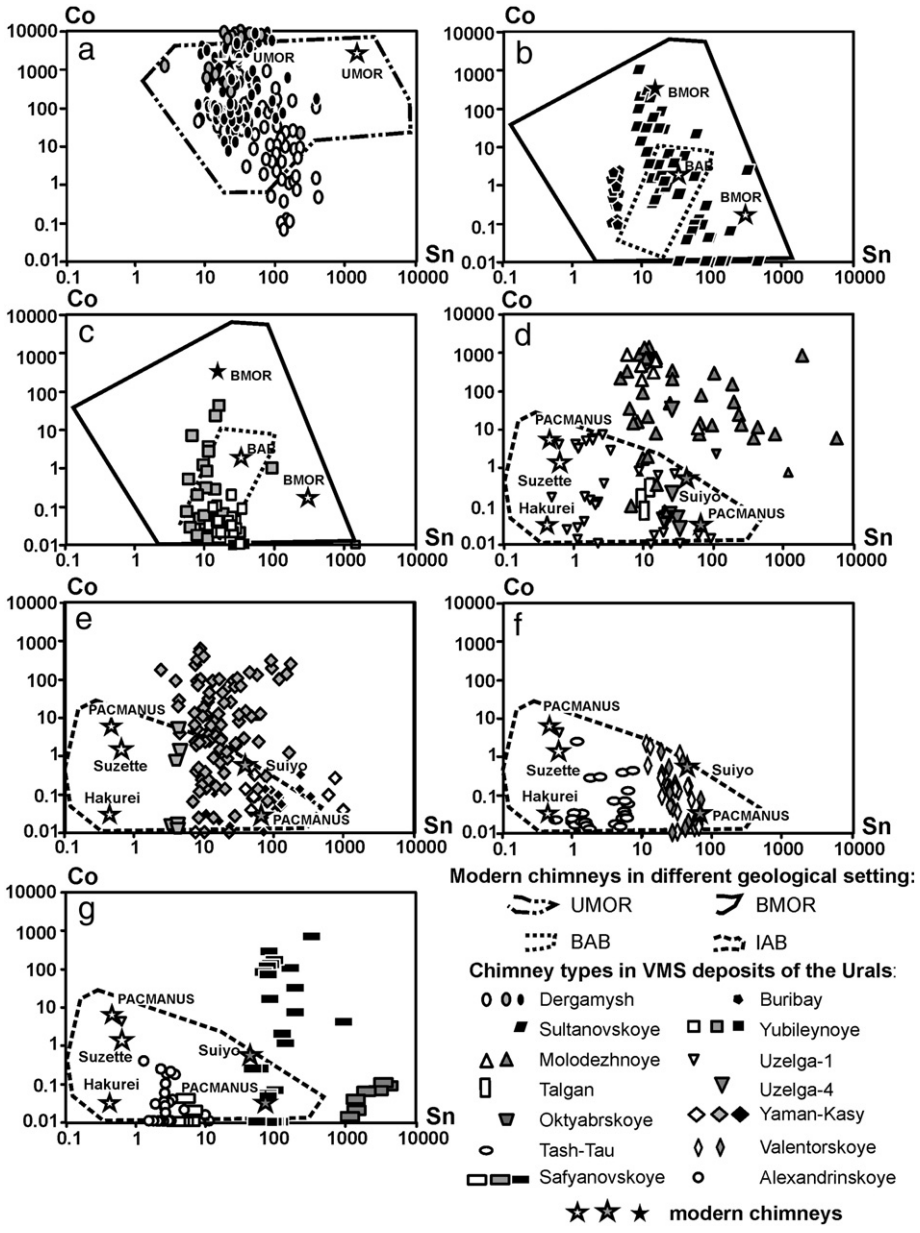

Fig. 9. Log–log plots of Co vs. Sn for chalcopyrite of chimneys from the Urals and modern vent sites. Most of Sn and Co data points are located within appropriate field of modern smokers. The highest contents of Co are typical of chalcopyrite of chimneys of Dergamysh VMS deposit and modern vent sites (Rainbow, Logatchev) hosted by ultramafic rocks (a). Chalcopyrite of chimneys of VMS deposits and modern vent sites located in bimodal felsic sequences (f – Valentorskoye, Tash-Tau and Oktyabrskoye deposit g – Alexandrinskoye deposit) displays lower Co contents. Chalcopyrite of chimneys from Safyanovskoye deposit associated with felsic rocks and carbonaceous shales has higher Sn contents. Chalcopyrite of chimneys from other deposits has intermediate Co and Sn contents. The lower Co and Sn contents are typical of modern white and clear smokers and their ancient counterparts. The color of black, grey and white symbols corresponds to black, grey and white (or clear) smokers, respectively. The line counters are field of data points of chalcopyrite composition for chimneys from different host rocks and of geological setting: UMOR – ultramafic-rich mid-ocean ridge; BMOR – basalt-rich mid-ocean ridge; HS – hot spots of the mid-ocean ridge; BAB – basalt basement of back-arc basins; IAB – bimodal mafic- and felsic-hosted vent sites in intra-arc or proximal arc basins.

($r = 0.54$), Pb–Ag ($r = 0.45$) and Bi–Ag ($r = 0.88$). The bornite-rich chimneys, however, display very strong positive correlation of Bi and Ag ($r = 0.96$) versus Pb and Ag ($r = 0.02$). This means that the strong positive correlation of Bi and Ag may be provided by bornite microinclusions too.

At the *Safyanovskoye* deposit, Bi and Pb contents in chalcopyrite decrease in the range from pyrite–chalcopyrite to barite-sphalerite-rich chimneys (Table 5; Fig. 10g). The Pb and Bi contents are mostly related to numerous microinclusions of galena. Invisible microinclusions of Bi telluride were identified by LA-ICP-MS in chalcopyrite-rich chimneys.

In many cases, high contents of Bi are typical for chalcopyrite of chalcopyrite-rich chimneys which could be analogs of black and grey smokers. Chalcopyrite of barite- and sphalerite-rich chimneys display low contents of Bi like in modern greyish white and clear smokers (Tables 5, 6).

4.2.1.4. Au–Ag. The Au contents in chalcopyrite from the *Dergamysh* chalcopyrite-rich chimneys vary from 0.001 to 10.5 ppm (Fig. 11a; Table 5). The Au contents in chalcopyrite are much higher in the chalcopyrite-rich chimneys (3.5–10.5 ppm, rarely, up to 12–168 ppm) than incalcite–pyrite diffusers (0.001–0.06 ppm) (Table 5). A significant part of Au and Ag in chalcopyrite from isocubanite-chalcopyrite-rich chimneys is observed as microinclusions of electrum ($Au_{0.56}Ag_{0.54}$, SEM analysis), which are most abundant in isocubanite.

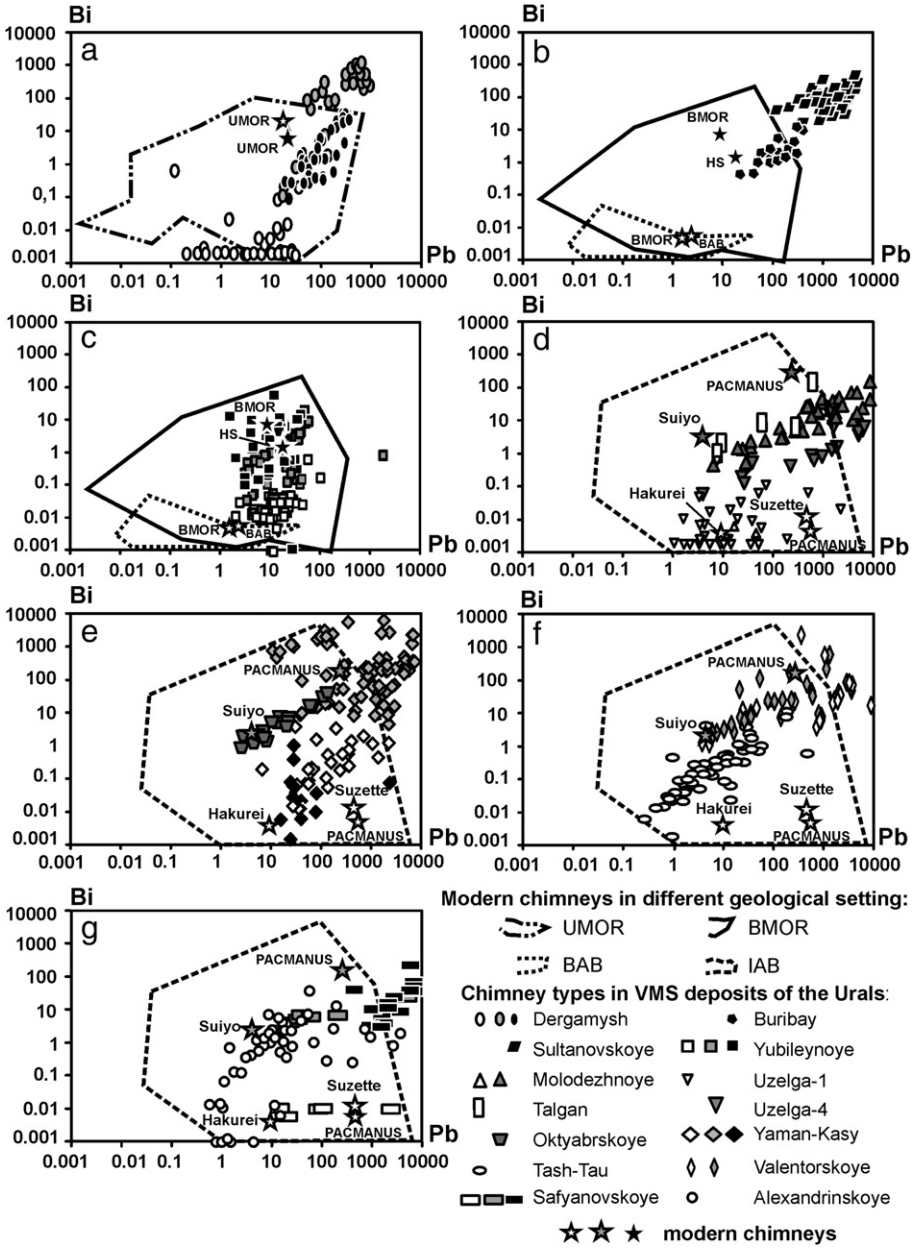

Fig. 10. Log–log plots of Bi vs. Pb for chalcopyrite of chimneys from the Urals VMS deposits and modern vent sites. The maximum Pb and Bi contents in chalcopyrite of modern chimneys increase in the range from ultramafic (a) and mafic (b) to bimodal mafic- and felsic-hosted (d–g) vent sites similarly to chimneys from the Urals VMS deposits. In most cases, except for the Rainbow site, the modern white and clear smokers and their ancient analogues display the lower Bi and Pb contents in comparison with black and grey smokers. The Uralian analogues of black and grey smokers have the higher maximum contents of these elements. The color of black, grey and white symbols corresponds to black, grey and white (or clear) smokers, respectively. The line counters are field of data points of chalcopyrite composition for chimneys from different host rocks and of geological setting: UMOR – ultramafic-rich mid-ocean ridge; BMOR – basalt-rich mid-ocean ridge; HS – hot spots of the mid-ocean ridge; BAB – basalt basement of back-arc basins; IAB – bimodal mafic- and felsic-hosted vent sites in intra-arc or proximal arc basins.

The Au (0.4–2.9 ppm) and Ag (8–334 ppm) contents in chalcopyrite from the *Buribay* chalcopyrite–pyrite chimneys are higher by one order of magnitude relative to those in chalcopyrite of the MOR modern black smokers (Tables 5, 6; Fig. 11b). The strongly variable Au (0.1–115 ppm) and Ag (3–1147 ppm) contents are typical of chalcopyrite from the *Sultanovskoye* chimneys (Fig. 11b). The Au–Ag positive correlation is related to microinclusions of native gold ($Au_{0.66}Ag_{0.34}$, SEM analysis). Similar data are obtained for chalcopyrite from all the *Yubileynoye* chimneys (Fig. 11c).

Most Au and Ag contents in chalcopyrite from the chalcopyrite-rich chimneys of the *Molodezhnoye*, *Uzelga-4* and *Yaman-Kasy* deposits are much higher than those in chalcopyrite from chimneys of the modern black and grey smokers (Tables 5, 6; Fig. 11d, e). The higher contents of these elements are related to microinclusions of sylvanite (Yaman-Kasy) and native gold. In the *Yaman-Kasy* chimneys, native gold (rather than sylvanite) is more common in chalcopyrite and increases with increasing amount of sphalerite, quartz and barite (Maslennikova and Maslennikov, 2007; Maslennikov et al., 2013). The Ag/Au ratio of chalcopyrite increases in the same direction due to the higher amount of microinclusions of hessite and tennantite in sphalerite-rich chimneys.

The Au (0.03–2.3 ppm) and Ag (1–65 ppm) contents in chalcopyrite from the *Oktyabrskoye* chimneys are much lower than those in previous examples (Fig. 11e). Significant amount of gold and tellurides is concentrated in sphalerite. No correlation between Ag and Au indicates that part of Ag is related to both native gold and hessite, which is confirmed by microscopic observations. The Au contents (0.001–12 ppm) in

chalcopyrite from the *Uzelga-1*, *Talgan*, *Tash-Tau*, *Alexandrinskoye* and *Safyanovskoye* chimneys are much lower relative to the chimneys of the Uralian type deposits (Fig. 11d–g). The barite–chalcopyrite–sphalerite chimneys of the deposit are dominated by gold–hessite–galena–tennantite assemblages free of altaite and tellurobismuthite. The sphalerite-rich chimneys of these deposits contain microinclusions of native gold in sphalerite, only. The variable Ag contents (2–134 ppm) are registered in chalcopyrite from chimneys of the all deposits. Silver is concentrated in galena, bornite, tennantite and hessite.

Hence, the Ag/Au ratios in chalcopyrite of both modern and ancient smokers are commonly higher than that typical of microinclusions of sylvanite, electrum and native gold. It is obvious that other minerals could also be enriched in Ag. Silver likely occurs as isomorphic substitution for Cu in chalcopyrite of black smokers, where no these minerals were identified. The higher Ag contents in grey smokers are due to microinclusions of hessite, bornite, Ag-bearing tennantite and tetrahedrite. However, the calculation shown no significant correlation between Ag and Cu for chimneys described here. In some cases, the positive correlation coefficients between Ag and Cu ($r = 0.5–0.7$) are typical of some chimneys from EPR 9°50′N, Galapagos Ridge and Rainbow vent sites and Alexandriskoye deposit. All these chimneys contain microinclusions of Ag-bearing bornite or covellite. The strong correlations of Ag with Bi and Cu ($r = 0.7–0.96$) are typical of massive sulfides enriched in these minerals.

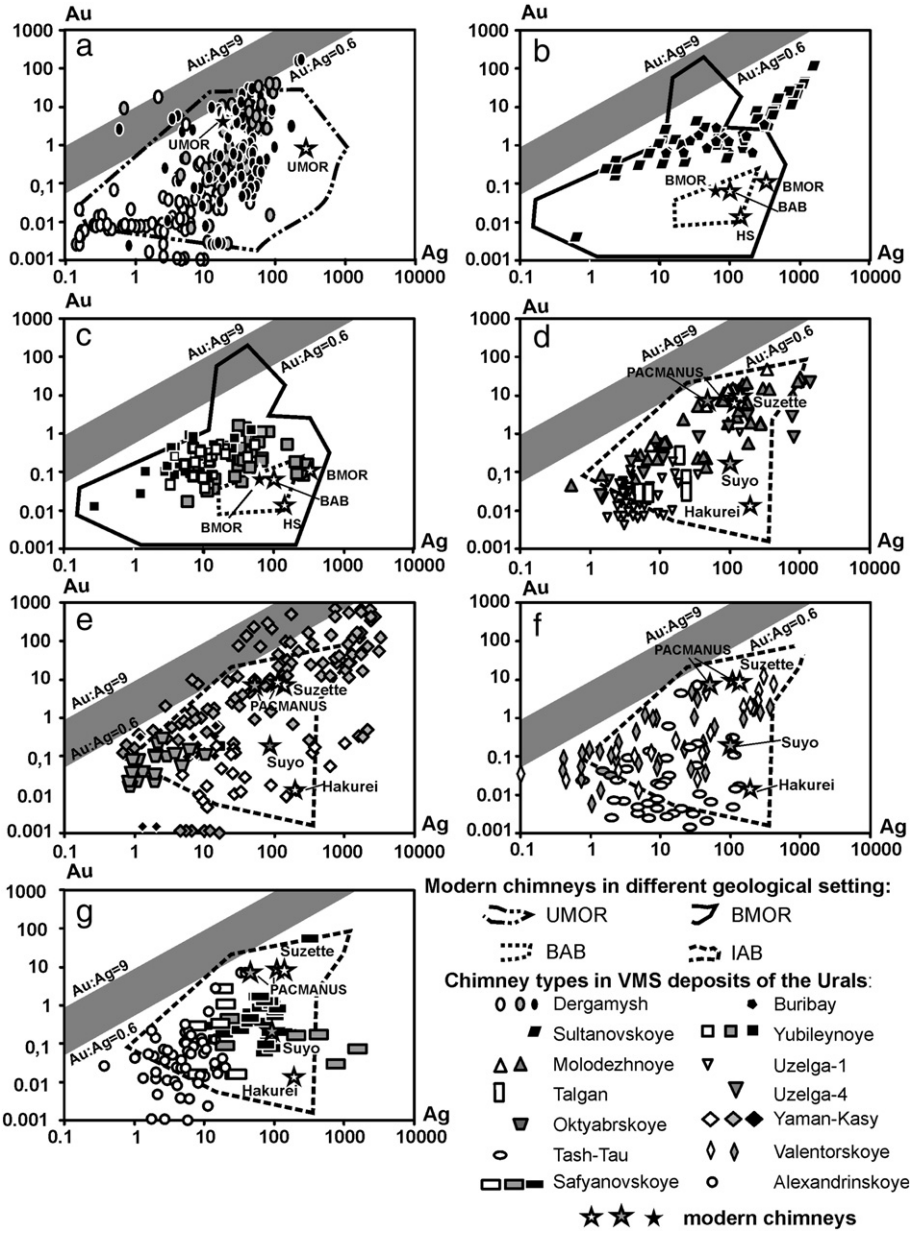

Fig. 11. Log–log plots of Ag vs. Au for chalcopyrite of chimneys from the Urals VMS deposits and modern vent sites. The fields of Ag and Ag contents are similar for the chimneys located in different geological settings of modern and ancient chimneys. The shaded area shows the composition of sylvanite or native gold and electrum microinclusions detected by microprobe analyses in modern and ancient chimneys. In the area, the data points appropriate to the microinclusions. The intergrowths of native gold and electrum with hessite and other Ag-rich minerals are supposed or anticipated to the left from the shaded area. The most analogues of black and grey smokers have the higher Au content in comparison with white and/or clear smokers. The color of black, grey and white symbols corresponds to black, grey and white (or clear) smokers, respectively. The line counters are field of data points of chalcopyrite composition for chimneys from different host rocks and of geological setting: UMOR – ultramafic-rich mid-ocean ridge; BMOR – basalt-rich mid-ocean ridge; HS – hot spots of the mid-ocean ridge; BAB – basalt basement of back-arc basins; IAB – bimodal mafic- and felsic-hosted vent sites in intra-arc or proximal arc basins.

4.2.2. Sphalerite

4.2.2.1. Fe–Cu. In the Cu–Fe plot, most data points of sphalerite from the *Dergamysh* chimneys occupy the field of the modern black and clear smokers associated with serpentinites (Fig. 12a; Table 7). A positive correlation between Cu and Fe ($r = 0.88$) is indicative of microinclusions of chalcopyrite and isocubanite in sphalerite, as well as in ultramafic-associated isocubanite–pyrite–sphalerite chimneys and diffusers from the Rainbow vent site. The data points beyond the chalcopyrite–isocubanite area are explained by Fe^{2+} for Zn^{2+} substitution, which is typical of sphalerite with low Cu contents (Fig. 12a).

The Fe contents in sphalerite from chimneys of the *Buribay*, *Sultanovskoye* and *Yubileynoye* deposits are 0.5–5 wt.% (Table 7; Fig. 12b). The Fe contents in sphalerite from the chalcopyrite-rich chimneys of the Buribay and Sultanovskoye deposits are largely related to inclusions of chalcopyrite. About half of sphalerite grains in sphalerite-rich Yubileynoe chimneys contain excessive iron most likely due to substitution of Fe^{2+} for Zn^{2+} or inclusions of pyrite.

Sphalerite from the chimneys of the *Molodezhnoye* deposit is characterized by Fe/Cu ratio of >0.88 (Fig. 12c). Finely dispersed dissemination of chalcopyrite, isocubanite, pseudomorphic pyrite after pyrrhotite and magnetite is observed in this sphalerite. The Fe/Cu ratio of ~0.88 is characteristic of sphalerite from the chalcopyrite–pyrite–sphalerite chimneys of the *Uzelga-4* deposit. This sphalerite is saturated with microinclusions of chalcopyrite only. Sphalerite contains microinclusions of isocubanite, magnetite and pyrite in some *Yaman-Kasy* chimneys and tennantite in other chimneys, which cause significant variations in Fe/Cu ratio (Fig. 12d).

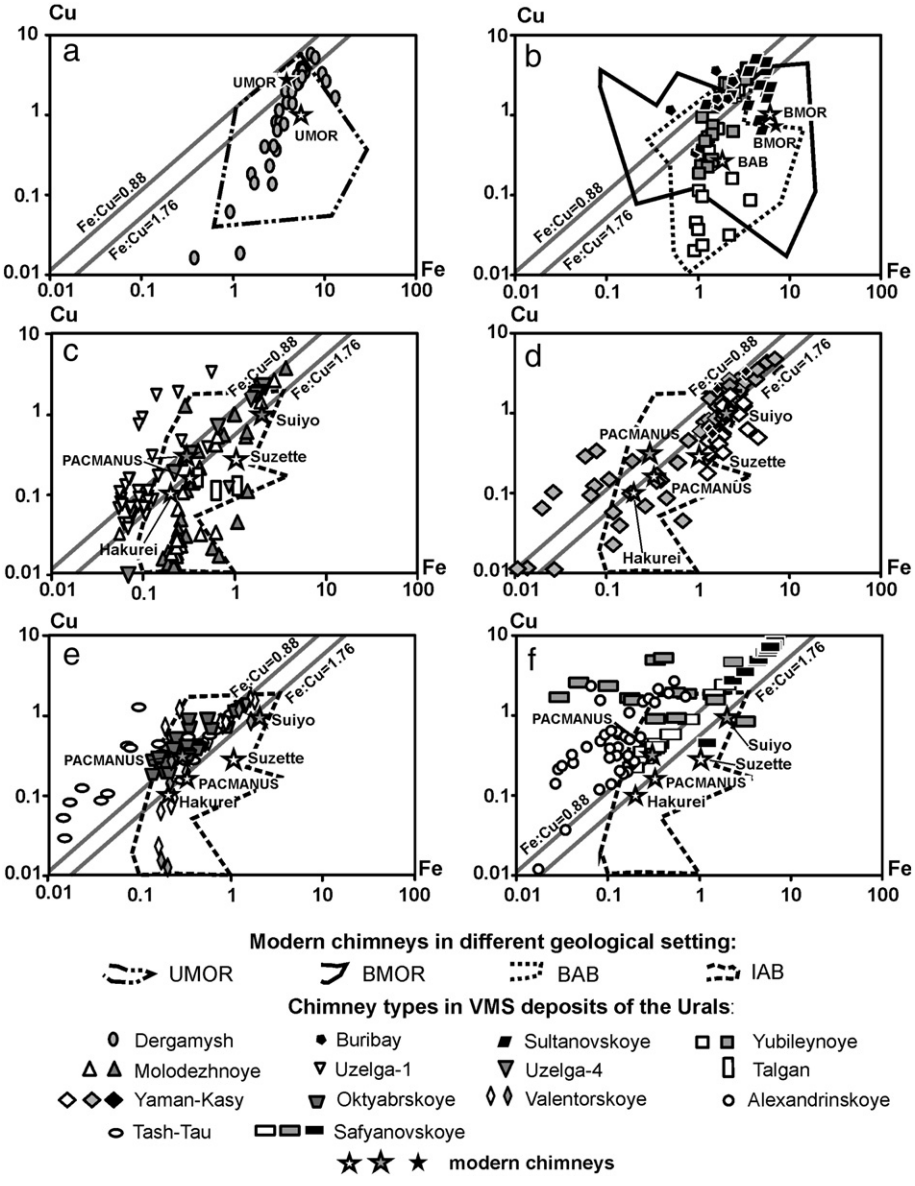

Fig. 12. Log–log plots of Fe vs. Cu for sphalerite of chimneys from the Urals VMS deposits and modern vent sites. The chalcopyrite microinclusions constrain the position of the shaded line with Fe/Cu ratio of 0.88. The shaded line separates the diagrams on the two part by Fe/Cu ratio 0.88. The data points corresponded to the microinclusions of isocubanite, pyrite, magnetite, hematite of substitution of Fe^{2+} for Zn^{2+} occur in the right part of the plot. The left area corresponds to the microinclusions of bornite, covellite, tennantite or tetrahedrite. The more variable Fe/Cu ratios are typical of sphalerite of chimneys formed on the MORBs (b). In the range of the deposits, the Fe/Cu ratio dramatically decreases due to change of the micromineral assemblages. In chimneys of the deposits and vent site hosted by serpentinite and basalts, the Fe/Cu ration of sphalerite is ≫0.88. Sphalerite in chimneys associated with bimodal felsic units displays Fe/Cu ration of ≪0.88. The color of black, grey and white symbols corresponds to black, grey and white (or clear) smokers, respectively. The line counters are field of data points of chalcopyrite composition for chimneys from different host rocks and of geological setting: UMOR – ultramafic-rich mid-ocean ridge; BMOR – basalt-rich mid-ocean ridge; HS – hot spots of the mid-ocean ridge; BAB – basalt basement of back-arc basins; IAB – bimodal mafic- and felsic-hosted vent sites in intra-arc or proximal arc basins.

Table 7
Average contents of trace elements in sphalerite of chimneys from the Urals VMS deposits (LA-ICP-MS, ppm and wt.%).

Dep	CH	SM	n/sd	Mn	Fe%	Co	Ni	Cu%	As	Se	Ag	Cd%	Sn	Sb	Te	Au	Tl	Pb	Bi
Der	Cu-Fe	bs	20	1547	4.6	1948	29	1.6	17	240	28	0.13	286	876	7.5	4.5	0.06	624	5.4
			sd	1099	3.3	2213	50	1.3	20	245	22	0.05	194	974	18	4.8	0.08	842	13.8
Der	Fe-Ca-Cu	cs	26	2194	4.1	1516	24	1.6	19	100	56	0.11	127	1368	1.5	19	0.10	460	2.0
			sd	1985	1.6	636	64	1.7	22	44	67	0.01	188	1351	2.3	64	0.4	501	1.6
Bur	Cu-Fe ± Zn	bs	7	83	1.4	2.6	0.2	1.5	8.3	192	30	0.19	13	18	15	0.4	0.11	57	1.6
			sd	14	0.4	2.7	0.4	1.0	7.5	122	22	0.01	18	18	16	0.3	0.09	49	2.4
Yub	Cu-Fe-Zn	gs	19	133	1.9	0.005	0.05	1.3	592	28	358	0.28	4.6	505	13	67	0.4	2310	4.5
			sd	75	0.9	0.010	0.11	1.2	596	20	364	0.02	4.0	529	11	243	0.5	3399	4.5
Yub	Zn-Fe-Cu	ws	15	149	1.8	0.009	1.0	0.5	44	15	144	0.29	3.6	432	1.9	0.7	0.7	202	0.01
			sd	113	0.9	0.011	2.4	0.7	59	3.2	230	0.04	2.2	750	1.5	0.8	1.9	248	0.01
Sult	Cu-Fe ± Zn	bs	11	0.7	4.7	251	0.3	2.4	64	350	24	0.09	24	49	48	1.2	0.9	454	25
			sd	0.5	1.2	181	0.3	1.3	37	30	5.1	0.01	21	23	8.9	0.4	0.5	117	12
Mol	Cu-Fe-Zn	gs	46	44	0.6	21	1.0	0.4	213	115	176	0.22	91	97	193	10	0.05	528	3.2
			sd	43	0.7	42	6.1	0.7	741	109	384	0.02	124	289	327	28	0.10	2243	6.4
Uz-4	Cu-Fe-Zn	gs	16	1.6	1.1	0.10	0.2	1.2	17	518	49	0.22	8.6	86	31	0.5	0.04	331	0.8
			sd	0.9	0.7	0.23	0.4	0.8	27	524	70	0.01	4.6	230	51	0.9	0.04	470	1.0
Uz-1	Zn-Cu	ws	36	40	0.1	0.103	0.01	0.3	1438	106	54	0.35	0.5	675	14	0.7	0.03	261	0.002
			sd	103	0.2	0.113	0.02	0.7	3759	73	158	0.04	1.0	1879	64	2.2	0.02	783	0.005
Tal	Cu-Zn-Fe	ws	3	14	0.7	0.009	0.01	0.1	217	9	297	0.25	2.9	990	12	1.8	0.3	7165	31
			sd	10	0.3	0.008	0.00	0.0	29	10	38	0.01	0.5	184	11	0.5	0.11	10,864	35
YK	Cu-Fe	bs	6	128	2.1	0.12	0.6	1.4	2661	18	192	0.20	13	2304	12	4.1	2.2	4294	0.01
			sd	97	0.8	0.12	0.7	1.1	1492	12	110	0.04	2.9	1979	6.8	2.4	1.3	3416	0.00
YK	Cu-Fe-Zn	gs	68	55	1.7	28	0.3	1.3	1525	6.3	61	0.18	30	300	220	6.1	1.7	2114	3.0
			sd	60	1.7	30	0.4	1.2	1608	6.0	114	0.09	36	425	1143	11	2.1	4250	6.8
YK	Zn-Fe-Cu	ws	31	43	1.9	0.3	0.1	0.8	2476	1.5	245	0.41	18	1048	38	0.7	0.2	487	0.2
			sd	35	0.8	0.8	0.2	0.4	2275	1.4	149	0.15	20	1000	39	3.3	0.2	891	0.2
Val	Cu-Zn-Fe	gs	38	171	0.7	0.1	0.8	0.7	102	56	49	0.17	4.2	44	77	4.7	1.1	674	24
			sd	93	0.5	0.2	3.8	0.6	387	44	51	0.06	5.0	103	128	9.2	3.5	2465	50
Okt	Zn-Cu-Fe	gs	25	39	0.5	0.002	0.03	0.6	376	50	2697	0.27	1.0	585	1630	34	0.2	187	28
			sd	18	0.4	0.002	0.09	0.4	540	42	11,160	0.01	0.5	740	6772	78	0.1	180	30
TT	Zn-Cu ± Fe	ws	29	17	0.3	0.010	0.05	0.4	81	54	138	0.38	5.5	368	2.8	23	0.2	297	0.9
			sd	7.2	0.3	0.011	0.08	0.3	223	51	263	0.04	8.4	931	6.4	68	0.5	401	0.7
Alex	Zn-Cu	ws	52	15	0.2	0.023	0.4	0.6	437	26	46	0.39	1.9	278	11	2.0	0.2	307	11
			sd	19	0.2	0.044	2.3	0.7	1799	50	43	0.06	2.2	477	28	4.6	0.7	586	18
Saf	Cu-Fe ± Zn	bs	17	3.3	5.1	0.8	0.2	5.9	42	343	85	0.40	266	149	3.8	0.1	0.6	715	13
			sd	10.7	1.1	1.5	0.4	1.6	32	183	27	0.06	187	191	3.0	0.1	0.6	778	11
Saf	Cu-Fe-Zn	gs	14	4.9	0.8	1.6	1.5	2.3	5345	111	812	0.52	150	3715	14	1.0	2.9	8080	196
			sd	6.7	1.0	2.1	3.9	1.5	5746	65	586	0.05	111	4214	10	0.6	2.5	15,422	191
Saf	Zn-Cu	ws	11	0.1	0.6	0.006	0.03	0.7	25	66	197	0.52	0.9	331	3.3	1.0	0.2	10,157	0.03
			sd	0.2	0.6	0.007	0.02	0.7	46	66	185	0.02	0.6	631	4.8	0.9	0.1	22,359	0.08

Dep – massive sulfide deposits: Der – Dergamysh, Bur – Buribay, Sult – Sultanovskoye, Yb – Yubileynoye, Mol – Molodezhnoye, Uz – Uzelga, Tal – Talgan, YK – Yaman-Kasy, Okt – Oktyabrskoye, Val – Valentorskoye, TT – Tash-Tau, Alex – Alexandrinskoye, Saf – Safyanovskoye.
CH – chemical chimney type; SM – supposed chimney smoke: bs – black, gs – grey, ws – white (greyish); cs – clear; n – number of analyses; sd – standard deviation.

Numerous microinclusions of both chalcopyrite and tennantite–tetrahedrite identified in sphalerite from the sphalerite-barite–calcite–chalcopyrite chimneys of the *Uzelga-1* deposit (Fig. 12c) are responsible for Fe/Cu ratio of <0.88. The *Oktyabrskoye* quartz–barite–chalcopyrite–sphalerite chimneys contain numerous inclusions of chalcopyrite and tennantite. The tennantite inclusions provide Fe/Cu < 0.88 (Fig. 12e). Sphalerite of the *Valentorskoye* chimneys is characterized by positive correlation between Cu and Fe due to microinclusions of chalcopyrite in contrast to sphalerite with the lower Cu and Fe contents (Fig. 12e). In the latter case, sphalerite contains microinclusions of hematite thus providing Fe/Cu ratio of >0.88 (Fig. 12e). Sphalerite with Fe/Cu ratio of <0.88 encloses numerous microinclusions of tennantite and bornite (*Tash-Tau* and *Alexandrinskoye* deposits) (Fig. 12e, f). Generally, the Fe contents in sphalerite from the chimneys of other Baymak type deposits are lower than those in sphalerite from the chimneys of abovementioned Atlantic, Cyprus and Uralian types of deposits.

Sphalerite of the *Safyanovskoye* chimneys has strongly variable Cu (0.2–10 wt.%) and Fe (0.03–6.9 wt.%) contents (Fig. 12f; Table 7). In most cases, the contents yielding Fe/Cu ratios of ~0.88 are related to the inclusions of chalcopyrite. Sphalerite with Fe/Cu ratio of <0.88 contains inclusions of tennantite, enargite and covellite. Rare sphalerite with Fe/Cu ratio of >0.88, in addition to chalcopyrite, contains inclusions of isocubanite.

In the Fe–Cu plot, the fields of the data points of sphalerite from the MOR modern black smokers and diffusers associated with both serpentinites and basalts are overlapped (Fig. 12). The Fe contents are 1–13 wt.% higher in sphalerite from the MOR chimneys. Sphalerite from clear smokers contains two–three times lower Fe contents, on average (Table 8). Most analyses are characterized by Fe/Cu ratio of >0.88, i.e., the ratio that is higher than that in stoichiometric chalcopyrite. This indicates that Fe is related to both finely dispersed chalcopyrite, isocubanite and pyrrhotite microinclusions. Sphalerite characterized by Fe/Cu ratio of <0.88 ratio contains microinclusions of tennantite, digenite, covellite and bornite. The Fe contents in sphalerite from the modern grey smokers associated with dacites vary from 0.09 to 2.6 wt.% (Table 8). Despite the fact that most analyses have Fe/Cu ratio of >0.88, the content of isomorphic Fe^{2+} is most likely lower than 1 wt.%. When the Fe/Cu ratio of sphalerite is below 0.88, it contains inclusions of tennantite, covellite or bornite.

4.2.2.2. As–Sb. The sphalerite of modern chimneys collected in MOR, the most of data points display Sb/As < 1.6 that is typical for tennantite. In the island arc system, Sb/As in sphalerite are much higher than 1.6. The chimneys comprise tetrahedrite-rich fahlores (Fig. 13). This pattern is not consistent with data on the Urals chimneys.

Sphalerite of the *Dergamysh* deposit is characterized by the highest Sb concentrations (up to 3925 ppm) and low As contents (up to 86 ppm) (Fig. 13a). The Sb/As ratio commonly exceeds 1. The high ratio is likely related either to microinclusions of tetrahedrite or to isomorphic presence of Sb in structure of sphalerite (Huston et al., 1995; Ciobanu et al., 2010).

The lowest As (0.1–20 ppm) and Sb (0.1–48 ppm) contents are characteristic of sphalerite of the *Buribay* chimneys (Fig. 13b). The contents of these elements are somewhat higher in sphalerite of the *Sultanovskoye* chimneys: 37–154 ppm As, 35–115 ppm Sb. In this group of the deposits, the highest As and Sb contents are determined in sphalerite from the chalcopyrite–sphalerite–pyrite–calcite–talc chimneys of the *Yubileynoye* deposit (1–2162 ppm As; 6–2581 ppm Sb) (Table 7; Fig. 13b). The enrichment in As and Sb is apparently related to the microinclusions of tetrahedrite–tennantite and tennantite, which are abundant in sphalerite from chimneys of this deposit.

The highest As and Sb contents in sphalerite from chimneys of the deposits related to bimodal complexes reach 1 wt.% (Fig. 13c–f). The Sb/As ratio commonly attains 1.6 in sphalerite from chimneys of the deposits studied that is typical of breakpoints of tetrahedrite–tennantite. The lowest Sb/As values (<0.01) in sphalerite from the *Yaman-Kasy* chimneys are related to microinclusions of cobaltite and loellingite.

4.2.2.3. Co–Sn and Ni. In sphalerite of the modern smokers, The Co, Sn, and Ni contents decrease across the range from ultramafic- and mafic- to bimodal mafic- and felsic-hosted vent sites (Table 7; Fig. 14). This range is consistent with the same range relating to the Urals chimneys.

The composition of sphalerite from the *Dergamysh* sphalerite–chalcopyrite–isocubanite chimneys and Rainbow smokers and diffusers completely coincides with the Co–Sn plot (Fig. 14a). These elements occasionally attain economic concentrations in sphalerite from the Dergamysh deposit.

The Sn contents in sphalerite from the *Buribay*, *Sultanovskoye* and *Yubileynoye* chimneys are mostly lower than 100 ppm (Table 7; Fig. 14b). Sphalerite from the pyrite–sphalerite–chalcopyrite chimneys of the Buribay and Sultanovskoye deposits is enriched in Co, as well as sphalerite of the MOR black smokers. The Co contents (<0.1 ppm) in sphalerite from the Yubileynoye sphalerite-rich chimneys correspond to those of the modern clear smokers.

By Co (0.06–204 ppm) and Sn (1–501 ppm) contents in sphalerite, the *Molodezhnoye* chimneys are similar to the MOR black smokers (Tables 7, 8). Sphalerite from the *Uzelga-4* sphalerite–pyrite–chalcopyrite and *Uzelga-1* sphalerite–chalcopyrite chimneys are similar to that of the IAB-associated grey and clear smokers in low Co (<1 ppm) and Sn (<1–20 ppm) contents (Fig. 14c).

The Sn (3–208 ppm) and Co (0.7–125 ppm) contents from the *Yaman-Kasy* chalcopyrite-rich chimneys are much higher relative to

Table 8
Average contents of trace elements in sphalerite of chimneys from the modern vent sites (LA-ICP-MS data, ppm and %).

VS	CH	CS	n/sd	Mn	Fe%	Co	Cu%	As	Se	Ag	Cd%	Sn	Sb	Te	Au	Tl	Pb	Bi
Rb	Cu ± Ca	bs	3	15	4.0	3008	2.9	62	2.0	413	0.2	32	15	0.1	0.4	8.3	2827	0.112
			sd	0.9	1.1	1532	2.6	25	1.6	446	0.1	47	21	0.0	0.3	4.0	931	0.157
Rb	Zn-Cu-Fe	cs	50	39	5.7	888	0.5	104	1.6	992	0.3	319	85	0.1	0.6	5.4	1215	0.550
			sd	24	4.3	808	0.4	591	1.1	996	0.2	327	114	0.1	1.2	18	1670	3.169
EPR	Cu-Fe ± Zn	bs	35	105	3.4	33	0.6	209	87	176	0.3	1.0	92	0.7	0.1	0.4	849	0.014
			sd	37	1.2	23	0.7	208	65	228	0.2	2.1	72	0.7	0.3	1.4	1516	0.039
BS	Cu-Zn-Fe	bs	26	225	10.2	212	1.1	148	225	42	0.2	72	96	18	0.5	0.1	326	0.330
			sd	104	2.4	483	2.7	283	314	66	0.2	164	169	23	0.7	0.3	740	1.046
SP	Cu-Fe-Zn	bs	27	64	8.4	412	0.6	415	116	242	0.3	42	368	1.6	1.8	1.8	535	1.370
			sd	21	2.6	737	1.0	491	170	509	0.1	39	189	1.8	5.1	5.0	790	3.356
SP	Zn-Cu-Fe	cs	21	140	6.2	0.07	1.0	405	2.7	465	0.5	80	262	0.2	3.3	6.8	2779	0.011
			sd	55	3.8	0.12	1.0	428	1.9	280	0.2	49	151	0.3	3.3	13.0	3647	0.027
TM	Fe-Cu-Zn	ws	6	16	0.2	0.04	1.4	181	1.5	1962	0.4	1.9	175	0.5	52	5.6	2027	0.222
			sd	9	0.1	0.04	1.3	39	3.2	1083	0.2	1.5	171	0.7	79	6.5	1492	0.423
GR	Fe-Cu-Zn	gs	21	26	26,157	5.4	4916	64	4.4	54	3389	16	163	0.06	0.05	0.01	396	0.03
			sd	11	16,182	15	3989	84	4.4	62	1943	28	130	0.05	0.05	0.02	566	0.03
MG	Ba-Cu-Zn-Fe	gs	13	98	1.2	25	1.1	455	16	138	0.2	0.7	419	0.3	0.5	0.8	1591	0.014
			sd	44	1.1	9.2	0.8	367	11	133	0.1	0.2	132	0.3	0.7	2.3	821	0.027
LS	Cu-Fe ± Zn	bs	3	12	0.9	1.7	1.0	195	8.6	20	0.2	0.2	10	0.7	0.03	0.4	523	0.007
			sd	3.4	0.8	2.2	0.8	36	9.2	21	0.1	0.1	4	0.4	0.03	0.3	803	0.011
AS	Zn-Ba-Fe-Cu	gs	21	394	6.6	33	0.6	408	469	389	0.3	5.2	592	0.1	1.0	0.3	911	0.021
			sd	145	2.5	53	0.4	449	637	731	0.2	12	668	0.1	1.2	0.6	1049	0.052
NL	Zn-Fe-Cu	cs	20	328	0.7	0.01	0.1	200	2.2	12	0.2	0.4	207	0.1	0.02	1.0	188	0.005
			sd	151	0.3	0.01	0.2	633	1.5	33	0.1	0.7	427	0.1	0.03	3.9	526	0.006
CL	Zn-Fe-Cu	cs	3	113	0.8	0.1	2312	39	0.9	306	5821	5.0	87	0.00	0.50	0.04	458	0.000
			sd	13	0.2	0.0	1407	19	1.2	265	2104	8.2	48	0.00	0.14	0.03	263	0.000
VW	Zn-Fe-Cu	cs	15	140	2.2	3.7	0.4	18	10	18	0.5	19	54	0.04	0.7	0.1	132	0.001
			sd	24	0.4	3.9	0.4	22	4.5	13	0.2	18	50	0.06	0.7	0.1	140	0.001
SV	Cu-Fe ± Zn	bgs	14	124	2.0	14	0.9	731	18	395	0.8	1.2	1307	0.4	33	2.0	2706	16.9
			sd	38	1.0	14	0.8	851	19	412	0.5	2.1	776	0.6	37	3.1	3671	31.3
Pac	Cu ± Fe ± Zn	gs	11	72	0.3	0.5	0.3	16,168	7.7	125	0.3	0.2	328	0.5	4.5	830	23,710	0.057
			sd	43	0.2	1.5	0.5	10,810	10	139	0.2	0.1	382	0.9	6.9	1264	20,715	0.057
Pac	Ba-Zn-Fe-Cu	ws	28	45	0.3	2.1	0.2	5939	3.4	251	0.4	0.2	1404	0.2	24	144	14,915	0.003
			sd	11	0.3	1.6	0.3	5269	1.3	367	0.3	0.0	1431	0.1	24	136	12,248	0.003
Suz	Ba-Zn-Fe-Cu	ws	15	34	1.0	1.0	0.3	9728	2.9	1066	6993	0.2	1814	0.1	51	178	17,047	0.005
			sd	17	1.7	1.0	0.2	6942	1.0	1045	3822	0.0	1792	0.1	26.1	143	11,202	0.003
Hak	Zn-Ba-Fe-Cu	cs	17	1716	0.2	0.1	0.1	65	2.3	58	3427	0.3	378	0.04	0.1	0.1	178	0.003
			sd	513	0.0	0.1	0.1	58	0.9	49	440	0.1	255	0.03	0.1	0.0	355	0.002

VS – vent sites: Rb – Rainbow, EPR – East Pacific Rise 9°11′N, BS – Broken Spur, SP – Snake Pit, TM – TAG-MIR, GR – Galapagos Ridge, MG – Menez Gwen, LS – Lucky Strike, AS – Axial Seamount, NL – Northern Lau, CL – Central Lau, VW – Vienna Wood, SV – Suiyo Volcano, Pac – PACMANUS (Solwara-4), Suz – Suzette (Solwara-1); Hak – Hakurei.
CH – chemical type of a chimney; CS – supposed color of chimney smoke: bs – black; gs – grey; ws – white (greyish white); cs – clear; bgs – black or grey; n – number of analyses; sd – standard deviation.

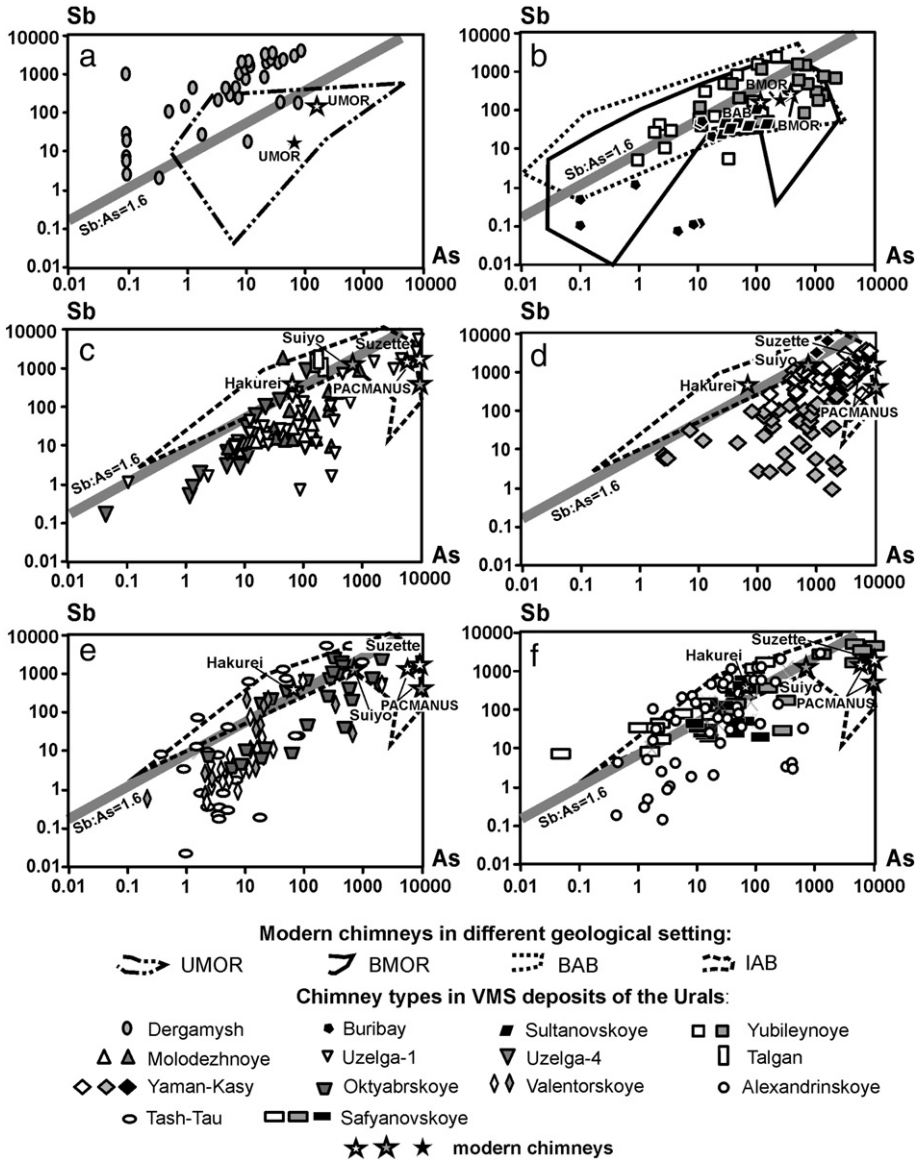

Fig. 13. Log–log plots of As vs. Sb for sphalerite of chimneys from the Urals VMS deposits and modern vent sites. The shaded line corresponds to the Sb/As ratio of 1.6, which reflects the boundary between tetrahedrite and tennantite. The enigmatically high Sb contents in sphalerite of the Dergamysh chimneys are above the field of the modern analogues. The Sb/As ratio in sphalerite of the chimneys decrease (a) in the range from ultramafic and mafic to bimodal mafic-hosted deposits due to increasing amount of inclusions of tennantite, arsenopyrite (d – Molodezhnoye, Uzelga-4), loellingite and cobaltite (d – Yaman-Kasy). The sphalerite of chimneys related to the bimodal felsic sequences (d – Uzelga-1; e – Oktyabrskoye, Valentorskoye, Tash-Tau; e – Alexandrinskoye and Safyanovskoye) (f) is enriched in tennantite and, to a lesser extent, in tetrahedrite–tennantite, as well as their modern arc-related analogues with inclusions of realgar and orpiment. The color of black, grey and white symbols corresponds to black, grey and white (or clear) smokers, respectively. The line counters are field of data points of chalcopyrite composition for chimneys from different host rocks and of geological setting: UMOR – ultramafic-rich mid-ocean ridge; BMOR – basalt-rich mid-ocean ridge; HS – hot spots of the mid-ocean ridge; BAB – basalt basement of back-arc basins; IAB – bimodal mafic- and felsic-hosted vent sites in intra-arc or proximal arc basins.

the IAB-associated grey and clear smokers. The fields of the data points of sphalerite in the Co–Sn plot are closer to the field of the modern black smokers (Tables 7, 8). The Co content is far below in sphalerite-rich chimneys (0.01–3 ppm) (Fig. 14d). These chimneys are considered to be the white or clear smokers (Maslennikov et al., 2009).

The low Co (0.001–0.1, rarely, up to 2 ppm) and Sn (0.01–7, rarely, up to 33 ppm) contents in sphalerite of the *Oktyabrskoye*, *Valentorskoye*, *Tash-Tau* and *Alexandrinskoye* quartz–pyrite–chalcopyrite chimneys correspond to that from modern white and clear smokers (Tables 7, 8; Fig. 14e, f).

In the *Safyanovskoye* chimneys, sphalerite is enriched in Sn (up to 454 ppm) and depleted in Co (0.1–6 ppm). The Sn (0.5–1.6 ppm) and Co (1–20 ppb) contents are much lower in sphalerite from the sphalerite-rich chimneys similarly to the modern clear smokers (Fig. 14f).

In general, the Co and Sn contents decrease in the range of chimneys under the increase in amount of felsic volcanic rocks. Within each deposit, the Co and Sn contents decrease with increasing amount of barite and sphalerite in chimneys and disappearance of isocubanite and pseudomorphic pyrite after pyrrhotite.

The highest Ni contents (20–60 pm) and very high Co/Ni ratios (10–80) are typical of sphalerite from the Dergamysh deposit in comparison with other deposits (Table 7). The lower Ni contents (0.01–0.09 ppm) and Co/Ni ratios (<0.1) are characteristic for sphalerite of chimneys from some deposits related to Baymak type (Uzelga-1, Talgan, Tash-Tau, Oktyabrskoye) (Table 7). Sphalerite from the Uralian and Cyprus type of deposits display intermediate Ni contents (0,01–1 ppm) at Co/Ni ratio of >5–80. Similar consistent pattern is registered in modern smokers (Table 8).

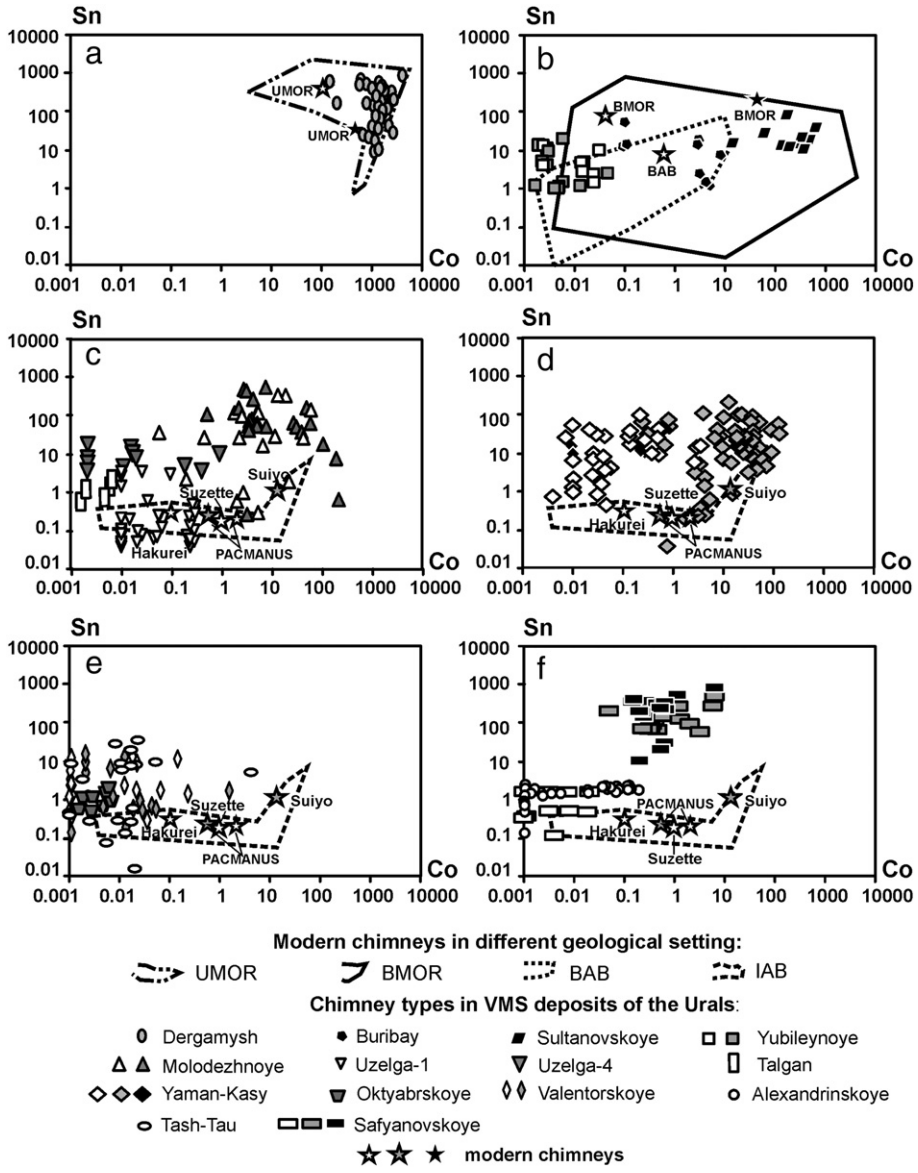

Fig. 14. Log–log plots of Sn vs. Co for sphalerite of chimneys from the Urals VMS deposits and modern vent sites. The Sn and Co contents decrease in sphalerite of chimneys in the range from ultramafic and mafic to bimodal mafic- and felsic-hosted VMS deposits. The analogues of black and grey smokers yield higher contents of these elements in comparison with those of white or clear smokers. The color of black, grey and white symbols corresponds to black, grey and white (or clear) smokers, respectively. The line counters are field of data points of chalcopyrite composition for chimneys from different host rocks and of geological setting: UMOR – ultramafic-rich mid-ocean ridge; BMOR – basalt-rich mid-ocean ridge; HS – hot spots of the mid-ocean ridge; BAB – basalt basement of back-arc basins; IAB – bimodal mafic- and felsic-hosted vent sites in intra-arc or proximal arc basins.

4.2.2.4. Au–Ag. Sphalerite of modern chimneys is enriched in Ag relative to native gold and even electrum (Fig. 15; Table 8).

Sphalerite from the *Dergamysh* chalcopyrite–isocubanite–sphalerite chimneys is characterized by highly variable Au and Ag contents. A positive correlation between Au and Ag (Fig. 15a) is consistent with the occurrence of microinclusions of electrum. However, the Au/Ag ratios are much lower than shaded area relating to composition of native gold and electrum.

The low Au/Ag ratio is characteristic of both sphalerite from the *Buribay*, *Sultanovskoye*, and *Yubileynoe* chimneys and modern smokers and diffusers associated with MOR and BAB basalts (Fig. 15b). Some data points of sphalerite from chimneys of the Urals deposits hosted by felsic volcanic rocks are observed in the compositional field of native gold and electrum in the Ag/Au plot (Fig. 15c–f). The larger part demonstrates the low Au/Ag values due to that, in addition to native gold, sphalerite of many chimneys contain abundant Ag-carriers such as galena, hessite, Ag-bearing tennantite and, occasionally (Alexandrinskoye), bornite.

4.2.3. Colloform pyrite

4.2.3.1. Co–Ni. The Co (1321–6400 ppm) and Ni (84–641 ppm) contents in the colloform pyrite of the *Dergamysh* pyrite–chalcopyrite chimneys are much higher than that of the Rainbow clear smokers and diffusers (Tables 9, 10; Fig. 16a). Colloform pyrite of the Dergamysh chimneys is characterized by elevated Co/Ni ratio (8–30).

Colloform pyrite from the *Buribay*, *Sultanovskoye* and *Yubileynoe* chimneys contains lower Co (0.01–359 ppm) and Ni (3–174 ppm) than that from the Dergamysh deposit (Fig. 16a). The highest Co (up to 359 ppm) contents are determined in chalcopyrite from the quartz–pyrite–chalcopyrite chimneys. Relatively low Co (<10 ppm) contents are characteristic of colloform pyrite in the talc–calcite–

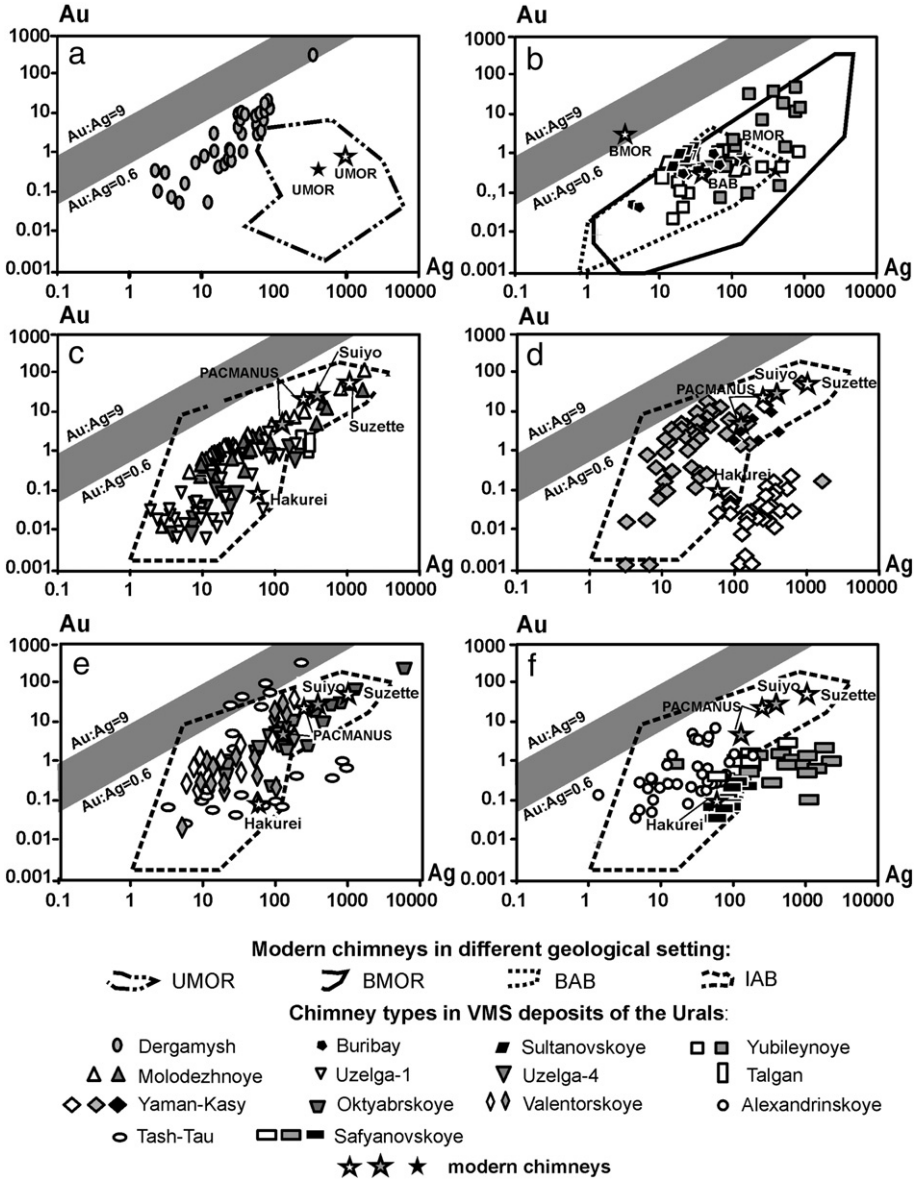

Fig. 15. Log–log plots of Ag vs. Au for sphalerite of chimneys from the Urals VMS deposits and modern vent sites. In comparison with composition of native gold and electrum microinclusions, the enigmatically low Au/Ag ratios are typical of modern smokers and their Uralian analogues, as well. The color of black, grey and white symbols corresponds to black, grey and white (or clear) smokers, respectively. The shaded line counters are field of data points of chalcopyrite composition for chimneys from different host rocks and of geological setting: UMOR – ultramafic-rich mid-ocean ridge; BMOR – basalt-rich mid-ocean ridge; HS – hot spots of the mid-ocean ridge; BAB – basalt basement of back-arc basins; IAB – bimodal mafic- and felsic-hosted vent sites in intra-arc or proximal arc basins.

chalcopyrite–pyrite, talc–calcite–sphalerite–chalcopyrite and pyrite–sphalerite chimneys of the Yubileynoe deposit. The Co/Ni ratio in colloform pyrite from these chimneys is the lowest (0.001–0.01) in comparison with sphalerite from other basalt-hosted deposits.

Colloform pyrite from the *Molodezhnoye* pyrite–sphalerite–chalcopyrite chimneys is characterized by high Co contents (90–1601 ppm) and high Co/Ni ratio (2–140), which is more typical of the MOR modern black smokers. The Co contents are slightly lower in calcite–pyrite–chalcopyrite chimneys of the *Uzelga-4* deposit (Table 9; Fig. 16b).

The Co and Ni contents in colloform pyrite from the *Yaman-Kasy* pyrite–chalcopyrite and sphalerite–marcasite–chalcopyrite chimneys are 0.4–917 and 2–171 ppm, respectively. The Co/Ni ratio varies from 0.01 to 49 at dominant Co/Ni ratio of >1 (Fig. 16b). The Co contents are lower in the chalcopyrite–quartz–barite–pyrite–sphalerite chimneys (0.01 to 49) at dominant Co/Ni ratio of <1.

The Co and Ni contents in colloform pyrite from most chimneys of the Baymak type deposits (*Oktyabrskoye*, *Valentorskoye* and *Alexandrinskoye*) belong to the field of the modern grey and clear smokers from the back-arc and intra-arc basins (Fig. 16b, c). As a rule, the Co contents in colloform pyrite of these deposits are the lowest. The Co/Ni ratio is commonly lower than 0.1.

Colloform pyrite of the *Safyanovskoye* chalcopyrite-rich chimneys corresponded to the black smoker chimneys by Se content is enriched in both Co and Ni (Table 9; Fig. 16c). Its Co/Ni ratio varies from 0.01 to 7.

4.2.3.2. Sb–As. Colloform pyrite from the *Dergamysh* chalcopyrite-rich chimneys has the lowest As content (99–193 ppm) similar to those of colloform pyrite from the modern black smokers associated with ultramafic rocks (Table 9; Fig. 17a). The Sb (75–155 ppm) contents in the *Dergamysh* colloform pyrite are higher by one–two orders of magnitude than that of colloform pyrite from the Rainbow diffusers. The As content

Table 9
Average contents of trace elements in colloform pyrite of chimneys from the Urals VMS deposits (LA-ICP-MS data, ppm).

Dep	CH	SM	n/sd	Mn	Co	Ni	Zn	As	Se	Ag	Sn	Sb	Te	Au	Tl	Pb	Bi
Der	Cu–Fe	bs	10	272	2337	440	207	133	28	15	2.8	109	32	1.3	14	118	12
			sd	278	803	105	245	38	11	6	3.4	31	23	0.3	4	58	8.7
Der	Fe-Ca-Cu	cs	14	122	1292	170	574	117	46	24	20	115	3.0	0.9	0.8	330	2.4
			sd	93	356	38	640	58	17	10	7.7	44	3.2	0.3	1.3	111	2.7
Bur	Cu-Fe ± Zn	bs	18	83	228	20	1549	285	68	60	0.5	46	107	4.4	5.2	485	33
			sd	48	175	10	2028	79	34	21	0.3	13	37	2.3	4.8	234	10
Sult	Cu-Fe ± Zn	bs	19	61	346	8.9	3324	1802	74	29	1.4	128	30	3.3	18	1907	11
			sd	51	700	5.6	3653	632	38	15	0.8	68	45	1.4	17	791	38
Yub	Cu-Fe	bs	16	383	83	36	3453	550	59	105	0.7	47	111	8.9	26	480	38
			sd	236	111	20	2567	221	76	88	0.5	36	104	6.8	17	254	24
Yub	Cu-Fe-Zn	gs	19	746	0.2	27	4186	917	69	209	0.8	85	73	7.2	66	12,448	19
			sd	543	0.2	18	5806	531	93	117	0.3	57	56	7.5	103	17,634	25
Yub	Zn-Fe-Cu	ws	16	413	0.3	37	1709	751	13	156	1.4	166	44	5.4	23	1957	0.09
			sd	238	0.2	34	3386	417	14	37	0.3	61	14	1.6	43	2529	0.06
Mol	Cu-Fe-Zn	gs	13	1146	377	95	2753	6350	78	878	1.1	163	898	26	12	4632	38
			sd	1255	446	143	5036	2870	81	1072	1.3	96	1194	40	11	5462	29
Uz-4	Cu-Fe-Zn	gs	11	187	41	25	1371	3717	164	209	0.2	235	303	6.8	8.0	3802	2.5
			sd	286	48	21	2312	2670	176	91	0.2	228	247	6.3	18	5488	2.8
YK	Cu-Fe	bs	8	693	1.1	39	1106	1675	9.2	112	5.6	578	11	7.7	35	3482	0.05
			sd	300	0.7	56	828	831	5.4	47	2.0	229	13	2.6	32	1240	0.08
YK	Cu-Fe-Zn	gs	27	543	105	18	2430	2327	14	154	4.7	872	1043	36	11	3290	6.1
			sd	785	179	23	3322	1647	19	134	4.2	957	1684	32	9.5	1686	10
YK	Zn-Fe-Cu	ws	10	25	6.8	6.2	6379	7667	2.6	3645	0.8	395	2942	1.5	12	6465	10
			sd	23	14	3.5	7957	6076	1.5	3037	0.7	289	2207	1.7	10	8716	12
Okt	Zn-Cu-Fe	gs	5	416	6	49	12,116	1827	54	8924	0.1	24	5191	46	16	1155	75
			sd	167	2.4	15	18,841	1175	17	16,874	0.1	19	9554	25	19	683	43
Val	Cu-Zn-Fe	gs	5	2297	0.4	11	5600	1810	27	139	0.2	38	233	52	9.5	626	120
			sd	906	0.4	6.7	1485	626	8.3	197	0.1	55	262	100	2.5	479	170
Tal	Cu-Zn-Fe	ws	7	47	0.1	11	3016	19,872	1.9	294	0.7	2926	22	13	43	7335	114
			sd	19	0.0	7.1	3141	11,517	1.6	204	1.6	1518	8.0	11	27	8236	69
Saf	Cu-Fe ± Zn	bs	12	585	266.7	157	3228	6722	53	403	18	818	7.1	6.8	128	2238	29
				424	261	166	2791	2938	37	367	18	589	5.6	5.6	120	1339	42

Dep – massive sulfide deposits: Der – Dergamysh, Bur – Buribay, Sult – Sultanovskoye, Yb – Yubileynoye, Mol – Molodezhnoye, Uz – Uzelga, Tal – Talgan, YK – Yaman-Kasy, Okt – Oktyabrskoye, Val – Valentorskoye, Saf – Safyanovskoye.
CH – chemical chimney types; CS – supposed chimney smoke: bs – black, gs – grey, ws – white (greyish); cs – clear; n – number of analyses; sd – standard deviation.

in colloform pyrite from the *Buribay*, *Yubileynoye* and *Sultanovskoye* is higher by one order of magnitude (225–2525 ppm) than that in the Dergamysh colloform pyrite (Table 9; Fig. 17a). The As and Sb contents are even higher in colloform pyrite of chimneys from the bimodal rhyolite–basalt and basalt–rhyolite complexes (*Yaman-Kasy*, *Molodezhnoye*, *Uzelga*, *Valentorskoye*, *Oktyabrskoye* and *Alexandrinskoye*) (Fig. 17b, c). In the As–Sb plot, the data points of this colloform pyrite occur in the field of grey smokers.

4.2.3.3. Au–Ag. Colloform pyrite from the *Dergamysh* pyrite–chalcopyrite and chalcopyrite–calcite–pyrite chimneys is characterized by low Au (0.6–1.5 ppm) and Ag (8–39 ppm) contents (Table 6). In the Au–Ag plot, its composition corresponds to the upper part of the fields of colloform pyrite from the modern smokers associated with serpentinite (Fig. 18a).

The Au (1–10 ppm, rarely, up to 29 ppm) and Ag (21–100 ppm, rarely, up to 433 ppm) contents in colloform pyrite from sphalerite–pyrite–chalcopyrite chimneys of the *Buribay*, *Sultanovskoye* and *Yubileynoye* deposits correspond to the maximum values of the modern white and clear smokers (Tables 9, 10; Fig. 18b).

The Au and Ag contents are high in colloform pyrite from the chalcopyrite-rich chimneys of the *Molodezhnoye*, *Uzelga*, *Yaman-Kasy*, *Safyanovskoye* and *Oktyabrskoye* deposits (Table 9, Fig. 18c, d). Judging from the positive correlation between Ag, Au and Te, colloform pyrite contains microinclusions of sylvanite and hessite in addition to nanoinclusions of native gold. The highest Ag contents (av. 3645 ppm) were determined in colloform pyrite from the Yaman-Kasy sphalerite-rich chimneys. Positive correlation between Ag and Te is indicative of microinclusions of hessite in these chimneys (Maslennikov et al., 2009, 2013). The data points of colloform pyrite from all chimneys correspond to maximum values typical of the modern grey smokers from the island-arc basins.

5. Discussion

5.1. Mineralogical comparison with modern chimneys

In the mid-ocean ridges, a diversity of black, grey, white and clear smokers is formed at the vent sites. Black smoker activity starts, when the hydrothermal fluids can produce enough sulfide particles, mainly, pyrrhotite, at temperatures above 300 °C. Some black smokers are grey or dark grey probably due to dilution or oxidation of the hot hydrothermal fluids. At temperatures between 100 and 300 °C, the white smoker chimneys begin to form and silica, anhydrite and barite precipitate from the hydrothermal fluids quenched by cold seawater. They are formed at the first stage, when the fluids are not hot enough to carry sufficient metals and sulfur or, alternatively, in a high-temperature system, where conductive cooling of subseafloor mixing results in loss of metals at depth (von Damm et al., 1985; Tivey et al., 1995; Hannington et al., 1995). Some of white smokes are greyish white (Halbach et al., 2003) indicative of some sulfide particulate in the vent fluid. In some low-temperature chimneys or diffusers, the fluids emanated from vent orifice are absolutely clear. Sphalerite- and/or pyrite-rich clear smokers with diffuse venting are commonly formed at the later stage of chimney growth (Fouquet et al., 1993; Bogdanov et al., 2006b).

Some textures and minerals revealed in chimneys from the Dergamysh deposit have been described in modern chimneys associated with serpentinites. Pseudomorphic chalcopyrite after colloform pyrite, pyrrhotite and pseudomorphic marcasite and pyrite after subhedral pyrrhotite are found in the Dergamysh and modern

Table 10
Average contents of trace elements in colloform pyrite of chimneys from the modern vent sites (LA-ICP-MS data, ppm).

VS	CH	SM	n/sd	Mn	Co	Ni	As	Se	Ag	Sn	Sb	Te	Au	Tl	Pb	Bi
Rb	Zn-Cu-Fe	cs	9	47	1200	1	31	0.5	18	1.1	2	0.04	0.4	14	81	0.001
			sd	59	1142	0.5	39	0.3	43	2.4	2	0.05	0.5	6	76	0.003
EPR	Cu-Fe ± Zn	bs	30	991	45	10	425	42	24	0.4	2	2.98	0.1	33	301	0.011
			sd	51	51	11	294	57	76	30	0.7	1.7	6.6	0.1	52	311
AS	Zn-Ba-Fe-Cu	gs	7	1084	5	10	539	9	150	0.1	11	0.03	0.8	137	405	0.006
			sd	585	11	11	200	9	320	0.1	20	0.02	0.6	74	495	0.008
BS	Cu-Zn-Fe	bs	17	584	81	3	340	5	14	0.3	2	0.10	2.1	111	401	0.010
			sd	263	131	1	195	8	21	0.3	2	0.15	2.0	110	451	0.013
TM	Fe-Cu-Zn	ws	3	324	0.03	5	133	1	196	1.3	40	0.01	5.7	40	398	0.006
			sd	458	0.02	5	62	0	178	1.2	37	0.00	6.8	22	201	0.004
SP	Cu-Fe-Zn	bs	5	339	15	7	481	2	2	0.4	1	0.15	1.0	119	208	0.004
			sd	69	20	5	266	1	3	0.5	1	0.14	0.3	110	189	0.003
SP	Zn-Cu-Fe	cs	3	693	0.2	3	311	1	80	0.5	9	0.34	2.4	43	904	0.010
			sd	404	0.2	1	148	1	46	0.5	6	0.07	0.7	26	477	0.007
LS	Cu-Fe ± Zn	bs	4	1156	345	9	271	14	20	0.1	5	0.13	0.9	64	300	0.001
			sd	496	507	3	52	19	9	0.1	5	0.13	0.4	26	106	0.001
GR	Fe-Cu-Zn	gs	28	126	3946	3.1	846	23	20	1.0	2.2	0.38	0.16	14.1	151	0.8
			sd	1976	6716	2.8	78	25	12	0.9	2.3	0.50	0.13	26.0	190	1.3
MG	Ba-Cu-Zn-Fe	gs	6	1577	25	5	663	13	168	0.3	11	0.47	0.6	333	1623	0.005
			sd	610	19	3	616	21	98	0.1	16	0.70	0.5	151	681	0.006
VW	Zn-Fe-Cu	cs	18	2346	0.2	10	798	2	75	0.4	2	0.09	4.9	705	1234	0.002
			sd	1351	0.3	3	709	1	118	0.1	3	0.12	5.6	815	1092	0.002
NL	Zn-Fe-Cu	cs	13	11,039	0.1	27	1256	2	61	0.1	32	0.07	0.5	1342	1350	0.002
			sd	3447	0.1	24	1011	1	14	0.1	29	0.13	0.2	941	979	0.003
CL	Zn-Fe-Cu	cs	7	109	0.05	6.0	120	0.8	65	2.7	4.6	0.04	2.2	77	483	0.001
			sd	33	0.04	5.7	84	0.9	41	3.9	6.5	0.02	1.7	68	367	0.001
SV	Cu-Fe ± Zn	bgs	7	2624	6.7	70	4250	4	123	0.1	12	0.12	3.9	1512	1155	0.160
			sd	1622	7.0	56	1276	2	212	0.1	4	0.13	2.0	432	350	0.094
Pac	Cu ± Fe ± Zn	gs	21	197	0.1	7	3851	2	173	0.1	33	0.39	32.6	705	1674	1.456
			sd	96	0.1	6	2420	1	141	0.1	45	0.57	50.8	702	1963	4.524
Pac	Ba-Zn-Fe-Cu	ws	16	480	29	13	10,801	2	160	0.1	204	0.15	7.5	3478	3478	0.002
			sd	285	39	8	6505	2	326	0.0	525	0.25	14.0	4815	7020	0.002
Suz	Ba-Zn-Fe-Cu	ws	9	312	6	24	8443	3	528	0.1	210	0.09	19.4	1001	3710	0.001
			sd	164	14	12	5697	2	888	0.0	426	0.08	34.5	1079	5974	0.001

VS – vent sites: Rb – Rainbow, EPR – East Pacific Rise 9°11′N, BS – Broken Spur, SP – Snake Pit, TM – TAG-MIR, GR – Galapagos Ridge, MG – Menez Gwen, LS – Lucky Strike, AS – Axial Seamount, NL – Northern Lau, CL – Central Lau, VW – Vienna Wood, SV – Suiyo Volcano, Pac – PACMANUS (Solwara-4), Suz – Suzette (Solwara-1).
CH – chemical type of a chimney; SM – supposed color of chimney smoke: bs – black; gs – grey; ws – white (greyish white); cs – clear; bgs – black or grey; n – number of analyses; sd – standard deviation.

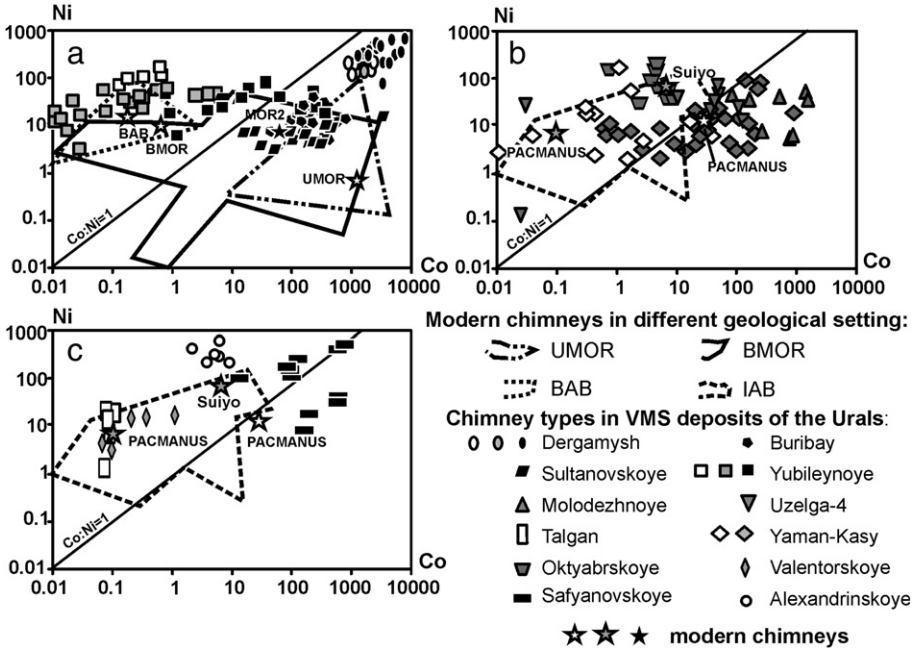

Fig. 16. Log–log plots of Co vs. Ni for colloform pyrite from chimneys from the Urals VMS deposits and modern vent sites. Colloform pyrite of ultramafic-associated modern smokers displays much higher Co contents in comparison with smokers associated with intra-arc and back-arc basins. The Co contents are highly variable in colloform pyrite of the MORB-associated modern smokers. Colloform pyrite of most ancient analogues of black smokers associated with ultramafic (Dergamysh), mafic (Buribay) and bimodal mafic (Sultanovskoye) sequences is characterized by the higher Co contents and Co/Ni ratio (>0.1) in comparison with most white and/or clear smokers. The grey smoker analogues display the intermediate position. The color of black, grey and white symbols corresponds to black, grey and white (or clear) smokers, respectively. The line counters are field of data points of chalcopyrite composition for chimneys from different host rocks and of geological setting: UMOR – ultramafic-rich mid-ocean ridge; BMOR – basalt-rich mid-ocean ridge; HS – hot spots of the mid-ocean ridge; BAB – basalt basement of back-arc basins; IAB – bimodal mafic- and felsic-hosted vent sites in intra-arc or proximal arc basins.

chimneys. Isocubanite is common at the Dergamysh deposit in contrast to Y-phases typical of the modern black smokers (Rainbow vent site). In contrast to modern black and clear smokers, bornite, diagenite, Co-Ni pentlandite, tellurides and various native metals (Table 4) are absent in chimneys from the Dergamysh deposit. The Co-bearing pyrite, electrum and cassiterite are present however.

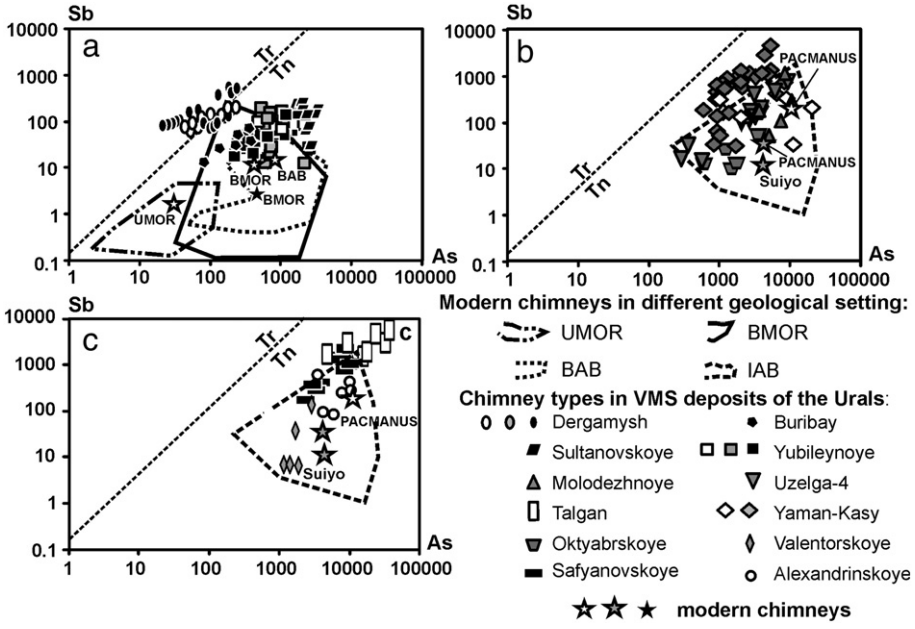

Fig. 17. Log–log plots of Sb vs. As for colloform pyrite of chimneys from the Urals VMS deposits and modern vent sites. In colloform pyrite of modern smokers, the As and Sb contents increase with increasing amount of felsic host rocks. The data points of the Urals chimneys are mostly located in the fields of modern chimneys except for the Dergamysh chimneys, which display much higher Sb contents. The color of black, grey and white symbols corresponds to black, grey and white (or clear) smokers, respectively. The line counters are field of data points of chalcopyrite composition for chimneys from different host rocks and of geological setting: UMOR – ultramafic-rich mid-ocean ridge; BMOR – basalt-rich mid-ocean ridge; HS – hot spots of the mid-ocean ridge; BAB – basalt basement of back-arc basins; IAB – bimodal mafic- and felsic-hosted vent sites in intra-arc or proximal arc basins.

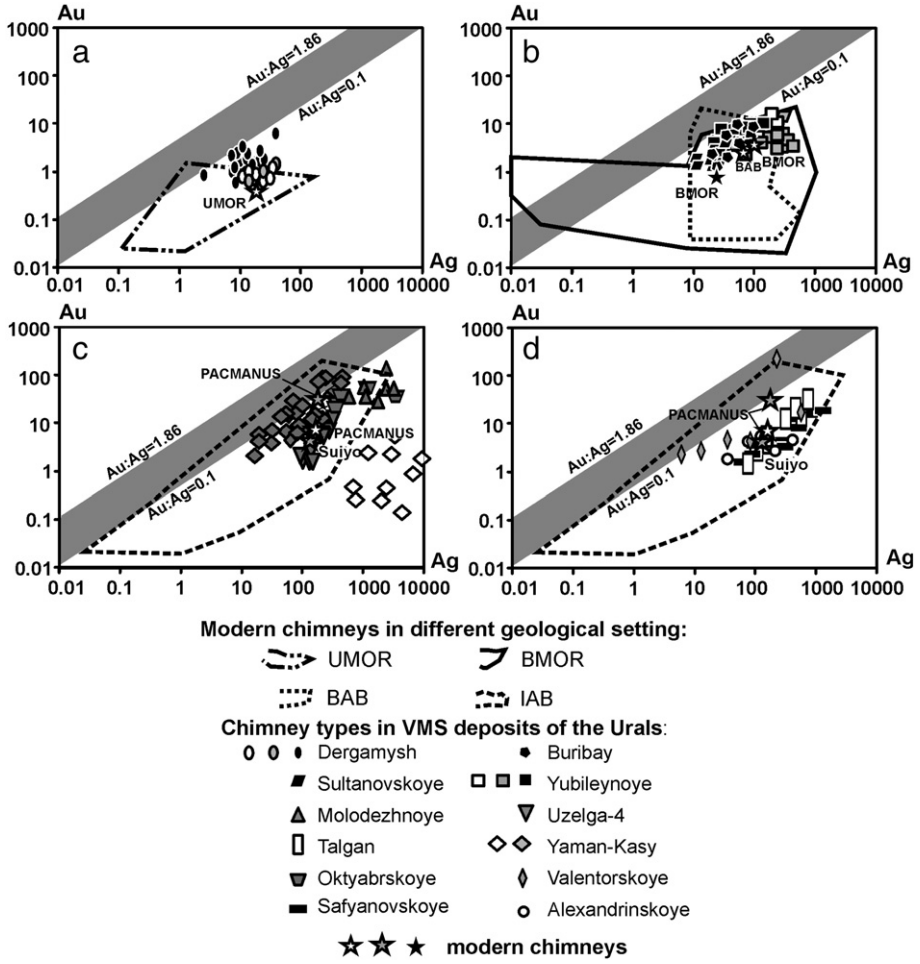

Fig. 18. Log–log plots and Au vs. Ag for colloform pyrite of chimneys from the Urals VMS deposits and modern vent sites The data points of colloform pyrite from the Urals chimneys correspond to the maximum values of modern smokers associated with corresponding host rocks. The Au and Ag contents increase in colloform pyrite of modern and the Urals chimneys in the range from ultramafic and mafic to felsic host rocks. The color of black, grey and white symbols corresponds to black, grey and white (or clear) smokers, respectively. The line counters are field of data points of chalcopyrite composition for chimneys from different host rocks and of geological setting: UMOR – ultramafic-rich mid-ocean ridge; BMOR – basalt-rich mid-ocean ridge; HS – hot spots of the mid-ocean ridge; BAB – basalt basement of back-arc basins; IAB – bimodal mafic- and felsic-hosted vent sites in intra-arc or proximal arc basins.

Some textures of the chimney fragments from the Buribay deposit are similar to those of black smokers from the basalt-hosted MORs (e.g., EPR) and mature back-arc (e.g., Fiji) basins. Black smokers have a typical mineral zonation of chimneys (Graham et al., 1988). The presence of the outer anhydrite wall with minor sulfides and hematite and their well-developed chalcopyrite- and isocubanite-lined conduit is the characteristic feature precisely of black smoker vents (Haymon, 1983). In older chimneys, anhydrite eventually dissolves in ambient cold seawater. Pyrrhotite is also abundant in some black smokers, but, in older chimneys, it tends to be replaced by marcasite and pyrite, which are more stable in seawater (Hannington et al., 1995). The outer wall of most black smokers is overgrown by crusts of colloform pyrite. Colloform pyrite, bladed chalcopyrite and pseudomorphic pyrite after pyrrhotite are typical of chimney fragments from the Buribay deposit. Isocubanite with lattice (exsolution) texture, bornite and barite, as well as silica-rich chimneys, are absent from this deposit thus far. In modern black smokers, silica or barite are generally lost in the hydrothermal plume (Hannington et al., 1995). Modern black smokers associated with basalts from fast-spreading ridges (EPR) (Scott, 1997) are poor in respect to the accessory minerals, similar to the chimneys from Buribay deposit and ancient Cyprus type of VMS deposits (Oudin and Constantinou, 1984; Little et al., 1999). Invisible Bi-tellurides only detected by LA-ICP-MS (this study) were found in euhedral pyrite of black smokers from the Broken Spur vents site.

Grey to greyish white barite–sphalerite–chalcopyrite smokers occur in the hot spot-related vent sites (Axial Seamount, Lucky Strike, Menez Gwen) (Hannington and Scott, 1988; Bogdanov et al., 2006b). In contrast to black smokers, rare galena, native gold, tetrahedrite–tennantite, jordanite and Pb-, As-, Sb-sulfosalts were occasionally found associated with the greyish white or grey smokers (Halbach et al., 2003) especially in assemblage with sphalerite, opal and barite (Fouquet et al., 1993; Scott, 1997; Halbach et al., 2003; Lein et al., 2003; Bogdanov et al., 2015). No this rare mineral assemblage was found in chimneys from the Buribay deposit.

In the Urals type of the deposits, all types of chimneys contain, at least, two zones, which mark the centrifugal external (zone A) and the centripetal internal (zones B, C) growth zone. The chalcopyrite of zone B may have a rhythmic structure evidently reflected the episodic character of hydrothermal activity. This two-fold structure is typical of many chimneys of modern black smokers (Haymon, 1983; Graham et al., 1988; Hannington and Scott, 1988; Halbach et al., 1993). It is suggested that two layers show opposite growth directions from the boundary layers between zones A and B. Successive layers were formed in response to the interaction of cold oxidized seawater and hot hydrothermal fluids carrying H_2S and dissolved metals (Graham et al., 1988). The textures of sulfides in the outer part of zone A are very fine-grained, suggesting that they have grown rapidly by quenching of hot fluids interacting with cold seawater. In the inner part of zone A, coarse-grained cubic pyrite may be recrystallized to early fine-grained pyrite.

Vuggy aggregates of botryoidal and dendritic pyrite grow outwards from this zone, suggesting that chimneys had highly permeable outer walls. There is little evidence in the ancient chimney material for the initial shell of anhydrite that characterizes modern chimney growth. However, relict bladed pyrite textures here are interpreted to replace crystals of subhedral pyrrhotite. This texture was described in some modern chimneys (Peter and Scott, 1988; Marchig and Rösch, 1988; Paradis et al., 1988) and ores from the Urals type of the deposits (Maslennikov et al., 2009, 2013). The pseudomorphs contain relict inclusions of pyrrhotite and display incomplete cleavages in pyrite characteristic of former pyrrhotite crystals (Zhabin and Samsonova, 1975). The pyrite net veining contour rim and porous textures are likewise typical of pseudomorphic pyrite after pyrrhotite crystals (Zierenberg et al., 1993). The amount of chalcopyrite increases toward the inner rim of zone A, where euhedral coarse-grained pyrite is the main phase. Euhedral pyrite can contain inclusions of relict pyrrhotite. Sphalerite and marcasite are rare or absent in zone A of chalcopyrite–pyrite chimneys but are abundant in quartz-rich varieties. The boundary between zone A and adjacent zone B is distinctive, marked by the disappearance of the granular aggregates of pyrite. Silica is ubiquitous as a matrix phase in numerous chimney fragments. The broad sulfide zonation and specific location of Te-bearing phases in the studied chimneys can be interpreted in terms of extreme gradients of temperature and oxygen–sulfur fugacity across the vent chimney walls as a result of interaction between high-temperature hydrothermal fluid in the central conduit of the chimney and cold seawater outside the external layers. This idea points to increased oxidation state of the fluids from Cu–Fe to Zn-rich chimneys due to subseafloor and seafloor modification processes (Maslennikov et al., 2009, 2013). Thus, the presence of abundant colloform and biomorphic pyrite, relict pyrrhotite, pseudomorphic pyrite and marcasite after euhedral pyrrhotite, isocubanite and altaite, which indicates the low-sulfidation condition, are typical features of chimneys from the Urals type of the deposits.

The chimneys from the Brothers volcano (de Ronde et al., 2011; Berkenbosch et al., 2012) and probably PACMANUS vent sites are possible analogues of those of the Urals type of the deposits because of abundant tellurides in chalcopyrite from the dark grey smokers. The vent sites are formed on andesites, andesitic dacite lavas and hyaloclastites surrounded by basalts and basaltic andesites. These sequences are typical host rocks of subtype U3 of the Urals type of the deposit or those transitional to Baymak type (Oktyabrskoye and Valentorskoye deposits). The chalcopyrite–barite–pyrite chimneys from the Lahanos VMS deposit (Pontides) with kawazulite, hessite, native gold and wittechenite are most likely Mesozoic analogues of these telluride-rich modern and Urals chimneys (Revan et al., 2014). Samples from the Suiyo volcano are considered to be the first example of the Kuroko type of sulfide mineralization (Watanabe and Kajimura, 1994; Ishibashi and Urabe, 1995) and probably examples of chalcopyrite chimneys from some Baymak type of deposits (Tash-Tau and Talgan). Sphalerite–chalcopyrite–barite chimneys from the Alexandrinskoye and Uzelga-1 deposits could be similar with greyish white to clear smokers from dacite/rhyodacite-hosted PACMANUS vent site in the Eastern Manus back-arc basin. This chimneys lack tellurides, except for rare hessite, and contain galena–tennantite assemblage with native gold. No realgar, orpiment and iordanite identified in modern chimneys (e.g., Marumo et al., 2008; Berkenbosch et al., 2012; Monecke et al., 2016) were found in those from the Urals and Pontides deposits.

Black and clear smokers from the Okinawa Trough (the nascent intracontinental back arc basin) are the anticipated analogues of chimneys from the Safyanovskoye deposit. The basement of the Okinawa Trough, as well as Safyanovskoye deposit, comprises dacites, rhyolites, andesites, andesitic basalts and organic-rich sediments underlain by rifted continental crust (Herzig and Hannington, 1995, 2000; Glasby and Notsu, 2003; Bogdanov et al., 2006b). Submarine hydrothermal fluid in the trough is strongly influenced by interaction with organic matter of sediment, which results in high alkalinity and high CO_2, N_2O, thermogenic CH_4, H_2 and NH^{4+} concentrations (Zengqian and Qiling, 1998; Glasby and Notsu, 2003). Methane and N_2 detected by gas chromatography are common in fluid inclusions of barite from the Safyanovskoye deposit (Safina et al., 2016). Galena–tetrahedrite assemblage with native gold typical of the sphalerite–barite–chalcopyrite chimneys of the Safyanovskoye deposit is similar, probably, with grey clear smokers of the Hakurei modern vent site. In chalcopyrite-rich chimneys of the deposit, arsenopyrite, enargite, Pb–As sulfosalts, terahedrite and chalcopyrite intergrowths with isocubanite occur, as well as in the Okinawa Trough black smokers (Lüders et al., 2001). However, no orpiment, cinnabar, realgar, native silver, stibnite, kermesite and enargite (Halbach et al., 2003; Marumo and Hattori, 1997; Glasby and Notsu, 2003) were found in the chimneys from the Safyanovskoye deposit. At the same time, no hessite, stannoidite, mawsonite and glaucodot typical of the Safyanovskoye chimneys were found in the Okinawa Trough vent sites. The presence of Bi-tellurides, sulfoarsenides and stannite in the chalcopyrite–pyrrhotite–barite–sphalerite–chalcopyrite chimneys from the Escanaba Trough reflect the influence of footwall organic-rich sedimentary rocks (Zierenberg et al., 1993). Sulfoarsenides, Bi-tellurides, and Cu–Sn-sulfides in the Safyanovskoye chimneys support the same idea. The common occurrence of low sulfidation (pyrrhotite, isocubanite, arsenopyrite) and high sulfidation (galena, sulfosalts, barite) assemblages are common conflicting characteristic of the modern and ancient chimneys formed on the sediment-rich basements.

In general, the Urals chimneys and modern smokers are characterized by following similar textures: (1) colloform pyrite in zone A (Fig. 19a1 and a2); (2) dendritic marcasite and pyrite overgrown by sphalerite in zone A (Fig. 19b1 and b2); (3) marcasite pseudomorphs after tabular crystals of pyrrhotite in zones A and C (Fig. 19c1 and c2); (4) euhedral pyrite in inner part of zone A at the boundary with chalcopyrite of zone B (Fig. 19d1 and d2); (5) spear chalcopyrite in zone B (Fig. 19e1 and e2); (6) lamellar chalcopyrite in isocubanite or γ-phase $Cu_2Fe_3S_5$ in zone B (Fig. 19f1 and f2); (7) dendritic intergrowths of sphalerite and chalcopyrite in zone C (Fig. 19g1 and g2) and (8) bornite (Bo) with chalcopyrite lattice (Fig. 19h1 and h2).

The textures 1, 2, 3 and 6 are typical of chimneys of the Atlantic, Cyprus and Urals type of the deposits and MOR smokers, but are very rare in chimneys of the Baymak type of the deposits and smokers from the island arc basins. Other textures are widespread in chimneys from different geological setting, excluding texture 8, which was not found in chimneys of the Urals type of the deposits. Colloform and detritic textures reflect rapid precipitation of sulfides from saturated fluids, are more typical of the MOR smokers (Hannington et al., 1995) and are also typical features of the chimneys of the Urals type of the deposits (Herrington et al., 1998).

5.2. Trace element comparison with modern chimneys

5.2.1. Selenium and tellurium

Chalcopyrite and pyrite from chimneys of both modern and ancient smokers are characterized by highly variable Se (0.1–3834 ppm) and Te (0.1–10,000 ppm) contents (Tables 5, 6, 9, 10). Less variable Se and Te contents are typical of sphalerite and wurtzite (Tables 7, 8). The high-temperature assemblages dominated by chalcopyrite and pyrite are expected to have elevated Se and Te concentration, since Te^{2-} and Se^{2-} substitute S^{2-} at high temperatures (Huston et al., 1995). Chalcopyrite crystals from the outer parts of modern (Butler and Nesbitt, 1999) and ancient (Maslennikov et al., 2009) chimneys generally show the lower Se concentrations relative to the inner part of the conduits. The general enrichment in Se depends on the fluid temperature, with very high solubilities of Se in fluids over 350 °C (Auclair et al., 1987; Hannington et al., 1991, 1995; Butler and Nesbitt, 1999). In contrast, Se-poor chalcopyrite has been found to precipitate at medium to low temperatures (Rouxel et al., 2004). Low Se contents (<10 ppm) are typical of diagenetic chalcopyrite (Maslennikov et al., 2009). The higher Se contents in high-temperature sulfides may reflect the strong temperature and

pH dependence of the dissociation constant for H_2Se (D'yachkova and Khodarkovskiy, 1968). This marked contrast in variations in Se contents between chalcopyrite from different chimney types suggests decreasing temperature of chalcopyrite deposition across the range from type 1 to type 3 chimneys of the Urals deposits. In general, host rocks control the relative Se and Te concentration in chalcopyrite. The positive correlation between Se and Te is observed only in chimneys from the deposits hosted by serpentinites (Dergamysh), basalts (Buribay, Yubileynoye, Sultanovskoye) or organic-rich (Safyanovskoye) sediments (Fig. 8a–g), which provide redox buffering to preserve Se^{2-} and Te^{2-} in the hydrothermal fluids. The positive correlation disappears in chalcopyrite of chimneys from bimodal mafic deposits (Urals type) and is completely absent in

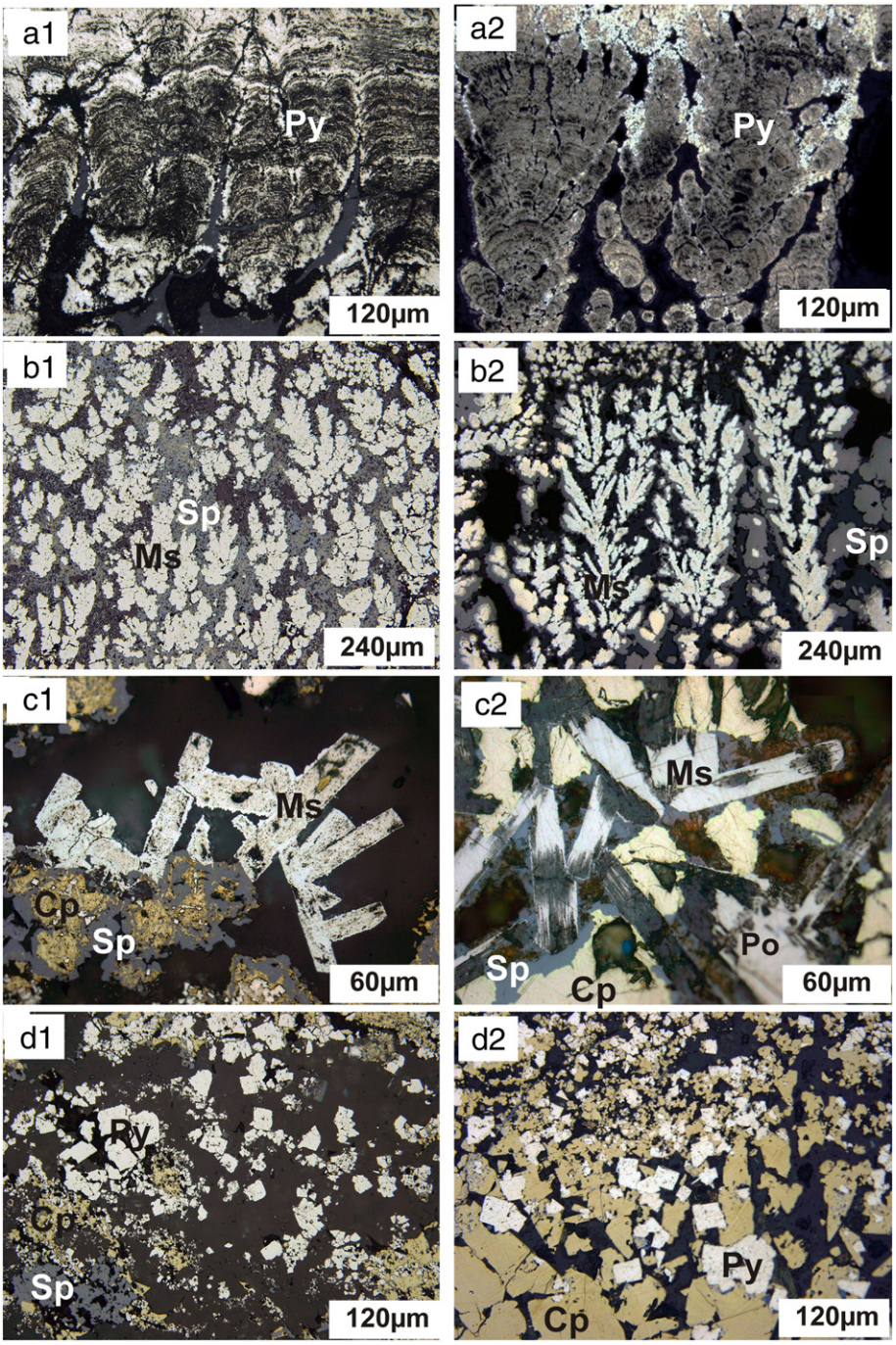

Fig. 19. Comparison of most important microtextures in chimneys from the Urals VMS deposits (a1–h1) and modern smokers (a2–h2). a – reniform colloform pyrite (Py) in subzone A1 (a1 – Yaman-Kasy deposit, sample 7380-32; a2 – EPR 9°N vent site, sample 4354-142-8/2); b – dendritic marcasite (Ms) overgrown by sphalerite (Sp) in subzone A1/A2 (b1 – Yaman-Kasy deposit, sample Y-SV-119; b2 – Broken Spur vent site, sample 4348-M1-2/1); c – pseudomorphic marcasite after tabular pyrrhotite (Po) crystals in subzone A2 (c1 – Yaman-Kasy deposit, sample Y-2002-44a; c2 – Rainbow vent site, sample 4402-M1-2/2c); d – euhedral pyrite in subzone A3 at the boundary with chalcopyrite (Cp) zone B (d1 – Yaman-Kasy deposit, sample Y-2003-29a; d2 – Lucky Strike vent site, sample 4383-M1-7в); e – spear chalcopyrite in zone B (e1 – Yaman-Kasy deposit, sample 7380-32; e2 – Broken Spur vent site, sample 4348-M1-2/1); f – lattice intergrowth of chalcopyrite and isocubanite (ISS) (f1 – Yaman-Kasy deposit, sample RF) and γ-phase $Cu_2Fe_3S_5$ (ISS) (f2 – Rainbow vent site, sample 4412-M1-9) in zone B3; g – dendritic intergrowths of sphalerite and chalcopyrite in zone C (g1 – Aleksandrinskoye deposit, sample AL-SV-I; g2 – EPR 9°N vent site, sample 4658-3); h – bornite (Bo) with chalcopyrite lattice (h1 – Aleksandrinskoye deposit, sample AOO-2C; h2 – Suzette vent site, sample SSu07CH-08-3). Reflected light. Tn, tennantite; Di, digenite.

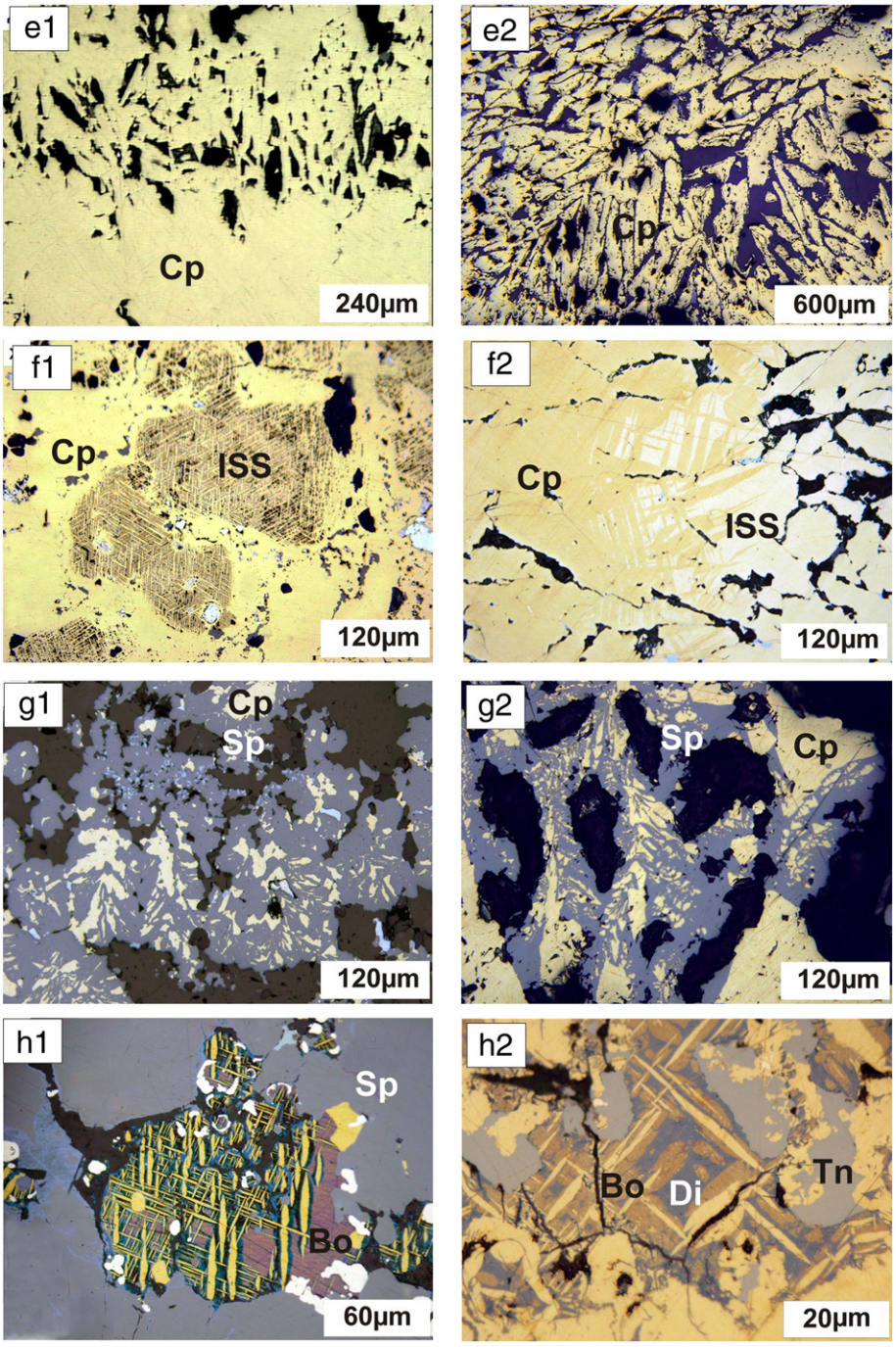

Fig. 19 (*continued*).

chimneys from bimodal felsic deposits (Baymak type) (Fig. 8d–g). These results are consistent with distribution of Se and Te in the modern chimneys.

Chalcopyrite of typical black smokers associated with MOR serpentinites (Rainbow, Logatchev, Ashadze fields) and basalts (Broken Spur, EPR 9°50′N fields) is characterized by elevated contents of both Se (300–3000 ppm and higher) and Te (7–285 ppm) (Table 6). The low contents of Se (1–12, up to 20 ppm) and Te (0.01–0.14 ppm) are typical of chalcopyrite from clear smokers and diffusers. The high Se and Te contents of 2734 ppm and 64 ppm, respectively, are found in a thin chalcopyrite zone within an anhydrite immature black smoker chimney from 9°50′N. Positive Se–Te correlation is characteristic of chalcopyrite of the modern chimneys related to MOR serpentinites and basalts, as well as for chimneys of the Urals deposits also hosted by serpentinites and basalts.

Dark grey barite–sphalerite–chalcopyrite smokers related to hot spots (Menez Gwen, Lucky Strike, Axial Seamount) are distinguished by the highest Se contents (up to 3834 ppm) and the lowest Te contents (<2 ppm) in chalcopyrite. Pyrite–chalcopyrite and sphalerite–pyrite–chalcopyrite chimneys of inactive Galapagos hydrothermal system also affected by the hot spot may be ascribed to this type.

The Se contents in chalcopyrite from the West Pacific arc-associated grey smokers are much lower (1–240 ppm) in comparison with those from MOR and hot spot black and grey smokers. The Se contents rarely

attain 200–2000 ppm in dark grey smokers (de Ronde et al., 2011). The Te contents in chalcopyrite from MOR black smokers and West Pacific grey smokers are similar, on average (Table 6). The Te content in chalcopyrite of the Cu-rich grey smoker chimneys of the PACMANUS field strongly varies (0.01–414 ppm). The Se and Te contents in chimneys from this site are similar to those of chimneys from the Urals type of the deposits and, especially, to the transitional subtype to Baymak type of the deposits (Oktyabrskoye and Valentorskoye deposits) (Table 5, Fig. 8e, f).

Moderate Se (32–204 ppm) and low Te (0.05–0.87 ppm) contents are typical of some white to clear barite–sphalerite-rich smokers from the PACMANUS field. Similar Se and Te contents were determined in chimneys from the Alexandrinskoye deposit (Fig. 8g). In general, no Se–Te correlation is observed in chalcopyrite from the modern island-arc smokers.

As was noted above, Se^{2-} and Te^{2-} substitute S^{2-} in chalcopyrite at high temperature. This causes strong positive correlation ($r = 0.60$–0.96) of Se^{2-} and Te^{2-} calculated for modern and ancient black smokers (Maslennikov et al., 2014) (Fig. 8).

However, unlike Se, a temperature dependence of Te in chalcopyrite is not so obvious (Maslennikov et al., 2009). Te-bearing minerals are generally scarce in chimneys from mafic and bimodal felsic-hosted deposits, but are abundant in chimneys from the Urals type related to bimodal mafic volcanic units. The high Te contents (>1000 ppm) in chimneys from the Urals type of the deposits and West Pacific island arc system are much higher compared to the MOR modern black smokers. The excess of Te and Se may be explained by contribution of Te from subducted sediments in the island arc system (Cook and McPhail, 2001; Ciobanu et al., 2006). Fluids reacted intensively with organic-rich sediments may have significantly more reduced compositions than any fluids interacted with basalts or other volcanic rocks (Hannington et al., 1995). Selenium can easily be reduced to H_2Se by interaction with additional H_2. In chalcopyrite-rich chimneys from the Safyanovskoye deposit, chalcopyrite displays the highest grades of Se, which are similar to those from the modern black smokers associated with basalts and serpentinites.

5.2.2. Tin

The high Sn contents are specific feature of the moderate- to high-temperature sulfides from VMS deposits (Hannington et al., 1999). The highest bulk Sn concentrations were found in the modern hydrothermal fields associated with ultramafic rocks (up to 2210 ppm; Evrard et al., 2015). In the Logatchev field, SEM-EDX data display high Sn concentrations, mostly, in sphalerite (3 to 5 wt.%) and chalcopyrite (1 to 2 wt.%) from high-temperature zone of the chimneys. The highest Sn concentrations are measured along the replacement front of sphalerite by chalcopyrite with inclusions of stannite (Evrard et al., 2015).

In our LA-ICP-MS study, the Sn contents are the highest in the isocubanite–chalcopyrite aggregates and sphalerite from grey and clear smokers or diffusers of the Rainbow vent site associated with ultramafic rocks. Black smokers display much lower Sn contents in chalcopyrite. This is consistent with Sn data from the Dergamysh chimneys, where chalcopyrite from chalcopyrite-rich analogues of black smokers contains the lower amount of Sn than the chalcopyrite-poor but pyrite-rich chimneys and diffusers considered the analogues of clear smokers. The variations in Sn contents in sphalerite from the Dergamysh chimneys are consistent with the Sn contents in sphalerite of ultramafic-hosted modern smokers.

In the ocean, sulfide deposits on basalts have relatively low Sn concentrations (<92 ppm, Fouquet et al., 2010). The low Sn contents were determined in chalcopyrite and sphalerite from chimneys of the Buribay deposit hosted by boninite–basalt units (Figs. 9b, 14b). Slightly higher Sn contents were identified in sphalerite and chalcopyrite from chimneys of the Urals type of deposits (Tables 5, 7). The highest Sn contents were detected in chalcopyrite from sphalerite–pyrite–barite chimneys, which are analogues of white or clear smokers (Maslennikov et al., 2009). The chimneys from the Baymak type of the deposits have much lower Sn contents, which are similar to those in chimneys of the West Pacific island arc system hosted by felsic rocks.

Chimneys from the Safyanovskoye deposit associated with both felsic rocks and black shales are exceptional. The highest concentration of Sn is found in chalcopyrite (up to 0.4 wt.%) and sphalerite from the pyrite–sphalerite–chalcopyrite chimneys. This is consistent with data on Sn contents from hydrothermal deposits located in sedimentary ridges (up to 1500 ppm; Koski et al., 1994).

The reasons for Sn enrichment are still unclear. Progressive Sn input from magmatic hydrothermal fluids was suggested for some VMS deposits (Hannington et al., 1999; Relvas et al., 2006; Huston et al., 2010). In this model, granitophile Sn usually precipitated as cassiterite along with low-temperature sulfides such as pyrite or sphalerite but, when the temperature increases, Sn is trapped in copper sulfides. In hydrothermal fluids, Fe^{2+} is oxidized to Fe^{3+} at high temperatures despite oxygen-free environments (Di Benedetto et al., 2005). The substitution of $Sn^{4+}Fe^{2+}$ for $2Fe^{3+}$ is therefore suggested to explain tin enrichment in sulfides (Kase, 1988).

At high temperatures, limited amount (up to 0.6 wt.%) of Sn can be incorporated in sulfides, as the structure of stannite (Cu_2FeSnS_4) is very similar to ZnS and $CuFeS_2$ (Moh, 1975). Enhanced concentrations of Sn in sphalerite and good correlation between Sn and Cu suggests a substitution mechanism such as $2Zn^{3+} \leftrightarrow Cu^{+} + Sn^{3+}$ or $3Zn^{3+} \leftrightarrow 2Cu^{+} + Sn^{4+}$ (Cook et al., 2009; Ye et al., 2011). However, the manners of substitution are difficult to validate without evidence for reduced state of Sn in sphalerite. At 250 °C, reduced acid fluids are suitable for the transport of $SnCl_2$ (Hannington et al., 1999). Substitution Sn^{2+} for Zn^{2+} is expected under strong reducing conditions (Maslennikov et al., 2009). The positive correlation coefficients ($r = 0.5$–0.7) between Sn, Zn, Fe have been calculated for chalcopyrite-rich chimneys from Yaman-Kasy and Safyanovskoye deposits only. For other chimneys discussed, very strong correlation of Sn with Cu and Se ($r = 0.70$–0.96) reflects influence of chalcopyrite "decease" on concentration of Sn in sphalerite (Maslennikov et al., 2014).

The higher Sn contents of moderate- to low-temperature isocubanite–pyrrhotite-rich clear smokers rather than of high-temperature bornite–chalcopyrite-rich black smokers must be explained. Probably, low redox potential and variable conductive cooling are other important factors for Sn^{2+} enrichment in hydrothermal fluids emanated from diffuse clear smokers, where mixing with oxygenated seawater is restricted. This is consistent with high Sn contents in chimneys with widespread Fe- and Co-rich sphalerite, isocubanite and pseudomorphic pyrite after pyrrhotite (Dergamysh, Molodezhnoye, Sultanovskoye, Yaman-Kasy, Safyanovskoye deposits). In general, ultramafites and organic-rich sediments provide reducing condition favorable for Sn^{2+} saturation in hydrothermal fluids and followed substitution of tin in structure of stannite and other sulfides of modern and ancient chimneys.

5.2.3. Cobalt and nickel

The Co and Ni contents in sphalerite and chalcopyrite of the modern smokers decrease in the range from ultramafic to basaltic to bimodal-hosted settings (Tables 6, 8). The highest Co contents are found in sphalerite and chalcopyrite from diffusers associated with ultramafic rocks. Chalcopyrite and sphalerite have elevated Ni contents in serpentinite-associated chimneys. Colloform pyrite displays the highest contents of Co and Co/Ni ratio (>10) in black smokers from ultramafic- and basaltic-hosted sites. Colloform pyrite in modern clear smokers from all geological settings has very low contents of Co and Ni and Co/Ni ratio of <1 (Table 10).

These data are in agreement with distribution of Co and Ni in different varieties of chimneys from the Urals deposits (Tables 5, 7, 9). The Co and Ni contents in sphalerite, chalcopyrite and colloform pyrite show similar correlation with host rock composition. The maximums of Co are much higher in chimneys from basalt- and serpentinite-hosted

deposits in comparison to chimneys from the Baymak type of deposits. The chimneys from the Urals type of deposit occupy intermediate position. In the other hand, chalcopyrite-poor chimneys (analogues of clear smokers) have lower Co contents in comparison with black smokers. Nickel is mainly contained in sulfides of chimneys related to the Atlantic type of the deposits (Dergamysh). Colloform pyrite from chimneys of the Atlantic, Cyprus and Urals type of the deposits display Co/Ni ratio of >1, while pyrite of chimney from the Baymak type of the deposits have Co/Ni ratio of <1. The latter is typical of the modern grey and clear smokers. Colloform pyrite, sphalerite and chalcopyrite from the Safyanovskoye deposit is enriched in Co and Ni in comparison with pyrite from the Baymak type of the deposits.

It is generally assumed that the host rocks strongly influence chemical composition of sphalerite and chalcopyrite. For example, Co and, to a lesser degree, Ni from mafic and ultramafic rocks are captured by sulfides of the chalcopyrite-rich chimneys of the Atlantic and Cyprus types of the deposits, as well as of modern black smokers.

It is known, that Co^{2+} enters sphalerite structure via the simple substitution of similar sized ions such as Zn^{2+}, Fe^{2+}, Mn^{2+} and Cd^{2+} (e.g., Vaughan and Rosso, 2006; Cook et al., 2009). The results of Vaughan and Rosso (2006) indicate that Ni and Co are commonly lattice bound in structure of pyrite. Nickel and Co are temperature-sensitive elements, which are typically enriched in chimney sulfides that precipitated at high temperatures (Maslennikov et al., 2009; de Ronde et al., 2011; Wohlgemuth-Ueberwasser et al., 2015; Keith et al., 2016). Previous studies have shown that Cu, Co and Ni precipitation occurs at temperatures below 350 °C (Metz and Trefry, 2000). Thus, the low Cu, Co and Ni contents in clear smokers and their ancient analogues in the Urals thus indicate low temperature of the fluid. Moderate temperatures and less reduced conditions result in precipitation of Co-rich frohbergite, Co-rich loellingite, cobaltite (Yaman-Kasy) and glaucodot (Safyanovskoye) rather than in substitution of Co and Ni in major sulfides (Maslennikov et al., 2009, 2013). Nevertheless, temperature is not only one parameter controlling the solubility of Co and Ni. Depletion in chlorinity due to phase separation may be one more reason of the low Co and Ni content (Keith et al., 2016). In chimneys from sediment-starved ridges, the Fe content in sphalerite is show to be a function of temperature (Keith et al., 2014). In this case, the positive correlation between elevated Co and Fe ($r = 0.6–0.8$) contents in sphalerite suggests the high- and moderate-temperature conditions for the modern black smokers and chimneys from the Urals deposit, respectively. Partitioning of Co and Ni depends on the temperature and host rock composition, as well as on fS_2 (Eremin, 1983). Increasing fS_2 and/or decreasing temperature favor substitutions, first, of Co^{2+} and then Ni^{2+} for Fe^{2+} in pyrite (Maslennikov et al., 2009). In general, Co/Ni ratio depends on the maturity of the hydrothermal system. Thermodynamic modeling displays extraction of Co ahead of Ni in immature hydrothermal system at the rock/seawater (ξ) ratio ($-Lg\xi = 3–1.5$) at 350 °C (Tret'yakov, 2015). The low Co/Ni ratios in pyrite of chimneys from the Baymak type of the deposits can be explained by the higher fS_2 of mature hydrothermal system.

5.2.4. Arsenic and antimony

The As and Sb contents in chimneys from the sediment-starved ridges are generally very low except for the high contents of Sb (up to 380 ppm) in some Sb-rich chimneys from the Rainbow vent site. In case of As–Sb substitution in chalcopyrite, no data on their concentration and mechanism of incorporation are available except for partition of microinclusions of fahlores or arsenopyrite (Berkenbosch et al., 2012; Wohlgemuth-Ueberwasser et al., 2015). Arsenic and Sb are most abundant in chalcopyrite of chimneys from the island arc basins due to numerous inclusions of tennantite and tetrahedrite, similar to the occurrences in the Urals chimneys. Chalcopyrite of chimneys from the Atlantic, Cyprus and subtype U1 of the Urals type of the deposits has lower As and Sb contents (Fig. 13). The contents of these elements are much higher in chalcopyrite of chimneys from the deposits associated with bimodal mafic and bimodal felsic units. High As and Sb contents reflect a variety of mineral inclusions in different deposits: loellingite, cobaltite, Sb-rich tellurobismuthite and sulfosalts (Yaman-Kasy), tennantite and arsenopyrite (Molodezhnoye), tennantite (Alexandrinskoye) and tetrahedrite, tennantite and glaucodot (Safyanovskoye).

The Sb and As contents in sphalerite from the MOR black smokers rarely reach 100–400 ppm (Table 7). These lower values are typical of sphalerite from vent sites associated with serpentinites. Sphalerite of the Dergamysh deposit is characterized by much higher Sb concentrations in comparison with modern analogues. The high Sb/As ratio (>1) is likely related either to microinclusions of tetrahedrite or isomorphic Sb (Huston et al., 1995; Cook et al., 2009). The As and Sb contents in sphalerite from chimneys of the Buribay deposit are even lower than those in chimneys from the basalt-hosted modern black smokers (Fig. 13b). The highest values of Sb and As (up to 1 wt.%) are determined in sphalerite from the modern grey smokers associated with bimodal complexes. This is consistent with data on chimneys from the Urals and Baymak type of the deposits.

In general, sphalerite from all modern and ancient smokers demonstrates positive correlation between Sb and As, which reflects the presence of microinclusions of fahlores. Microscopic inclusions of fahlores are rare in sphalerite from the MOR chimneys in contrast to sphalerite from the IAB-associated grey and clear smokers with elevated As and Sb contents. In the island arc-related vent sites, the enrichment of sphalerite from grey smokers in As and Sb is related to microinclusions of fahlore, realgar and orpiment. No realgar and orpiment, however, were found in chimneys of the Urals deposits.

The As and Sb contents of colloform pyrite from modern chimneys increases in the range of host rock composition from ultramafic to basaltic and bimodal complexes (Table 10). Similar distribution of As is observed in colloform pyrite from chimneys of the Urals type of the deposits (Table 9, Fig. 17). The higher As and Sb content in colloform pyrite is controlled by inclusions, probably, of tennantite and tetrahedrite due to the correlation between As and Sb, as well as Cu and Zn (Wohlgemuth-Ueberwasser et al., 2015). The lack of this correlation may mean the presence of nanoinclusions of realgar and orpiment; the high As contents in colloform pyrite could be a result of lattice substitution.

In modern and ancient chimneys associated with ultramafic rocks, the low As contents are caused by serpentinization (Keith et al., 2016). Depletion in As is probably one of the reasons for the relative enrichment in Sb in modern and ancient deposits associated with serpentinites. Thermodynamic modeling of peridotite/seawater (ξ) interaction shows that enrichment in Sb is possible in relatively mature hydrothermal system (with $-Lg\xi = 1.5–0.5$) at 350 °C (Tret'yakov, 2015) and, in general, the As and Sb contents are elevated in mature systems. Differences in maturity can explain the variation in contents of these elements in chimneys related to the same host rocks. For example, we suggest that the hydrothermal systems of the Sultanovskoye and Yubileynoye deposits were more mature relative to that of the Buribay deposit in spite of their similar host basalts. Arsenic and Sb are evidence of the high temperature fluids reacting with more felsic rocks (Stanton, 1994; Hannington et al., 1995) and/or input of magmatic volatiles (Wohlgemuth-Ueberwasser et al., 2015). In the other hand, the buffer capacity with respect to the effect of seawater is generally much lower for felsic rocks than for basalts and this results in more rapid evolution of arc hydrothermal systems and their enrichment in As and Sb. The hydrothermal fluids in the sediment/seawater system are also relatively enriched in As and Sb because of their higher contents in organic-rich sedimentary rocks in comparison with dacites and andesites (Grichuk, 2012; Tret'yakov, 2015). This could explain much higher Sb and As contents in chimneys from the Safyanovskoye deposit compared with chimneys from the Baymak type of the deposits.

5.2.5. Lead and bismuth

The systematic variations are observed in distribution of Pb and Bi in chalcopyrite and colloform pyrite, which are much higher in the minerals of black smokers compared to clear smokers, probably, due to

higher temperature and, consequently, higher concentration of these elements in hydrothermal fluids.

In general, the maximum Pb and Bi contents in sulfides depend on the host rock composition: ultramafic rocks → MOR basalts → basaltic and bimodal complexes of island-arc basins (Tables 5–10). The high Pb contents are typical only of felsic-hosted systems with Pb being derived from the breakdown of feldspars and clays (Barrie and Hannington, 1999), whereas Bi migrates in magmatic volatiles from the degassing of felsic magma chamber (de Ronde et al., 2011; Berkenbosch et al., 2012). Lead and Bi contents can reach 0.1–0.6 wt.% in chalcopyrite of modern grey smokers associated with felsic rocks in the island-arc basins, e.g., Brothers volcano (Berkenbosch et al., 2012) and PACMANUS (this study) vent sites. The elevated Pb and Bi contents are related to numerous microinclusions of galena and tellurobismuthite similarly to chimneys from the Urals type and Baymak type of the deposits located in felsic rocks. In some Urals deposits (Molodezhnoye, Yaman-Kasy), Pb is also related to the presence of altaite, whereas, in the Baymak type, Bi and Pb occur together in the kochkarite–rucklidgeite series. In addition to felsic rocks, the sediments can be one more source for Pb and Bi. The Bi and Pb contents are high in chimneys of the Safyanovskoye deposit (Table 5) with both felsic and organic-rich sedimentary rocks in the footwall. The high Bi (up to 633 ppm) and Pb (up to 6707 ppm) contents in pyrite from the JADE field reflect influence of footwall sediments in comparison with the sediment-starved back-arc and intraoceanic arc vent sites (Keith et al., 2016). The high Bi and Pb contents in seafloor sulfides are believed to reflect a contribution of sediments to the hydrothermal system (Koski et al., 1988; Zierenberg et al., 1993).

5.2.6. Gold and silver

Mechanisms of gold enrichment and genetic models for gold-rich deposits have been reviewed for both ancient and modern setting (Hannington et al., 1986, 1999; Huston and Large, 1989; Large et al., 1989; Hannington and Scott, 1989; Large, 1992; Sillitoe et al., 1996; Huston, 2000; Dubé et al., 2007; Galley et al., 2007; de Ronde et al., 2011; Mercier-Langevin et al., 2011; Vikentyev, 2015). The processes of Au and Ag enrichment are related to the water-rock interaction, phase separation, input of magmatic volatiles, conductive cooling and subsurface mixing with seawater.

In the Au–Ag plots, compositions of the modern and ancient chimneys associated with different host rocks are overlapped. The lowest Au (0.001–1 ppm, rarely, up to 3 ppm) contents are characteristic of sulfides from basalt-hosted black smokers in both Pacific and Atlantic MORs, excluding sulfides from chimneys of inactive MIR site (TAG field), which contains up to 150 ppm Au (this study). The chimneys from bimodal-hosted vent sites and ancient deposits are characterized by much higher Ag and Au contents (up to 1000 ppm).

In contrast to Ag, the Au contents decrease from modern black to clear smokers, probably, due to the temperature decrease and depletion of hydrothermal fluid in Au and, to a lesser extent, in Ag. Positive correlation between Au and Ag is consistent with the presence of microinclusions of electrum and native gold or rare sylvanite. Generally, the decrease in Au/Ag ratio means the presence of microinclusions of hessite and sylvanite or substitutions of Ag^+ for Cu^+ in chalcopyrite.

Ultramafic rocks could probably be one of the sources for high Au contents in serpentinite-associated gold and VMS deposits (Leblanc, 1991) and modern black smokers (Murphy and Meyer, 1998). As was previously suggested for the Australian VMS deposits (Large et al., 1989; Huston and Large, 1989) and Logatchev vents site (Murphy and Meyer, 1998), the abundant gold in chalcopyrite and sphalerite of the modern and ancient chimneys may be a result of two different methods of transport: via $Au(HS)_2^-$ complex at low temperatures in association with zinc and $AuCl^{2-}$ complex at higher temperatures in association with copper. Hannington and Scott (1989) attributed rare primary Cu–Au association in seafloor sulfides to high-temperature oxidation of $Au(HS)_2^-$. However, the deficit in H_2S of hot fluids of serpentinite-hosted vents (Perner et al., 2013) suggests a significant role of $AuCl_2^-$ in the high-temperature hydrothermal transport of gold.

In basalt-hosted chimneys, it is assumed that gold enters the pyrite structure, because the high-temperature fluids are undersaturated in respect to gold (Bortnikov et al., 2003; Vikentyev, 2015). The low Au contents in some basalt-hosted deposits reflect low fO_2–fS_2 fluids buffered by basalts, which are unfavorable for Au transport (e.g., Hannington and Scott, 1989; Huston and Large, 1989). The results of physico-chemical modeling may explain the differences in Au content in basalt-hosted vent sites and deposits. Mature hydrothermal seawater/basalt system is more productive for the higher Au and Ag contents (Tret'yakov, 2015). In this case, the Sultanovskoye deposit represents more mature hydrothermal system than Buribay deposit, as well as TAG vs. EPR 9°50′ N vent sites.

The modeling results indicate that the low buffer capacity of felsic rocks causes fairly rapid complete scavenging of Ag and Au in comparison with seawater/basalt system (Grichuk, 2012). In the subtype U2 of the Urals type of the deposit, the Au contents in chalcopyrite from most chimneys are higher than those in sphalerite. The $AuCl_2^-$ complex in the high-temperature fluid may be the main carrier of gold (Huston and Large, 1989; Large, 1992). Associations of high Te, Bi and Au contents, along with Se, are indicative of magmatic source (Spooner, 1993). The correlation between Au with Bi and Te suggests that magmatic volatiles may deliver the high Au contents at high temperatures in this type of chimneys, as well as in modern counterparts from the Brothers vent site (de Ronde et al., 2011; Berkenbosch et al., 2012). The low melting point of Bi (271.4 °C) means that liquid Bi droplets can be transported in hydrothermal fluids and thus have the ability to transport Au (Ciobanu et al., 2010), however, this seems unlikely. Bismuth is most likely transported mainly as chloride complexes (Monecke et al., 2016).

In contrast to the chimneys from the Urals type of the deposits, sphalerite is a major carrier of Au in the Bi–Te–Se-poor chimneys of the Baymak type of the deposits. The lower Au contents in chalcopyrite indicate undersaturation in respect to gold under high-temperature conditions favorable for precipitation of chalcopyrite. With the decrease in temperature, native gold can precipitate in sphalerite. It is suggested that primary fluids, which were responsible for the formation of the Baymak type chimneys, could contain lower Au contents. Tellurides are very rare in chimneys from the Baymak type, as well as from Kuroko type VMS deposits and many modern analogues (e.g., Suiyo vent sites).

In the Safyanovskoye deposit, chalcopyrite and sphalerite have low Au contents in comparison to the chimneys from other Urals deposits. This is consistent with low Au contents in Sn-rich deposits (Hannington et al., 1999). At 250 °C, the reduced acid fluids, which transport $SnCl_2$, are well outside the range of maximum solubility of gold as $Au(HS)_2^-$ or $AuCl_2^-$. Gold is most readily transported in near-neutral conditions and much higher fO_2 (Huston and Large, 1989; Hannington and Scott, 1989; Hannington et al., 1999). In contrast to gold, Ag is transported as $Ag(Cl)_2^-$ over much wider range of temperature, pH, and oxidation state, and the solubility differences are consistent with very high Ag/Au ratios in chimneys from the Safyanovskoye deposit.

6. Conclusions

1. Sulfide mounds of the Urals VMS deposits associated with ultramafic (Atlantic type), mafic (Cyprus type), bimodal mafic (Urals type) and bimodal felsic (Baymak type) sequences yield a wide range of well-preserved chimneys. The combination of geological, mineralogical and trace element data provide a general outline of their comparison with modern counterparts. Chimneys from the Dergamysh serpentinite-hosted deposit display affinity with those from the Rainbow and other vent sites associated with ultramafic rocks of the Atlantic Ocean. Chimneys from the Buribay deposit are similar

to black smokers from the EPR vent sites. Chimneys from the Urals type of the deposits resemble dark grey smokers from the Brothers volcano and PACMANUS vent sites. Chimneys from the Baymak type of the deposits are typical of grey to white smokers of the PACMANUS and grey smokers of the Suiyo vent sites. Finally, chimneys from the Safyanovskoye deposit have similar features with black and clear smokers from the Okinawa Trough.

2. The formation of the specific mineral assemblages is controlled by composition of host rocks and physico-chemical conditions of ore-forming processes. The amount of colloform pyrite, isocubanite and pseudomorphic pyrite and marcasite after pyrrhotite decreases and the amount of sphalerite, galena, bornite, fahlores, native gold and barite increases in chimneys of this range of the VMS deposits. Chimneys from the Urals type of the deposits occupying the intermediate position contain abundant tellurides and sulfoarsenides, whereas these mineral are rare or absent in those from the Baymak type of the deposit. In general, across the same range, the buffering capacity of host rocks decreases and fS_2 and fO_2 increase.
3. In the Urals deposits, the chimneys include consecutive Fe–Cu to Cu–Zn–Fe and Zn–Cu types with decrease in the amount of isocubanite, colloform pyrite and marcasite and their pseudomorphs after pyrrhotite and increase in amount of sphalerite, quartz and barite. Each chimney type displays own mineralogical ranges with decrease in amount of chalcopyrite and increase in amount of quartz and/or barite and talc. The mineral zonation of different chimney types is broadly comparable with that of modern black, grey, white or clear smokers and can be interpreted in terms of extreme gradients of temperature and oxygen and sulfur fugacity across the chimney walls. The absence of the outer anhydrite zone and minerals unstable under metamorphism (e.g., realgar, orpiment) in ancient chimneys is the difference between the Urals and modern counterparts.
4. Each type of the Urals VMS deposit is characterized by its own mineral range of chimneys from black and grey to white or clear smokers. The range from chalcopyrite–pyrite to pyrite–chalcopyrite chimneys with subordinate sphalerite is typical of the ultramafic- and mafic-hosted deposits. The range from chalcopyrite to sphalerite–barite–chalcopyrite chimneys is common for some deposits of the Baymak type (Uzelga-1, Alexandrinskoye). The most complete range from chalcopyrite–pyrite to pyrite–marcasite–sphalerite–chalcopyrite and quartz–barite–sphalerite–pyrite–chalcopyrite is characteristic of the Urals type of the deposits and Safyanovskoye deposit, as well. The chalcopyrite–pyrite type lacks accessory minerals owing to high temperature and/or reducing conditions prevented precipitation of tellurides (Maslennikov et al., 2009, 2013). The chalcopyrite-sphalerite-pyrite chimneys contain abundant tellurides and sulfoarsenides, which indicates optimal temperature and redox conditions for their precipitation and, probably, magmatic contribution. Most chimneys of barite-sphalerite- and quartz-pyrite-rich chimneys contain lower amount of tellurides and sulfoarsenides, whereas native gold, Fe-poor sphalerite, barite, tennantite, tetrahedrite and galena are most pervasive minerals due to the higher fS_2 and fO_2. The specific mineral changes in the local ranges of chimneys are similar to the general changes in chimneys of the types of VMS deposits. The local variations can be interpreted by enhanced contribution of cool oxygenated seawater to processes of mineralization.
5. In the local ranges from black to clear smokers, the trace element variations can be explained by local variations in physico-chemical parameters of the hydrothermal fluids. Selenium in chalcopyrite and Fe and Co in sphalerite can indicate the decrease in reduction capacity and temperature of hydrothermal fluids for both modern smokers and the Urals chimneys. In general, the contents of trace elements in sulfides of the Urals chimneys, as well as their modern counterparts, are functions of the host rock composition, which affects the physico-chemical parameters of the fluids. This coherence can be proved only by comparison of genetically same homonymous minerals from specific zones of chimneys: hydrothermal chalcopyrite (zone B) and sphalerite (zones A and C) and hydrothermal-sedimentary colloform pyrite. Chalcopyrite in ultramafic-hosted chimneys (Atlantic type) has elevated Se, Sn, Co, Ni and Au contents. Chalcopyrite of chimneys associated with mafic rocks (Cyprus type) display high concentrations of Co and Se, whereas contents of Bi, Au и Pb are lower relative to all other types of the deposits. High concentration of Te, Au, Bi, Pb and Co and moderate contents of Se are typical of chalcopyrite from the Urals type of the deposits hosted by bimodal mafic sequences. The variable As contents coincide with Co concentrations in these chimneys due to inclusions of Co sulfoarsenides. In chimneys of the Baymak type of the deposits in bimodal felsic units, chalcopyrite displays high contents of As, Sb, Mo and Pb, moderate contents of Bi and lower contents of Co and Se. Similar variations in trace elements are identified in sphalerite and colloform pyrite from chimneys of this range of the deposits. In sphalerite, the contents of Bi, Pb, Ag, Au and Sb increase versus Fe, Se and Co in the range from ultramafic and mafic to bimodal series. The decrease in Fe contents may indicate intensification in $fS2$ and $fO2$ or general temperature degression due to subsurface mixing with cold seawater. The common results indicate the decrease in the buffer capacity in the range from the ultramafic and mafic to felsic rocks. Interaction of seawater with felsic rocks causes the fairly rapid complete scavenging of elements metals in comparison with seawater/basalt system (Grichuk, 2012).
6. Some exception is shown by atypical Safyanovskoye deposit, which is hosted by felsic rocks and black shales. In this deposit, pyrite- and chalcopyrite-rich chimneys are similar to those from the Atlantic and Cyprus type of the deposits by abundant colloform pyrite, isocubanite and pseudomorphic pyrite and marcasite after pyrrhotite. The difference is that it shows atypical combination of low sulfidation (glaucodot, arsenopyrite and stannite) and high sulfidation (barite, tetrahedrite, tennantite, galena, enargite) assemblages in chimneys from the deposit. As well as Fe–Co–Sn-rich chimneys associated with ultramafic rocks, the chimneys from the Safyanovskoye deposit yield high concentration of Pb, Bi, Ag, As and Sb, which are typical trace element contents in chimneys of felsic-hosted VMS deposits. High concentration of Fe, Co and Sn and lower contents of Au can be the result of hydrothermal transport by reduced fluids interacting with organic-rich sediments.

Conflicts of interest

No conflicts of interest.

Acknowledgments

The authors thank C. Stanley, K. Becker, J. Spratt, T. Wighton, T. Greenwood, V. Kotlyarov, I. Blinov, E. Churin, Yu. Kraynev and Dr. D. Steele for their assistance in microprobe analyses. The authors express their gratitude to A.P. Lisitsin, Yu.A. Bogdanov, A.M. Sagalevich, I. Jonasson, T. Urabe and M. Gibson for access to many of the modern chimneys. The reviews of Sebastian Fuchs, one anonymous reviewer and handling editor Olga Yu. Plotinskaya helped us greatly to improve the manuscript. The mineralogical study was supported by the Russian Foundation for Basic Research (project no. 14-05-00630). LA-ICP-MS analyses were carried out during visiting programs (2005, 2009, 2012, 2013, 2015) sponsored by the ARC Centre of Excellence grant to CODES, University of Tasmania. Chemical interpretation and preparation of the paper was supported by the Russian Science Foundation (project no. 14-17-00691).

Appendix A. Trace elements in chalcopyrite of chimneys from the Urals VMS deposits (LA-ICP-MS, ppm)

Deposit	Sample name	File name	Mineral	Zone	Chemical	Stympoeke	n	stat	V51	Mn55	Fe57
Dergamysh	D13-6-7cpy	SE28a657	Chp	B1'	Cu-Fe	bs			*0.03*	0.70	305000
Dergamysh	D13-6-7cpy	SE28a658	Chp	B1'	Cu-Fe	bs			1.76	89.0	341000
Dergamysh	D13-6-7cpy	SE28a660	Chp	B1'	Cu-Fe	bs			0.30	3.42	312000
Dergamysh	D13-6-7cpy	SE28a662	Chp	B1'	Cu-Fe	bs			0.21	1.55	310000
Dergamysh	D13-6-7cpy	SE28a663	Chp	B2'	Cu-Fe	bs			*0.03*	5.16	315000
Dergamysh	D13-6-7cpy	SE28a664	Chp	B2'	Cu-Fe	bs			*0.03*	2.76	305000
Dergamysh	D13-6-7cpy	SE28a665	Chp	B2'	Cu-Fe	bs			0.25	44.6	315000
Dergamysh	D13-6-7cpy	SE28a666	Chp	B2'	Cu-Fe	bs			0.64	35.3	310000
Dergamysh	D13-6-7cpy	SE28a667	Chp	B2'	Cu-Fe	bs			0.30	46.5	310000
Dergamysh	D13-6-7cpy	SE28a668	Chp	B2'	Cu-Fe	bs			0.46	8.34	305000
Dergamysh	D13-6-7cpy	SE28a669	Chp	B2'	Cu-Fe	bs			*0.03*	5.99	308000
Dergamysh	D13-6-7cpy	SE28a670	Chp	B2'	Cu-Fe	bs			1.38	13.3	305000
Dergamysh	D13-6-7cpy	SE28a671	Chp	B2'	Cu-Fe	bs			0.27	2.06	305000
Dergamysh	D13-6-7cpy	SE28a676	Chp	B2'	Cu-Fe	bs			0.32	11.0	305000
Dergamysh	D13-6-7cpy	SE28a677	Chp	B2'	Cu-Fe	bs			3.03	14.1	305000
Dergamysh	D13-6-7cpy	SE28a679	Chp	B2'	Cu-Fe	bs			0.06	0.71	305000
Dergamysh	D13-6-7cpy	SE28a680	Chp	B2'	Cu-Fe	bs			0.01	11.3	305000
Dergamysh	D13-6-7cpy	SE28a681	Chp	B2'	Cu-Fe	bs			*0.03*	2.43	305000
Dergamysh	D13-6-7cpy	SE28a682	Chp	B2'	Cu-Fe	bs			*0.03*	1.47	305000
Dergamysh	D13-6-7cpy	SE28a683	Chp	B2'	Cu-Fe	bs			*0.03*	*0.70*	305000
Dergamysh	D13-6-7cpy	SE28a684	Chp	B2'	Cu-Fe	bs			*0.03*	4.62	305000
Dergamysh	D13-6-7cpy	SE28a685	Chp	B2'	Cu-Fe	bs			0.19	6.88	305000
Dergamysh	D13-6-7cpy	SE28a687	Chp	B2'	Cu-Fe	bs			4.01	23.7	305000
Dergamysh	D13-6-7cpy	SE28a689	Chp	B2'	Cu-Fe	bs			0.45	10.9	305000
Dergamysh	D13-6-7Cb	SE28a473	Chp + ISS	B3'	Cu-Fe	bs			0.43	8.51	400000
Dergamysh	D13-6-7Cb	SE28a474	Chp + ISS	B3'	Cu-Fe	bs			0.58	9.55	390000
Dergamysh	D13-6-7Cb	SE28a475	Chp + ISS	B3'	Cu-Fe	bs			0.24	22.8	405000
Dergamysh	D13-6-7Cb	SE28a476	Chp + ISS	B3'	Cu-Fe	bs			0.83	8.65	395000
Dergamysh	D13-6-7Cb	SE28a477	Chp + ISS	B3'	Cu-Fe	bs			0.38	33.5	430000
Dergamysh	D13-6-7Cb	SE28a478	Chp + ISS	B3'	Cu-Fe	bs			0.09	25.2	415000
Dergamysh	D13-6-7Cb	SE28a479	Chp + ISS	B3'	Cu-Fe	bs			0.13	4.34	418000
Dergamysh	D13-6-7Cb	SE28a480	Chp + ISS	B3'	Cu-Fe	bs			0.09	16.2	410000
Dergamysh	D13-6-7Cb	SE28a481	Chp + ISS	B3'	Cu-Fe	bs			0.58	60.5	390000
Dergamysh	D13-6-7Cb	SE28a482	Chp + ISS	B3'	Cu-Fe	bs			0.36	14.2	415000
Dergamysh	D13-6-7Cb	SE28a483	Chp + ISS	B3'	Cu-Fe	bs			0.28	10.3	415000
Dergamysh	D13-6-7Cb	SE28a484	Chp + ISS	B3'	Cu-Fe	bs			0.06	4.96	430000
Dergamysh	D13-6-7Cb	SE28a485	Chp + ISS	B3'	Cu-Fe	bs			0.22	4.09	446000
Dergamysh	D13-6-7Cb	SE28a486	Chp + ISS	B3'	Cu-Fe	bs			0.32	10.9	410000
Dergamysh	D13-6-7Cb	SE28a487	Chp + ISS	B3'	Cu-Fe	bs			0.01	4.47	415000
				Derg	Cu-Fe	bs	39	av	0.47	15.0	348333
								sd	0.81	18.5	52395
								med	0.25	8.65	310000
								geom	0.17	7.90	344663
								max	4.01	89.0	446000
Dergamysh	D13CphISSB1	SE28a427	Chp	B1'	Cu-Zn ± Fe	bs			10.3	237	290000
Dergamysh	D13CphB1	SE28a428	Chp	B1'	Cu-Zn ± Fe	bs			*0.06*	1.77	300959
Dergamysh	D13CphISSB1	SE28a429	Chp	B1'	Cu-Zn ± Fe	bs			1.26	100	300000
Dergamysh	D13CphISSB1	SE28a430	Chp	B1'	Cu-Zn ± Fe	bs			2.26	239	285000
Dergamysh	D13CphISSB1	SE28a435	Chp	B1'	Cu-Zn ± Fe	bs			5.26	108	325000
Dergamysh	D13CphB1	SE28a437	Chp + ISS	B1'	Cu-Zn ± Fe	bs			3.95	31.6	375000
Dergamysh	D13CphissB2	SE28a438	Chp	B2'	Cu-Zn ± Fe	bs			4.10	20.2	305000
Dergamysh	D13CphissB2	SE28a439	Chp + ISS	B2'	Cu-Zn ± Fe	bs			3.10	58.2	372000

References

Auclair, G., Fouquet, Y., Bohn, M., 1987. Distribution of selenium in high-temperature hydrothermal sulfide deposits at 13° North, East Pacific Rise. Can. Mineral. 87, 577–587.

Ayupova, N.R., Maslennikov, V.V., Maslennikova, S.P., Blinov, I.A., Danyushevsky, L.V., Large, R.R., 2015. Rare mineral and trace element assemblages in submarine supergene zone at the Devonian Molodezhnoye VMS deposit, the Urals, Russia. Proceedings of the 13 SGA Biennial Meeting. Mineral Resources in a Sustainable World. Nancy, France, pp. 2051–2054.

Barrie, C.T., Hannington, M.D., 1999. Classification of volcanic-associated massive sulfide deposits based on host-rock composition. Rev. Econ. Geol. 8, 1–11.

Berkenbosch, H.A., de Ronde, C.E.J., Gemmell, J.B., McNeill, A.W., Geomann, K., 2012. Mineralogy and formation of black smoker chimneys from Brothers submarine volcano, Kermadec arc. Econ. Geol. 107, 1613–1633.

Binns, R.A., 2014. Bikpela: A large siliceous chimney from the PACMANUS hydrothermal field, Manus basin, Papua New Guinea. Econ. Geol. 109 (8), 2243–2259.

Binns, R.A., Scott, S.D., 1993. Actively forming polymetallic sulfide deposits associated with felsic rocks in the eastern Manus back-arc basin, Papua New Guinea. Econ. Geol. 88, 2226–2236.

Bogdanov, Yu.A., Lein, A.Yu., Ul'yanov, A.A., Maslennikov, V.V., Ul'yanova, N.V., Sagalevich, A.M., 2006a. Initial stage of the hydrothermal ore accumulation within the field at 9°50′ N on the East Pacific Rise. Oceanology 46 (1), 81–94.

Bogdanov, Yu.A., Lisitzin, A.P., Sagalevich, A.M., Gurvich, E.G., 2006b. Hydrothermal Oregenesis of the Oceanic Floor. Nauka, Moscow (527 pp. in Russian).

Bogdanov, Yu.A., Lein, A.Yu., Maslennikov, V.V., Li, S., Ul'yanov, A.A., 2008. Mineralogical–geochemical features of sulfide ores from the Broken Spur hydrothermal vent field. Oceanology 48, 679–700.

Bogdanov, Yu.A., Lein, A.Yu., Lisitsin, A.P., 2015. Polimetallic Ores in Rifts of the Mid-Atlantic Ridge (15–40°N): Mineralogy, Geochemistry, Genesis. GEOS, Moscow (256 pp. in Russian).

Borodaev, Yu.S., Mozgova, N.N., Gablina, I.F., 2004. Zonal chimneys of the hydrothermal vents (black smokers) from the Rainbow hydrothermal field (Mid–Atlantic Ridge 36°14′ of Northern Latitude). Vestn. Mosk. Univ. Geol. 3, 35–48.

Bortnikov, N.S., Vikentyev, I.V., 2005. Modern base metal sulfide mineral formation in the world ocean. Geol. Ore Deposits 47, 16–51.

Bortnikov, N.S., Cabry, L., Vikentyev, I.V., Tagirov, B.R., McMahon, G., Bogdanov, Yu.A., Stavrova, O.O., 2003. Invisible gold in sulfides from modern sulfide edifices. Geol. Ore Deposits 2, 510–542.

Bortnikov, N.S., Simonov, V.A., Bogdanov, Yu.A., 2004. Fluid inclusions in minerals from modern sulfide edifices: physicochemical conditions of formation and evolution of fluids. Geol. Ore Deposits 46, 64–75.

Butler, I.B., Nesbitt, R.V., 1999. Trace element distribution in the chalcopyrite wall of a black smoker chimney: insights from laser ablation inductively coupled plasma mass spectrometry (LA–ICP–MS). Earth Planet. Sci. Lett. 167, 335–345.

Ciobanu, C.L., Cook, N.J., Spry, P.G., 2006. Telluride and selenide minerals in gold deposits – how and why. Mineral. Petrol. 87, 163–169.
Ciobanu, C.L., Birch, W.D., Cook, N.J., et al., 2010. Petrogenetic significance of Au–Bi–Te–S associations: the example of Maldon, Central Victorian gold province, Australia. Lithos 116, 1–17.
Cook, D.R., McPhail, D.C., 2001. Epithermal Au-Ag-Te mineralization, Acupan, Baguio Philippines; numerical simulations of mineral deposition. Econ. Geol. 96, 109–131.
Cook, N.J., Ciobanu, C.L., Pring, A., Skinner, W., Shimizu, M., Danyushevsky, L., Saini-Eidukat, B., Melcher, F., 2009. Trace and minor elements in sphalerite: a LA-ICP-MS study. Geochim. Cosmochim. Acta 73, 4761–4791.
Danyushevsky, L.V., Robinson, R., Gilbert, S., Norman, M., Large, R., McGoldrick, P., Shelley, J.M.G., 2011. Routine quantitative multi-element analysis of sulfide minerals by laser ablation ICP-MS: standard development and consideration of matrix effects. Geochem. Explor. Environ. Anal. 11, 51–60.
de Ronde, C.E.J., Massoth, G.J., Butterfield, D.A., Christenson, B.W., Ishibashi, J., Ditchburn, R.G., Hannington, M.D., Brathwaite, R.L., Lupton, J.E., Kamenetsky, V.S., Graham, I.J., Zellmer, G.F., Dziak, R.P., Embley, R.W., Dekov, V.M., Munnik, F., Lahr, J., Evans, L.J., Takai, K., 2011. Submarine hydrothermal activity and gold-rich mineralization at Brothers Volcano, Kermadec Arc, New Zealand. Mineral Deposits 46, 541–584.
Detrick, R.S., Honnorez, J., Adamson, A.C., Brass, G., Gillis, K.M., Humphris, S.E., Mevel, C., Meyer, P., Petersen, N., Rautenschlein, M., Shibata, T., Staudigel, H., Yamamoto, K., Wooldridge, A.L., 1986. Drilling the Snake Pit hydrothermal sulfide deposit on the Mid-Atlantic Ridge, lat 23°22' N. Geology 14, 1004–1007.
Di Benedetto, F., Andreozzi, G.B., Bernardini, G.P., Borgheresi, M., Caneschi, A., Cipriani, C., Gatteschi, D., Romanelli, M., 2005. Short-range order of Fe^{2+} in sphalerite by Fe-57 Mossbauer spectroscopy and magnetic susceptibility. Phys. Chem. Miner. 32, 339–348.
Dubé, B., Gosselin, P., Mercier-Langevin, P., Hannington, M., Galley, A., 2007. Gold-rich volcanogenic massive sulphide deposits: Geological Association of Canada. Mineral Deposits 5, 75–94.
Duckworth, R.C., Knott, R., Fallick, A.E., Rickard, D., Murton, B.J., Dover, Van, 1995. Mineralogy and sulfur isotope geochemistry of the Broken Spur sulfides, 29° N Mid-Atlantic Ridge. Hydrothermal vents and processes (Parson et al., eds.) Spec. Publ. Geol. Soc. London. 87, 175–189.
D'yachkova, I.B., Khodarkovskiy, I.L., 1968. Thermodynamic equilibria in the system S–H_2O, Se–H_2O and Te–H_2O in the 25–300 °C temperature range and their geochemical interpretation. Geochem. Int. 5, 1108–1125.
Eldridge, C.S., Barton, P.B., Ohmoto, H., 1983. Mineral textures and their bearing on formation of the Kuroko orebodies. Econ. Geol. 5, 241–281.
Eremin, N.I., 1983. Differentiation of Volcanogenic Sulfide Deposits. MSU, Moscow (256 pp. in Russian).
Eremin, N.I., Sergeeva, N.E., Dergachev, A.L., 2007. Rare minerals from massive sulphide ores: typomorphic features and geochemical trend. Vestn. Mosk. Univ. Geol. 2, 85–106.
Evrard, C., Fouquet, Y., Moelo, Y., Rinnert, E., Etoubleau, J., Langlade, J.A., 2015. Tin concentration in hydrothermal sulfides related to ultramafic rocks along the Mid-Atlantic Ridge: a mineralogical study. Eur. J. Mineral. 27, 627–638.
Fouquet, Y., Charlou, J.L., von Stackelberg, U., Wiedicke, M., Erzinger, J., Herzig, P.M., Muehe, R., 1993. Metallogenesis in back-arc environments: the Lau basin example. Econ. Geol. 88, 2154–2181.
Fouquet, Y., Cambon, P., Etoubleau, J., Charlou, J.L., Ondreas, H., Barriga, F.J., Cherkashov, G., Semkova, T., Poroshina, I., Bohn, M., Donval, J.P., Henry, K., Murphy, P., Rouxel, O., 2010. Geodiversity of hydrothermal processes along the Mid-Atlantic Ridge and ultramafic-hosted mineralization: a new type of oceanic Cu-Zn-Co-Au volcanogenic massive sulfide deposit. Geophys. Monogr. Ser. 188, 231–367.
Franklin, J.M., Gibson, H.L., Jonasson, I.R., Galley, A.G., 2005. Volcanogenic massive sulfide deposits. In: Hedenquist, J.W., Thompson, J.F.H., Goldfarb, R.J., Richards, J.P. (Eds.), Econ. Geol. One Hundredth Anniversary Volume. Soc. Econ. Geol., Inc., Littleton, Colorado, pp. 523–560 (1905–2005).
Galley, A.G., Hannington, M.D., Jonasson, I., 2007. Volcanogenic massive sulphide deposits. Geol. Assoc. Canada, Min. Dep. Div. Spec. Publ. 5, 141–161.
Gena, K., Chiba, H., Kase, K., 2005. Tin-bearing chalcopyrite and platinum-bearing bismuthinite in the active Tiger sulfide chimney, Yonaguni Knoll IV seafloor hydrothermal system, Okinawa Trough, Japan. OKAYAMA Univ. Earth Sci. Rep. 12 (1), 1–5.
Glasby, G.P., Notsu, K., 2003. Submarine hydrothermal mineralization in the Okinawa Trough, SW of Japan: an overview. Ore Geol. Rev. 23, 299–339.
Grabezhev, A.I., Moloshag, V.P., Sotnikov, V.I., Murzin, V.V., Korovko, A.V., Zhuxlistov, A.P., 2001. Metasomatic aureole of Safyanovskoye zinc-copper deposit (Middle Urals). Petrologiya 9, 294–312 (in Russian).
Graham, U.M., Bluth, G.J., Ohmoto, H., 1988. Sulfide-sulphate chimneys on the East Pacific Rise, 11 and 13°N latitudes. Part 1: mineralogy and paragenesis. Can. Mineral. 26, 487–504.
Grichuk, D.V., 2012. Thermodynamic model of ore-forming processes in a submarine island-arc hydrothermal system. Geochem. Int. 50 (13), 1069–1100.
Halbach, P., Pracejus, B., Maerten, A., 1993. Geology and mineralogy of massive ores from the Central Okinawa Trough, Japan. Econ. Geol. 88, 2210–2225.
Halbach, P.E., Fouquet, Y., Herzig, P., 2003. Mineralization and compositional patterns in deep-sea hydrothermal systems. In: Halbach, P.E., Tunnicliffe, V., Hein, J.R. (Eds.), Energy and Mass Transfer if Marine Hydrothermal. Dahlem Univ, Berlin, pp. 85–122.
Hannington, M.D., Scott, S.D., 1988. Mineralogy and geochemistry of hydrothermal silica-sulfide-sulfate spire in the Caldera of Axial Seamount, Juan de Fuca Ridge. Can. Mineral. 26, 603–625.
Hannington, M.D., Scott, S.D., 1989. Sulfidation equilibria as guides to gold mineralization in volcanogenic massive sulfides: evidence from sulfide mineralogy and composition of sphalerite. Econ. Geol. 84, 1978–1995.
Hannington, M.D., Peter, J.M., Scott, S.D., et al., 1986. Gold in sea-floor polymetallic sulfide deposits. Econ. Geol. 81 (8), 1867–1883.
Hannington, M.D., Herzig, P.M., Scott, S.D., Thompson, G., Rona, P.A., 1991. Comparative mineralogy and geochemistry of gold-bearing sulfide deposits on the mid-ocean ridges. Mar. Geol. 101, 217–248.
Hannington, M.D., Jonasson, I.R., Herzig, P.M., Petersen, S., 1995. Physical, chemical processes of seafloor mineralization at Mid-Ocean Ridges. In: Humphris, R.A., et al. (Eds.), Seafloor Hydrothermal Systems: Physical, Chemical, Biological, and Geological Interactions. Geophys. Monograph 91, pp. 115–157.
Hannington, M.D., Bleeker, W., Kjarsgaard, I., 1999. Sulfide mineralogy, geochemistry and ore genesis of the Kidd Creek deposit: Part I. North, Central and South orebodies. The Giant Kidd Creek Volcanogenic Massive Sulfide Deposit, Western Abitibi Subprovince, Canada. Econ. Geol. Monograph 10, pp. 163–224.
Haymon, R.M., 1983. Growth history of hydrothermal black smoker chimneys. Nature 305, 695–698.
Herrington, R.J., Maslennikov, V.V., Spiro, B., Zaykov, V.V., Little, C.T.S., 1998. Ancient vent chimney structures in the Silurian massive sulfides of the Urals. In: Mills, R.A., Harrison, K. (Eds.), Modern Ocean Floor Processes and the Geological Record. Geol. Soc. London Spec. Publ. vol. 148, pp. 241–257.
Herrington, R.J., Armstrong, R.N., Zaykov, V.V., Maslennikov, V.V., Tessalina, S.G., Orgeval, J.-J., et al., 2002. Massive sulfide deposits in the South Urals: geological setting within the framework of the Uralide orogen. In: Brown, D., Juhlin, C., Puchkov, V.N. (Eds.), Mountain Building in the Uralides: Pangea to the PresentGeophys. Monograph vol. 132. American Geophysical Union, Washington (DC), pp. 155–182.
Herrington, R., Maslennikov, V., Zaykov, V., Seravkin, I., Kosarev, A., Buschmann, B., et al., 2005a. Classification of VMS deposits: lesson from the South Uralides. Ore Geol. Rev. 27, 203–237.
Herrington, R., Zaykov, V., Maslennikov, V., Brown, D., Puchkov, V., 2005b. Mineral deposits of the Urals and links to geodynamic evolution. Econ. Geol.: One Hundredth Anniv. Vol., pp. 1069–1095
Herzig, P.M., Hannington, M.D., 1995. Polymetallic massive sulfides at the modern seafloor: a review. Ore Geol. Rev. 10, 95–115.
Herzig, P.M., Hannington, M.D., 2000. Polymetallic massive sulfides and gold mineralization at mid-ocean ridges and in subduction-related environments. In: Cronan, D.S. (Ed.), Handbook of Marine Mineral Deposits. CRC Press, Boca Raton, Florida, pp. 347–368.
Huston, D.L., 2000. Gold in volcanic-hosted massive sulfide deposits: distribution, genesis, and exploration. Rev. Econ. Geol. 13, 401–426.
Huston, D.L., Large, R.R., 1989. A chemical model for the concentration of gold in volcanogenic massive sulfide deposits. Ore Geol. Rev. 4, 171–200.
Huston, D.L., Sie, S.H., Suter, G.F., Cooke, D.R., Both, R.A.Q., 1995. Trace elements in sulfide minerals from eastern Australian volcanic hosted massive sulfide deposits. Part I. Proton microprobe analyses of pyrite, chalcopyrite, and sphalerite, and Part II. Selenium levels in pyrite comparison with $\delta^{34}S$ values and implication for the source of sulfur in volcanogenic hydrothermal systems. Econ. Geol. 90, 1167–1196.
Huston, D.L., Pehrsson, S., Eglington, B.M., Zaw, K., 2010. The geology and metallogeny of volcanic-hosted massive sulfide deposits: variations through geologic time and with tectonic setting. Econ. Geol. 105, 571–591.
Ishibashi, J., Urabe, T., 1995. Hydrothermal activity related to back-arc magmatism in the Wester Pacific. In: Taylor, B.C. (Ed.), Backarc Basins; Tectonics and Magmatism. Plenum Press, New York, pp. 451–495.
Karetin, Yu.S., 2000. Geology and Volcanic Formation of Ultradeep Borehole SG-4 in the Urals. Institute of Geology and Geochemistry Press, Yekaterinburg (278 pp. in Russian).
Kase, K., 1988. Tin, arsenic, zinc and silver vein mineralization in the Besshi mine, Central Shikoku, Japan. Mining Geol. 38, 407–418.
Keith, M., Haase, K.M., Schwarz-Schampera, U., Klemd, R., Petersen, S., Bach, W., 2014. Effects of temperature, sulfur and oxygen fugacity on the composition of sphalerite from submarine hydrothermal vents. Geology 48, 699–702.
Keith, M., Häckel, F., Haase, K.M., Schwarz-Schampera, U., Klemd, R., 2016. Trace element systematics of pyrite from submarine hydrothermal vents. Ore Geol. Rev. 72, 728–745.
Kimura, M., 1990. Genesis and formation of the Okinawa Trough, Japan. Mem. Geol. Soc. Jpn. 34, 77–88.
Kontar, E.S., 2013. Geological-Industrial Types of the Cu, Zn, and Pb Deposits in the Urals: Geological Conditions of Setting, History of the Formation, and the Prospects. Department of Subsoil-Using in the Urals Federal District (Urals Subsoil-Using), Yekaterinburg (199 pp. (in Russian).
Koroteev, V.A., de Boorder, H., Necheukhin, V.M., Sazonov, V.N., 1997. Geodynamic setting of the mineral deposits of the Urals. Tectonophysics 276, 291–300.
Koski, R.A., Shanks, W.C., Bohrson, W.A., Oscarson, R.L., 1988. The composition of massive sulfide deposits from the sediment-covered floor of Escanaba Trough, Gorda Ridge: implications for depositional processes. Can. Mineral. 26, 655–674.
Koski, R.A., Jonasson, R.I., Kadko, D., Smith, V.K., Wong, F.L., 1994. Compositions, growth mechanisms, and temporal relations of hydrothermal sulphide–sulphate–silica chimneys at the northern Cleft segment, Juan de Fuca Ridge. J. Geophys. 99, 4813–4832.
Kristall, B., Nielsen, D., Hannington, M.D., Kelley, D.S., Denaney, J.R., 2011. Chemical microenvironments within sulfide structures from the Mothra Hydrothermal Field: evidence from high-resolution zoning of trace elements. Chem. Geol. 290, 12–30.
Krivtsov, A.I., 1999. Metallogeny of Andesite-like Volcanic-plutonic Belts. Part II. TsNIGRI, Moscow (268 pp. in Russian).
Large, R., 1992. Australian volcanic-hosted massive sulfide deposits: features, styles, and genetic models. Econ. Geol. 87, 113–128.
Large, R.R., Huston, D.L., McGoldrick, P.J., Ruxton, P.A., McArthur, G., 1989. Gold distribution and genesis in Australian volcanogenic massive sulfide deposits and their significance for gold transport models. Econ. Geol. Monogr. 6, 503–536.
Leblanc, M., 1991. Platinum-group elements and gold in ophiolitic complexes: distribution and fractionation from mantle to oceanic floor. In: Peters, T., et al. (Eds.),

Ophiolite Genesis and Evolution of the Oceanic Lithosphere, Oman. Kluwer, Dordrecht, pp. 231–260.
Lein, A.Yu., Ulyanova, N.V., Sagalevich, A.M., Bogdanov, Yu.A., Gurvich, E.G., Cherkashev, G.A., Stepanova, T.V., Torokhov, M.P., Ulyanov, A.A., 2003. Mineralogy and geochemistry of sulfide ores from the Logachev-2 and Rainbow fields: similar and distinctive features. Geochem. Int. 41 (3), 271–274.
Lein, A.Yu., Bogdanov, Yu.A., Maslennikov, V.V., Syaoli, Li, Ulyanova, N.V., Maslennikova, S.P., Ulyanov, A.A., 2010. Sulfide minerals in the Menez Gwen Nonmetallic Hydrothermal Field (Mid_Atlantic Ridge). Lithol. Miner. Resour. 45 (4), 305–323.
Little, C.T.S., Herrington, R., Maslennikov, V.V., Morris, N.J., Zaykov, V.V., 1997. Silurian high-temperature hydrothermal vent community from the southern Urals, Russia. Nature 385 (9), 3–6.
Little, C.T.S., Herrington, R.J., Haymon, R.M., Danelian, T., 1999. Early Jurassic hydrothermal vent community from the Franciscan Complex, San Rafael Mountains, California. Geology 27 (2), 167–170.
Lüders, V., Pracejus, B., Halbach, P., 2001. Fluid inclusion and sulfur isotope studies in probable modem analogue Kuroko-type ores from the JADE hydrothermal field (Central Okinawa Trough, Japan). Chem. Geol. 173, 45–58.
Marchig, V., Rösch, H., 1988. Mineralogical zonation and radiochronological relations in a large sulfide chimney from the East Pacific Rise at 18°25′S. Can. Mineral. 26, 541–554.
Marques, A.F.A., Barriga, F.J.A.S., Scott, S.D., 2007. Sulfide mineralization in an ultramafic-rock hosted seafloor hydrothermal system: from serpentinization to the formation of Cu–Zn–(Co)-rich massive sulfides. Mar. Geol. 245, 20–39.
Marumo, K., Hattori, K.H., 1997. Seafloor hydrothermal clay alteration at Jade in the back-arc Okinawa Trough: mineralogy, geochemistry and isotope characteristics. Geochim. Cosmochim. Acta 63, 2785–2804.
Marumo, K., Urabe, T., Goto, A., Takano, Y., Nakashima, M., 2008. Mineralogy and isotope geochemistry of active submarine hydrothermal field of Suiyo Seamount, Izu-Bonin Arc, West Pacific ocean. Resour. Geol. 58 (3), 220–248.
Maslennikov, V.V., 1999. Sedimentogenesis, Halmyrolysis and Ecology of the Massive Sulfide Paleohydrothermal Fields (on the Example of the Southern Urals). Geotur, Miass (348 pp. (in Russian).
Maslennikov, V.V., 2006. Lithogenesis and Massive Sulfide Deposits Formation. IMin UB RAS, Miass (384 pp. (in Russian).
Maslennikov, V.V., Maslennikova, S.P., Large, R.R., Danyushevsky, L.V., 2009. Study of trace element zonation in vent chimneys from the Silurian Yaman-Kasy VMS (the Southern Urals, Russia) using laser ablation inductively coupled plasma mass spectrometry (LA-ICP MS). Econ. Geol. 104, 1111–1141.
Maslennikov, V.V., Ayupova, N.R., Herrington, R.J., Danyushevskiy, L.V., Large, R.R., 2012. Ferruginous and manganiferous haloes around massive sulphide deposits of the Urals. Ore Geol. Rev. 47, 5–41.
Maslennikov, V.V., Maslennikova, S.P., Large, R.R., Danyushevskiy, L.V., Herrington, R.J., Stanley, C.J., 2013. Tellurium-bearing minerals in zoned sulfide chimneys from Cu-Zn massive sulfide deposits of the Urals, Russia. Mineral. Petrol. 107, 67–99.
Maslennikov, V.V., Ayupova, N.R., Maslennikova, S.P., Tret'yakov, G.A., Danyushevskiy, L.V., Large, R.R., Melekestseva, I.Yu., Safina, N.P., Belogub, E.V., Tseluyko, A.S., Gladkov, A.G., Kraynev, Yu.D., 2014. Toxic Elements in Massive Sulfide Forming Systems (Yekaterinburg, 340 pp. (in Russian with English abstract)).
Maslennikova, S.P., Maslennikov, V.V., 2007. Paleozoic "black Smoker" Sulfide Chimneys (After the Example of Ural) (Yekaterinburg, 312 pp. (in Russian with English abstract)).
Melekestseva, I.Yu., Zaykov, V.V., Nimis, P., Tret'yakov, G.A., Tesalina, S.G., 2013. Cu-(Ni-Co-Au)-bearing massive sulfide deposits associated with mafic-ultramafic rocks of the Main Urals Fault, South Urals: geological structures, ore textural and mineralogical features, comparison with modern analogs. Ore Geol. Rev. 52, 18–37.
Melekestseva, I.Yu., Tret'yakov, G.A., Nimis, P., Yuminov, A.M., Maslennikov, V.V., Maslennikova, S.P., Kotlyarov, V.A., Beltenev, V.E., Danyushevsky, L.V., Large, R., 2014. Barite-rich massive sulfides from the Semenov-1 hydrothermal field (Mid-Atlantic Ridge, 13°30.87′ N): evidence for phase separation and magmatic input. Mar. Geol. 349, 37–54.
Mercier-Langevin, P., Hannington, M.D., Dubé, B., Bécu, V., 2011. The gold content of volcanogenic massive sulfide deposits. Mineral Deposits 46, 509–539.
Metz, S., Trefry, J.H., 2000. Chemical and mineralogical influences on concentrations of trace metals in hydrothermal fluids. Geochim. Cosmochim. Acta 64, 2267–2279.
Moh, G.H., 1975. Tin-containing mineral systems. Part II: phase relations and mineral assemblages in the Cu-Fe-Zn-SnS system. Chem. Erde 34, 1–6.
Moloshag, V.P., Grabezhev, A.I., Gulyaeva, T.Ya., 2002. Conditions of telluride formation in ores of the Urals massive sulfide and copper-gold-porphyry deposits. Zap. Vses. Mineral. O-va. 131 (5), 40–53 (in Russian).
Monecke, T., Petersen, S., Hannington, M.D., Grant, H., Samson, I.M., 2016. The minor element endowment of modern sea-floor massive sulfides and comparison with deposits hosted in ancient volcanic successions. Econ. Geol. 18, 245–306.
Moss, R., Scott, S.D., 2001. Geochemistry and mineralogy of gold-rich hydrothermal precipitates from the eastern Manus Basin, Papua New Guinea. Can. Mineral. 39, 957–978.
Mozgova, N.N., Krasnov, S.G., Batuyev, B.S., Borodaev, Y.S., Efimov, A.V., Markov, V.F., Stepanova, T.V., 1996. The first report of cobalt pentlandite from a Mid-Atlantic Ridge hydrothermal deposits. Can. Mineral. 34, 23–28.
Mozgova, N.N., Borodaev, Yu.S., Cherkashev, G.A., et al., 2008. Mineralogy of massive sulfides from the Ashadze Hydrothermal Field, 13° N, Mid–Atlantic Ridge. Can. Mineral. 46, 545–567.
Murphy, P.J., Meyer, G., 1998. A gold-copper association in ultramafic-hosted hydrothermal sulfides from the Mid-Atlantic Ridge. Econ. Geol. 93, 1076–1083.
Norman, M.D., Griffin, W.L., Prearson, N.J., Garcia, M.O., O'Reilly, S.Y., 1998. Quantitative analysis of trace element abundances in glasses and minerals: a comparison of laser ablation inductively coupled plasma mass spectrometry, solution inductively coupled plasma mass spectrometry, proton microprobe and electron microprobe data. J. Anal. At. Spectrom. 13, 477–483.
Oudin, E., Constantinou, G., 1984. Black smoker chimney fragments in Cyprus sulfide deposits. Nature 308, 349–353.
Paradis, S., Jonasson, I.R., Le Cheminant, G.M., Watkinson, D.H., 1988. Two zinc-rich chimneys from the plume site, Southern Juan de Fuca Ridge. Can. Mineral. 26, 637–654.
Perner, M., Hansen, M., Seifert, R., Srauss, H., Koschinsky, A., Petersen, S., 2013. Linking geology, fluid chemistry, and microbial activity of basalt- and ultramafic-hosted-deep sea hydrothermal vent environments. Geobiology 11 (4), 340–355.
Peter, J.M., Scott, S.D., 1988. Mineralogy, composition, and fluid-inclusion microthermometry of seafloor hydrothermal deposits in the Southern Trough of Guaymas Basin, Gulf of California. Can. Mineral. 26, 567–587.
Petersen, S., Herzig, M., Hannington, M.D., Gemmel, J.B., 2003. Gold-rich massive sulfides from the interior of felsic-hosted PACMANUS massive sulfide deposit, Easter Manus Basin (PNG). In: Eliopolis, et al. (Eds.), Mineral Exploration and Sustainable Development. Millpress, Rotterdam, pp. 171–174.
Prokin, V.A., 1977. Regularities in Localization of Massive Sulfide Deposits in the Southern Urals. Nedra, Moscow (174 pp. (in Russian).
Prokin, V.A., Buslaev, F.P., 1999. Massive copper-zinc sulfide deposits in the Urals. Ore Geol. Rev. 14, 1–69.
Prokin, V.A., Seravkin, I.B., Vinogradov, A.M., 2011. Geological conditions of distribution and prognostic perspectives of large massive copper-sulfide deposits in the Urals. Litosfera 6, 123–133 (in Russian).
Puchkov, V.N., 2010. Geology of the Urals and Cis-Urals: Urgent Problems of Stratigraphy, Tectonics, Geodynamics and Metallogeny. DizainPoligraphServis, Ufa (280 pp. (in Russian).
Reeves, E.P., Seewald, J.S., Saccocia, P., Bach, W., Craddock, P.R., Shanks, W.C., Sylva, S.P., Walsh, E., Pichler, T., Rosner, M., 2011. Geochemistry of hydrothermal fluids from the PACMANUS, Northeast Pual and Vienna Woods hydrothermal fields, Manus Basin, Papua New Guinea. Geochim. Cosmochim. Acta 75 (4), 1088–1123.
Relvas, J.M.R.S., Barriga, F.J.A.S., Ferreira, A., Noiva, P.C., Pacheco, N., Barriga, G., 2006. Hydrothermal alteration and mineralization in the Neves-Corvo volcanic-hostemassive sulfide deposit, Portugal. I. Geology, mineralogy, and geochemistry. Econ. Geol. 101, 753–790.
Revan, M.K., Genç, Y., Maslennikov, V.V., Maslennikova, S.P., Large, R.R., Danyushevsky, L.V., 2014. Mineralogy and trace-element geochemistry of sulfide minerals in hydrothermal chimneys from the Upper-Cretaceous VMS deposits of the eastern Pontide orogenic belt (NE Turkey). Ore Geol. Rev. 62, 129–149.
Rona, P.A., 2008. The changing vision of marine minerals. Ore Geol. Rev. 33, 618–666.
Rouxel, O., Fouquet, Y., Ludden, J.N., 2004. Subsurface processes at the Lucky Strike hydrothermal field, Mid-Atlantic ridge: evidence from sulfur, selenium, and iron isotopes. Geochim. Cosmochim. Acta 68, 2295–2311.
Safina, N.P., Melekestseva, I.Yu., Nimis, P., Ankusheva, N.N., Yuminov, A.M., Kotlyarov, V.A., Sadykov, S.A., 2016. Barite from the Safyanovka VMS deposit (Central Urals) and Semenov-3 hydrothermal sulfide fields (Mid-Atlantic Ridge): a comparative analysis of formation condition. Mineral Deposits 51, 491–507.
Sakai, H., Gamo, T., Ishibashi, J., Shitashima, K., Kim, E.S., Yanagisawa, F., Tsutsumi, M., Sano, Y., Wakita, H., Tanaka, T., Matsumoto, T., Naganuma, T., Mitsuzawa, K., 1990. Unique chemistry of the hydrothermal solutions in the mid-Okinawa Trough back arc basin. Geophys. Res. Lett. 17, 2133–2136.
Scott, S.D., 1981. Small chimneys from Japanese Kuroko deposits. In: Seminars on Seafloor Hydrothermal Systems. Goldie, R., Botrill, T.J. (eds). Geosci. Can. 8, 103–104.
Scott, S.D., 1997. Submarine hydrothermal systems and deposits. In: Barnes, H.L. (Ed.), Geochemistry of Hydrothermal Ore Deposits. Wiley, New York, pp. 797–876.
Seravkin, I.B., 2010. The Metallogeny of the Southern Urals and the Central Kazakhstan. Gilem, Ufa (281 pp. (in Russian).
Shadlun, T.N., 1991. Some sulfide intergrowths typical for modern oceanic and ancient massive sulfide ores. Geol. Ore Deposits 33, 110–118 (in Russian).
Shadlun, T.N., Bortnikov, N.S., Bogdanov, Y.A., Tufar, W., Murav'yev, K.G., Gurvich, Y.G., Muravitskaya, G.N., Korina, Y.A., Topa, T., 1993. Mineralogy, textures, and formation conditions of modern sulfide ores, manus basin rift zone. Internat. Geol. Rev. 35 (2), 127–145.
Shikasono, N., Kusakabe, M., 1999. Mineralogical characteristics and formation mechanism of sulfate-sulfide chimney from Kuroko Area, Mariana Trough and Mid-Ocean Ridges. Resour. Geol. 20, 1–11.
Shimazaki, H., Horikoshi, E., 1990. Black pre chimney from the Hanaoka Kuroko deposits, Japan. Min. Geol. 40 (5), 313–321.
Sillitoe, R.H., Hannington, M.D., Thompson, J.F.H., 1996. High sulfidation deposits in the volcanogenic massive sulfide environment. Econ. Geol. 91, 204–212.
Slack, J.F., Foose, M.P., Flohr, J.H., Scully, M.V., Belkin, H.E., 2003. Exhalative and subseafloor replacement processes in formation of the Bald Mountain massive sulfide deposit, northern Main. Econ. Geol. Monogr. 11, 513–547.
Solomon, M., Tornos, F., Large, R.R., Badham, J.N.P., Both, R.A., Kin, Z., 2004. Zn-Pb-Cu volcanic-hosted massive sulfide deposits criteria for distinguishing brine pool-type from black smoker-type sulfide deposition. Ore Geol. Rev. 25, 259–283.
Spooner, E.T.C., 1993. Magmatic sulfide volatile interaction as a mechanism for producing chalcophile element enriched, Archean Au-Quartz, epithermal Au-Ag and Au skarn hydrothermal ore fluids. Ore Geol. Rev. 7, 359–379.
Stanton, R.L., 1994. Ore Elements in Arc Lavas. Oxford Univ, New York (391 pp.).
Tessalina, S.G., Maslennikov, V.V., Surin, T.N., 1998. Alexandrinka VMS deposit (East Magnitogorsk paleoisland arc, Urals). Institute of Mineralogy, Miass 228 p. (in Russian).
Tessalina, S.G., Bourdon, B., Maslennikov, V.V., Orgeval, J.-J., Birck, J.-L., Gannoun, A., Capmas, F., Allègre, C.-J., 2008. Osmium isotope distribution within the Palaeozoic Alexandrinka seafloor hydrothermal system in the Southern Urals, Russia. Ore Geol. Rev. 33, 70–80.

Tivey, M.K., Humphris, S.E., Thompson, G., Hannington, M.D., Rona, P.A., 1995. Deducing patterns of fluid flow and mixing within the TAG active hydrothermal mound using mineralogical and geochemical data. J. Geophys. Res. 100, 12527–12555.
Tret'yakov, G.A., 2015. Mineral assemblages and behavior of ore-forming elements at the rock-seawater interaction in hydrothermal. Litosfera 5, 147–151 in Russian.
Vaughan, D.J., Rosso, K.M., 2006. Chemical bonding in sulfide minerals. Rev. Mineral. Geochem. 61, 231–264.
Vikentyev, I.V., 2004. Formation conditions and metamorphism of massive sulfide ores. Nauchnyi Mir, Moscow 344 p. (in Russian).
Vikentyev, I.V., 2006. Precious metal and telluride mineralogy of large volcanic-hosted massive sulfide deposits in the Urals. Mineral. Petrol. 87, 305–326.
Vikentyev, I.V., 2015. Invisible and microscopic gold in pyrite: methods and new data for massive sulfide ores of the Urals. Geol. Ore Deposits 57 (4), 237–265.
Vikentyev, I.V., Belenkaya, Yu.A., Ageev, B.I., 2000. Alexandrinskoye polymetallic massive sulfide deposit (the Urals, Russia). Geol. Ore Deposits 42, 221–246.
von Damm, K.L., Edmond, J.M., Grant, B., Measures, C.I., 1985. Chemistry of submarine hydrothermal solutions at 21 N, East Pacific Rise. Geochim. Cosmochim. Acta 49 (11), 2197–2220.
Watanabe, K., Kajimura, T., 1994. The hydrothermal mineralization at Suiyo Seamount, in the central part of the Izu-Ogasawara Arc. Resour. Geol. 44, 133–140.
Wohlgemuth-Ueberwasser, C.C., Viljoen, F., Petersen, S., Vorster, C., 2015. Distribution and solubility limits of trace elements in hydrothermal black smoker sulfides: an in-situ LA-ICP-MS study. Geochim. Cosmochim. Acta 159, 16–41.
Ye, L., Cook, N.J., Ciobanu, C.L., Liu, Y.P., Zhang, Q., Gao, W., Yang, Y.L., Danyushevsky, L.V., 2011. Trace and minor elements in sphalerite from base metal deposits in South China: a LA-ICPMS study. Ore Geol. Rev. 39, 188–217.
Zaykov, V.V., 2006. Volcanism and Sulfide Mounds of Paleocean Margins (After the Example of Ural's and Siberia's Massive Sulfide-bearing Zones). Nauka, Moscow (428 pp. (in Russian).
Zaykov, V.V., Maslennikov, V.V., 1987. About seafloor sulfide mounds in the massive sulfide deposits of the Urals. Dokl. AS USSR 293 (1), 181–184 in Russian.
Zaykov, V.V., Maslennikov, V.V., Zaykova, E.V., Herrington, R., 2001. Ore-formational and Ore-facies Analysis of the Massive Sulfide Deposits of Ural Paleo-ocean. IMin UB RAS, Mias (315 pp. (in Russian).
Zengqian, H., Qiling, Z., 1998. CO_2-hydrocarbon fluids of the Jade hydrothermal field in the Okinawa trough: fluid inclusion evidence. China Earth Sci. 41, 408–415.
Zhabin, A.G., Samsonova, N.S., 1975. Traces of disappeared pyrrhotite in massive sulfide deposits. Zap. Vses. Mineral. O-va. 104, 346–350 (in Russian).
Zierenberg, R.A., Koski, R.A., Morton, J.L., Bouse, R.M., 1993. Genesis of massive sulfide deposits on a sediment-covered spreading center, Escanaba trough, Southern Gorda Ridge. Econ. Geol. 88, 2069–2099.